Title
Binding energy in antibody catalysis

Permalink
https://escholarship.org/uc/item/01s5w8fn

Author
Wade, Herschel VonEdward

Publication Date
2000

Peer reviewed|Thesis/dissertation

BINDING ENERGY IN ANTIBODY CATALYSIS

by

Herschel VonEdward Wade

DISSERTATION

Submitted in partial satisfaction of the requirements for the degree of
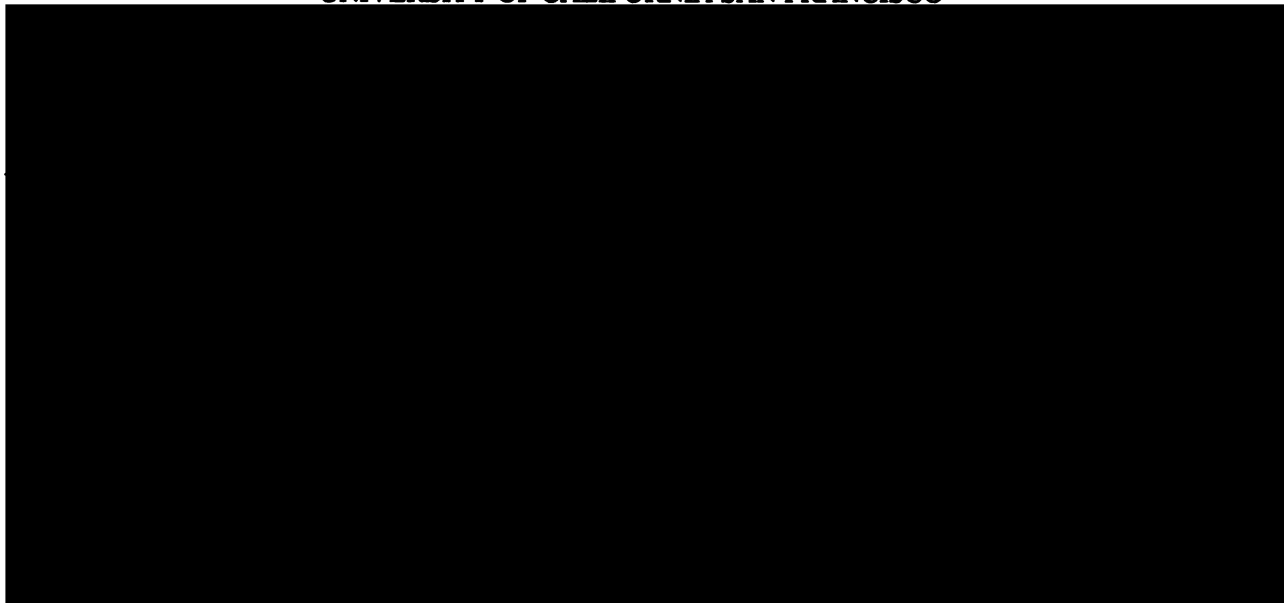
DOCTOR OF PHILOSOPHY

in

Pharmaceutical Chemistry

in the

GRADUATE DIVISION

of the

UNIVERSITY OF CALIFORNIA SAN FRANCISCO

Date   University Librarian

Degree Conferred: . . . .

Dedicated to

My mother, Williette Wade,

my sisters, Sharon, Sabrina, Shaunice, and Stacy,

and my late father William Leon Wade

Acknowledgements

I would first like to thank the creator and my spiritual guides for me with the strength, guidance, courage, perseverance, and determination for every part of this journey call life.

I would like thank Professor Thomas S. Scanlan for his support of my research, his advice concerning my scientific maturity and my career, and for his sternness when I needed to be put back on the right track. I also thank Tom for providing me with a significant amount of freedom (and money) which has forced me to learn from my mistakes and has helped me start to build a solid foundation for my scientific future. I feel truly fortunate to have been connected with Tom in my scientific endeavors, especially this particular part.

Professors Susan Miller, Paul Ortiz de Montellano, David Agard, and Robert Fletterick deserve special mention for their part in my research. I thank these scientists for always taking the time to have fruitful, sometimes lengthy, discussions with me, for always taking the time to write great letters of recommendations, and for being superior scientific models (and role models). I cannot express how important the participation of these scientists has been in my graduate training.

For providing me with strength, I thank my family: Mom, dad, sisters, nieces, nephews, grandmother, Tommie Dell, and aunt Dorthy.

The support from every last one of them has helped me though this part of my life.

I would like to thank my friends that have been silent and vocal supporters of my endeavors from the start: Stacy Mitchell and family, Tina Farris and family, Benjamin Watkins and family, Victor Alexander and family, Darryl Flowers, James Buckman, Van Hoang, Angela Wilks and family, Michael Stevenson and family, Joanne Trejo, Elizabeth Montangne, Tamara Barnes and family, Jennifer Harris, Mark Dresser, Luke Lightning, Bodo Stern, Carla Washington, Nicole Samuels, Dr. John Watson and family, Robert Otillar, Lisa Uyechi, Diane Wong, Lisa Shapiro, and James Goodfellow.

I would also like to thank the black faculty and staff at UCSF. With them I would not have been provided the opportunity to be here and probably any other place. Your smiles, encouraging fist pumps, and support will never go unappreciated.

Finally, I would like to the faculty and STAFF in the Department of Pharmaceutical Chemistry, especially Judy, Liza, and Christina, for their invaluable help.

"At first I did not know what I wanted. But in the end I understood this language. I understood it, I understood it, I understood it, all wrong perhaps. This is not what matters... Does this mean that I am freer now than I was? I do not know. I shall learn."
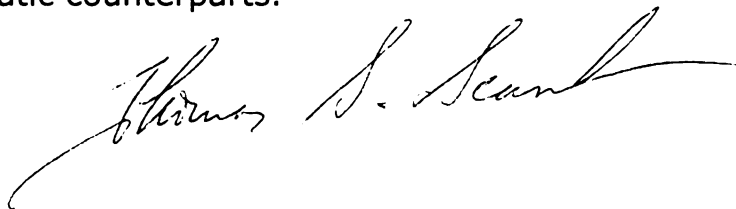
Samuel Beckett

Abstract

The haptens used to generate catalytic antibodies are expected to elicit active site-substrate binding interactions that are reminiscent of those found to be important in enzymatic catalysis. The work presented in this dissertation describes the investigation of how such binding interactions are used in the catalytic mechanism of the antibody 17E8. Kinetic and thermodynamic studies using alternative substrate and phosphonate transition-state analogs have provided insight to the catalytic and binding response to the hapten used to generate 17E8. The results from these studies indicate that the hapten does indeed elicit antibody active site binding interactions that are reminiscent of those found in enzyme active sites as these 'programmed' interactions are used for overall transition-state stabilization (to increase k_{cat}/K_M). It is also found that hapten elicitation does not necessarily result in an antibody active site that enforces the differential use of binding interactions between ground-state substrate complex and the transition-state complex so that the interactions can be used to increase catalytic turnover (k_{cat}). Calorimetric studies of 17E8–phosphonate binding reactions reveal that there may be thermodynamic differences between the desired properties of hydrolytic active site and those needed for hapten

binding, making it difficult to obtain efficient catalysts from screens based on the tight binding of transition-state analogs.

Together, these studies provide a conceptual framework for understanding how catalytic antibodies may use binding interactions in their mechanisms. I believe that the results from these studies may help bring chemists a step closer to be able to experimentally elucidate why antibodies have large shortcomings as catalysts compared to their enzymatic counterparts.

Table of Contents

List of Tables

List of Figures

Chapter 1. Introduction

Catalysis and Binding Energy

A

$$E + S^{\ddagger}$$

$$[E{\bullet}S]^{\ddagger}$$

$$G$$

$$E + S$$

$$(E{\bullet}S)$$

$$(E{\bullet}P)$$

$$E + P$$

B

$$E + S^{\ddagger}$$

$$[E{\bullet}S]^{\ddagger}$$

$$G$$

$$(E{\bullet}S)$$

$$(E{\bullet}P)$$

$$E + S$$

$$E + P$$

Figure 1.1 Free–energy diagrams for the reaction, S → P, in the absence (grey lines) and the corresponding reaction, E + S ↔ E•S → E + P, in the presence (black lines) of a catalyst. The catalyst is just a spectator in the uncatalyzed reaction. Key: E, enzyme; S, substrate; $S^{\ddagger}$, transition state; P, product; (E•S), enzyme•substrate complex; (E•P), enzyme•product complex. Note that the free-energy of the ground-state (E•S) and (E•P) complexes depend on [S] and [P]. **A.** [S] > K_S **B.** [S] < K_S, where K_S is the dissociation constant for the substrate.

Catalysts primarily function by stabilizing transition–states.

Because reaction rates are faster in the presence of a catalyst than in

their absence, the free–energy of activation is lower and thus, in thermodynamic terms, the transition-state is more stable.[1-4] Catalysts can also provide alternative reaction pathways provided that the free-energy of activation is lower than that of the uncatalyzed reaction. The free–energy diagram of a simple chemical reaction is shown in Figure 1.1 as is the corresponding reaction in the presence of a enzyme catalyst. The main difference between the two reactions (in addition to the lower free energy of activation) is that in the presence of a catalyst, there are obligatory association steps between the substrate and the catalyst. With chemical catalysts including general acids or bases and nucleophilic catalysts, the association with substrates is purely chemical–the catalyst only associates with the reaction center.[3,5-7] With catalysts such as enzymes, the association has a chemical and a binding component.[3,4,8-10] These catalysts associate with the substrate at the reaction center and at non-reacting portions. Studies with model systems have shown that both the chemical and binding components contribute significantly to the catalytic power of enzymes.[3,11-14]

How enzymes use binding interactions for catalysis is intriguing for several reasons. The rate enhancements afforded by enzymes are always orders of magnitude higher than those obtained with small molecule chemical catalysts.[3,5-7,12,15,16] The differences

between these rate enhancements undoubtedly have something to do with the fact that enzymes are able to utilize specific binding interactions in their catalytic mechanisms.[8,17-22] In addition, unlike chemical catalysts, enzymes use binding energy not only to determine which substrates will enter the active site and bind, but also to determine which substrates will undergo the requisite chemistry and at appropriate rate.[17]

Early questions concerning the use of specific binding interactions in enzyme catalysis were addressed by asking how enzymes catalyze reactions with their physiological substrates so effectively, and why so poorly with molecules that they were not designed to react upon. Indeed, it is easy to understand why substrates that cannot for steric reasons fit in an enzyme active site to react. The interesting question comes about when trying to understand why substrates that can bind to the active site react slowly or not at all.[17] A well-known investigation of binding in catalysis involves the enzyme, hexokinase.[23] This enzyme transfers the γ-phosphate group from ATP to the C6-hydroxyl group of glucose 4 x 10^4 times faster than it transfers the phosphate group to the chemically similar hydroxyl group of water. Chymotrypsin, a pancreatic endopeptidase, cleaves the ethyl ester of N-acetyl-L-tyrosine 4 x 10^7 times faster than it does the much smaller substrate,

ethyl acetate, although the chemical reactivities of these substrates are similar.[24-26] These large increases in catalytic rates with the additional substrate groups indicates the power of binding interactions in catalysis.

$$E + S \xrightarrow{k_{uncat}} E + S^{\ddagger} \longrightarrow E + P$$

$$k_{cat}/K_M \searrow \quad \Big\uparrow K_{TS}$$

$$[E{\bullet}S]^{\ddagger} \longrightarrow E + P$$
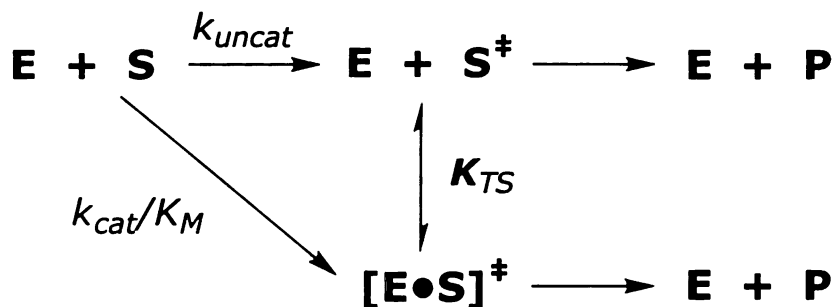
Figure 1.2 Catalytic proficiency results from transition-state binding.

The use of binding energy to promote catalysis can be presented with the thermodynamic box shown in Figure 1.2, which illustrates that the magnitude of the proficiency $((k_{cat}/K_M)/k_{uncat})$ of an enzyme is governed by how tightly the enzyme binds the transition-state (K_{TS}) of the reaction.[21,22,27,28] The importance of this ratio can easily be seen with the use of the free-energy diagram which indicates that it is from this ratio that the overall transition-state stabilization provided by an enzyme can be measured (Figure 1.1). The thermodynamic box is misleading in that it implies that enzymes are able to actually bind the transition-states of substrates that form in solution. A more accurate idea is that enzyme active sites provide a more stabilizing environment for transition-states than does aqueous solution.

4

Catalytic proficiency is different from the rate enhancement (k_{cat}/k_{uncat}) provided by enzymes. The rate enhancement, as shown with the thermodynamic box in Figure 1.3, depends on how tightly the enzyme binds the transition–state relative to its affinity for the unreacted substrate.[27,29,30] The rate enhancement rate is often awkward because k_{cat} values are always first order, whereas k_{uncat} values are often second or third order (the uncatalyzed reaction in Figure 1.3 is a first-order reaction). Chemists often apply a correction factor accounting for entropic requirement of bringing the reactants together to make comparisons between catalyzed and uncatalyzed reactions less awkward.[31]

$$E + S \xrightarrow{k_{uncat}} E + S^{\ddagger} \longrightarrow E + P$$

$$\Big\updownarrow K_S \qquad \Big\updownarrow K_{TS}$$

$$(E{\bullet}S) \xrightarrow{k_{cat}} [E{\bullet}S]^{\ddagger} \longrightarrow E + P$$
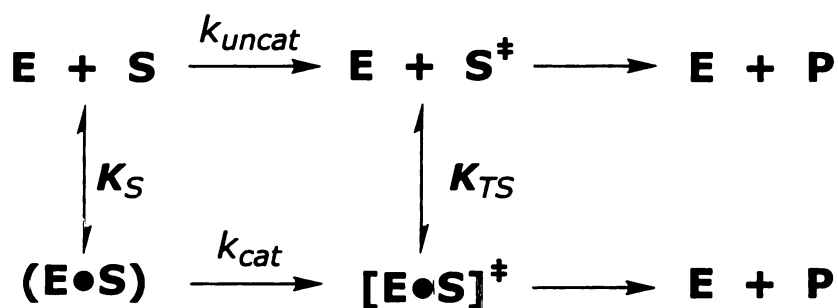
Figure 1.3 Binding to the transition–state more tightly than to the ground–state substrate results in large rate enhancements.

Binding tightly to transition–states is too simple an explanation of how enzymes use binding energy to promote catalysis. It turns out that enzymes have evolved several mechanisms for the utilization of

binding energy.[4,17] For example, induced fit is a mechanism that involves using binding energy to change an enzyme's conformation so that the catalytic groups in the active site are placed in the correct position relative to the substrate's reactive groups so that the catalyzed reaction can take place.[32,33] Studying the effect of turning intermolecular chemical reactions into intramolecular reactions has shown that decreasing a reaction's entropic requirement is another mechanism for the utilization of binding energy.[11,34-37] Binding energy can be used to eliminate the substrate's access to multiple, iso-energetic binding modes, of which only one is productive, so that efficient catalysis can take place.[24,38,39] The mechanism of binding to transition-states tightly (discussed above) has been placed under the mechanism of strain.[20,40,41] Because there are often geometric and electronic differences between a substrate's transition-state and ground-state, having an active site that is complementary to the transition-state has the consequence of being not complementary to the ground-state. Thus, 'strain' will be placed on the ground-state to distort it into the transition-state (called the 'Circe effect' by Jencks).[17] This strain could be due to unfavorable substrate•enzyme interactions that are relieved in the transition-state, or to enzyme providing binding interactions to the transition-state that are not provided to the ground-state substrate.[3,20,40-42] The

tighter binding of transition–state analogs, molecules that possess the geometric and electronic qualities of reaction transition–states (or high energy intermediates), relative to ground–state substrates has provided evidence of this type of strain.[22,27,28,30,43]

Binding Energy and Hydrolytic Antibodies

The 'strain' mechanism has been exploited for the generation of antibodies that catalyze ester hydrolysis.[44-47] The accepted mechanism for the base-promoted uncatalyzed hydrolysis reaction is shown in Figure 1.4.[3,48] The antibodies that catalyze this reaction have been generated with several types of haptens, most of which share the geometric and/or electronic properties of the putative anionic tetrahedral intermediate that is flanked by two
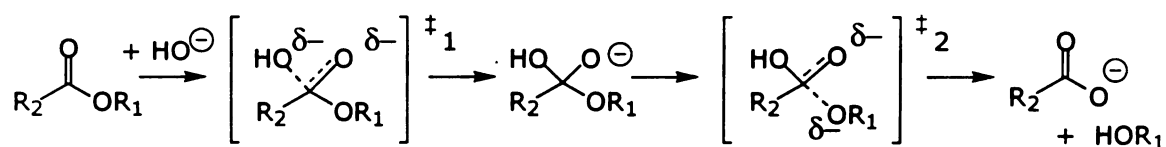
Figure 1.4 Base-promoted ester hydrolysis.

transition–states that are of similar structure and charge.[49-52] Of the haptens used, the phosphonate (**A**, Figure 1.5) and phosphonamidate (**B**) transition state analogs generally produce the most active antibodies.[49-52] Generating antibodies to these types

of molecules is expected to elicit immunoglobulin binding sites that are

electronically and/or geometrically complementary to the analogs and

thus provide stabilizing interactions (relative to bulk solution) for the

otherwise unstable tetrahedral intermediate and the flanking

transition-states.[46,47,53-55]
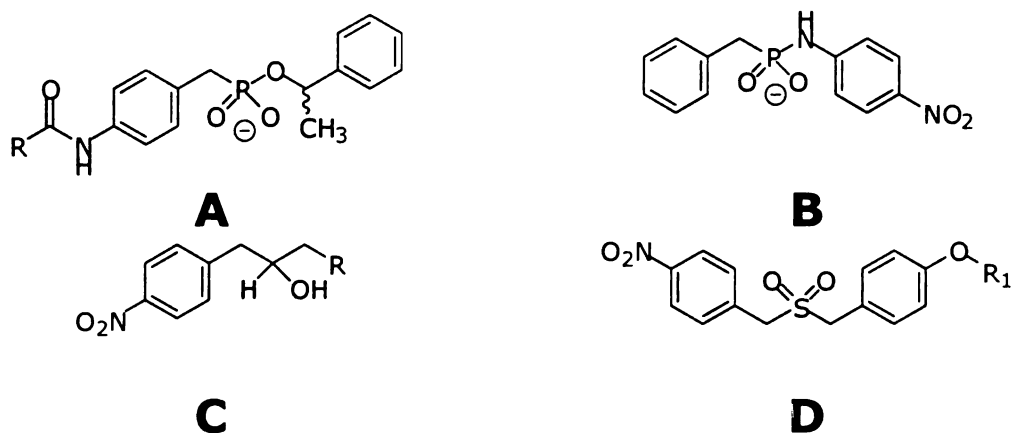
Figure 1.5 Types of haptens used to generate esterolytic antibodies. (A) phosphonate, (B) phosphonamidate, (C) secondary alcohol, and (D) sulfone.

This design consideration is supported by the fact that phosphonates,

phosphonamidates, phosphonimidates, and phosphonic acids are

potent inhibitors for enzymes that perform amide and ester

hydrolysis.[56-59] However, theoretical studies question how well

phosphonates, phosphonamidates, and phosphinates replicate the

geometry and electrostatic properties of the transition-states ($\ddagger$1 and

$\ddagger$2, Figure 1.4) and the tetrahedral intermediate.[60-62] The studies

do suggest that the binding sites should bind the transition-state

(primarily $\ddagger$2) and the tetrahedral intermediate more tightly than the

substrates and products. Structural studies of hydrolytic

antibody•phosphonate complexes provide support for the design

rationale and theoretical studies.[63,64] In all of the complexes, the

partially charged oxygen atoms of the anionic phosphonate moiety

form several hydrogen bonds in the antibody binding site (Figure

1.6).[65-69] The interactions are thought to mimic those between

the antibodies and their respective transition state (or tetrahedral

intermediate) anions.

A   **B**

48G7   **D2.3**
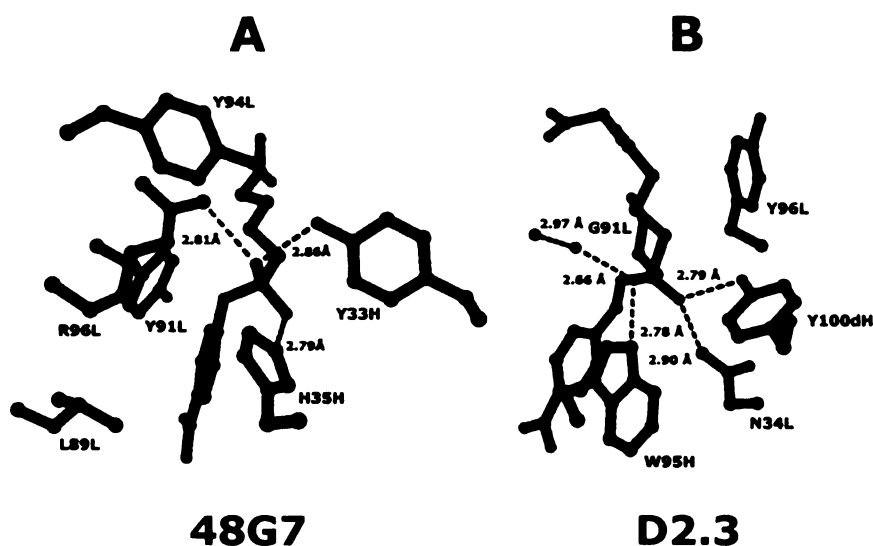
Figure 1.6 Important active site interactions in esterolytic antibodies. (**A**) 48G7, p-nitrophenyl esterase [65]. (**B**) D2.3, p-nitrobenzylesterase [66].

Examples of the Use of Binding Energy in Catalysis

Most of the discussion of binding energy in catalysis thus far has

focused on transition–state binding, but during a catalytic process

enzymes must recognize substrates, transition–states, and stable intermediates.**[4,70,71]** Numerous studies have shed a great deal of light on how enzymes have developed a 'distribution of labor' among active site–substrate interactions to accomplish this task. This 'distribution of labor' among active site interactions allows enzymes to use binding energy to decrease activation barriers, optimize equilibrium constants, and determine specificity.**[4]**

Detailed kinetic studies on the wild-type and site-directed mutants of tyrosyl-tRNA synthetase from *Bacillus stearothermophilus* have exemplified the profound role of binding energy in enzyme catalysis. This enzyme system is particularly interesting for addessing questions regarding binding energy and catalysis because it is probably one of the few whose catalytic power stems solely from the use of enzyme-substrate binding energy.**[70,72]** More importantly, the key interaction energies are determined for all species that are present on the reaction coordinate, including ground-state enzyme-substrate, enzyme-transition-state, enzyme-intermediate, and enzyme-product complexes.**[4,70-72]** Studies on this enzyme system have provided illustrative examples of uniform binding, the preferential stabilization of the transition-state(s), and the differential binding of ground-state species (enzyme-intermediate

complementarity), all of which are thought to be important for enzyme action.[4,18,73-75]

The tyrosyl-tRNA synthetase catalyzes the formation of tyrosyl-tRNA^{Tyr} in a two step reaction: (1) the amino acid is activated by the formation of an enzyme-bound aminoacyl adenylate (Figure 1.7) and (2) the activated amino acid is transferred to to the tRNA (not shown).

$$E \underset{\substack{k_{+T}[T] \\ k_{-T}}}{\overset{\substack{k_{+A}[A] \\ k_{-A}}}{\rightleftharpoons}} \begin{matrix} E{\bullet}A \\ E{\bullet}T \end{matrix} \underset{\substack{k'_{+A}[A] \\ k'_{-A}}}{\overset{\substack{k'_{+T}[T] \\ k'_{-T}}}{\rightleftharpoons}} E{\bullet}T{\bullet}A \underset{k_{-3}}{\overset{k_3}{\rightleftharpoons}} E{\bullet}T\text{-}A{\bullet}PP \underset{k_{+PP}[PP]}{\overset{k_{-PP}}{\rightleftharpoons}} E{\bullet}T\text{-}A + PP$$

Figure 1.7 Kinetic mechanism for step 1 of the tyrosyl–tRNA synthetase reaction. Key: E, enzyme; A, ATP (as Mg^{2+} salt); T, tyrosine; PP, pyrophosphate (as Mg^{2+} salt); E•A, enzyme–ATP complex; E•T, enzyme–tyrosine complex; E•T•A, enzyme–tyrosine–ATP complex; E•T–A•PP, enzyme–tyrosyl adenylate–pyrophosphate complex; E•T–A, enzyme tyrosyl adenylate complex.

The three-dimensional structures of the enzyme complexed with tyrosyl-adenylate (reaction intermediate) as well as tyrosine (substrate) have been solved.[76,77] A noteworthy feature of the complexes that Fersht and colleagues have taken advantage of is the number of active site hydrogen bonds provided by residue side-chains (Figure 1.8). Because the protein backbone is not involved in these interactions, this system is ideal for protein engineering. Manipulating hydrogen bonds in many cases allows for specific protein-substrate interactions to be removed without disturbing others.[78] In

contrast, manipulating van der Waal and hydrophobic interactions by site-directed mutagenesis to examine their roles in catalysis is not as straightforward because these forces are not as specific and/or directional. In most cases, removing these types of interactions by site-directed mutagenesis usually perturbs several others. Indeed, it is difficult to imagine examining a specific interaction energy between
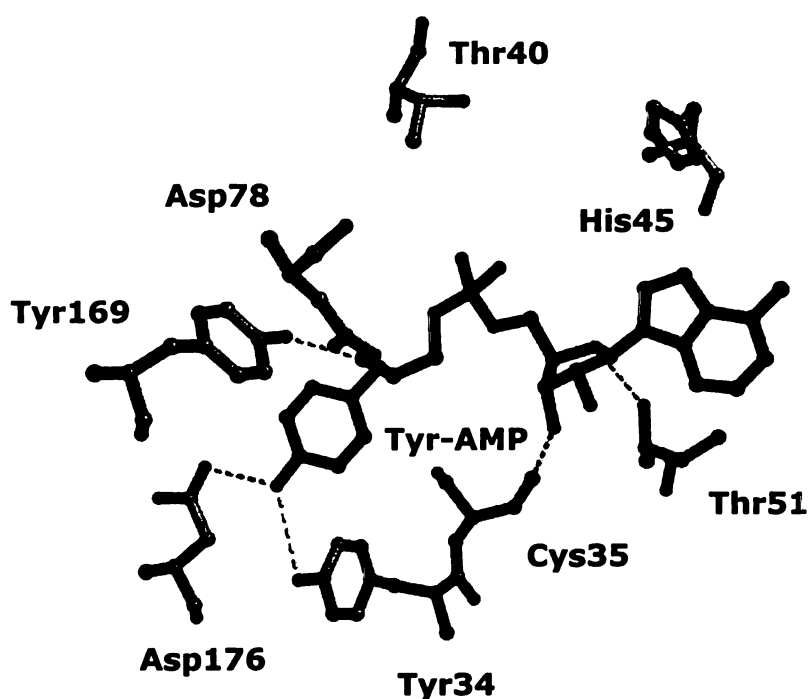
Figure 1.8 Enzyme active-site hydrogen bonding interactions with tyrosyl adenylate. Figure adapted from ref. [76].

a protein binding site and a hydrophobic methylene group on a ligand. Mutating a protein residue to remove this interaction is likely to remove interactions with the moieties that are covalently bonded to the ligand's methylene group, making the analysis of binding energy

involving this group difficult. The unfavorable situation of deleting multiple interactions also comes about when studying hydrogen bond networks. The removal of chemical groups involved in salt bridges is also not desirable because of the energetic desolvation penalties. In both situations it is likely that local structural rearrangements will accompany the mutation making the analysis difficult.[78,79]

Enzyme	k_3 (s^{-1})	k_{-3} (s^{-1})	$^aK_{tyrosine}$ (μM) $^aK'_{ATP}$ (μM)
Wild-type	38	17	12 4.7
Tyr34Phe	35	22	29 4.4
Tyr169Phe	35	14	1300 4.6

Table 1.1. Kinetic consequence of the removal of interactions involved in uniform binding. Data taken from ref. **[78]** . ^{a}These values are actual dissociation constants.
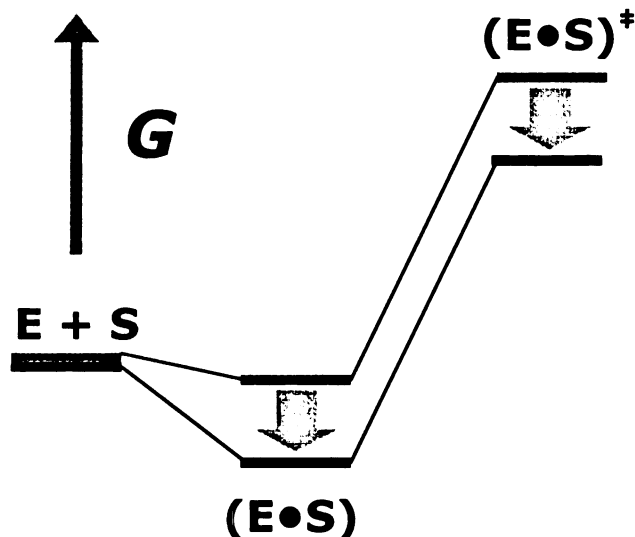
Figure 1.9 Free–energy diagram illustrating the effects of Uniform Binding. The additional binding interactions (grey → black) stabilize ground–state (E•S) and transition–state (E•S)‡ equally resulting in a zero change in the free–energy difference between (E•S) and (E•S)‡. In this reaction, k_{cat}/K_M value is increased, K_M value is decreased, but k_{cat} is unchanged.

Uniform Binding. The three-dimensional structure of the enzyme•tyrosyl-adenylate complex shows that the residues Tyr34 and Tyr169 form hydrogen bonds with the substrates' tyrosyl hydroxyl group and α-ammonium group, respectively (Figure 1.8). These same interactions are present in the enzyme•tyrosine complex.[76] The removal of the hydroxyl groups from these tyrosine residues (Tyr34Phe and Tyr169Phe) does not significantly affect the rate constant k_3 for activation, but just weakens the binding of tyrosine (Table 1.1) indicating that the hydroxyl moieties of Tyr34 and Tyr169 interact equally well with the tyrosine substrate when it is in its

unreacted forms ((E•T), (E•T•A), and (E•T-A)) and when it is in the

transition-state ((E•T•A)⁺) of the reaction.[80,81] The results

demonstrate that recognizing groups that are similar among the

chemical species is one solution to an enzyme being able to

simultaneously recognize substrates, transition–states, intermediates,

and products. These results imply that this use of binding energy will

be important recognizing, binding, and orienting substrates in the

enzyme active site, but at the same time, will probably not be

dominant in enzyme catalysis because it does not assist in increasing

catalytic turnover (Figure 1.9).[4,18]
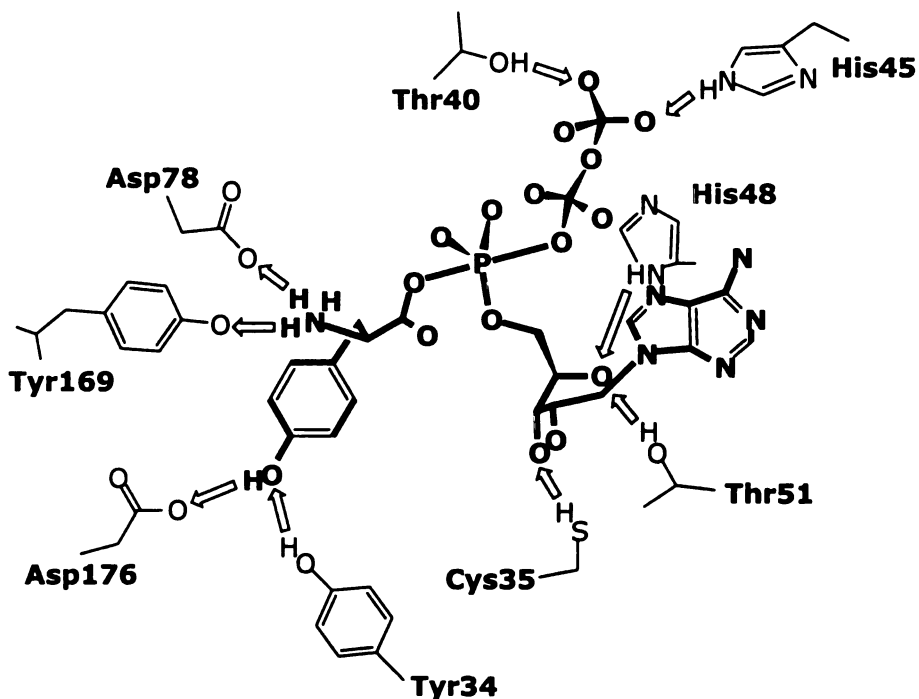
Figure 1.10 Model of hydrogen bonding interactions between the pentacoordinate transition-state of amino acid adenylation reaction and active site side-chains of tyrosyl-tRNA synthetase. This drawing is adapted from the model deduced by Fersht *et al* [82].

Preferential Transition-state Stabilization. To identify the amino acid residues involved in catalytic turnover, the pentacoordinate transition-state was modeled into the active site of the enzyme using the crystallographic structure of the tyrosyl-adenylate (E•Tyr-AMP) complex and a realistic length for the P-O axial bonds.[81,82] Two residues, Thr40 and His45, were identified and postulated to interact with the γ-phosphate group via their β-OH and ε-NH groups, respectively (Figure 1.10). These residues are distant from the seat of the reaction at the α-phosphate and they do not interact with the tyrosyl adenylate intermediate (Figures 1.8 and 1.10). Analysis of the His45Gly and Thr40Ala mutants reveals that the rate constant, k_3, is significantly reduced in both cases. In contrast, the mutations have little effect on the dissociation constants of tyrosine, ATP, and the tyrosyl adenylate (Tyr-AMP), indicating that the binding interactions involving these side-chains are used to preferentially stabilize the transition-state and probably do not interact strongly with ATP. This is a good example of an enzyme taking advantage of the geometric differences between the ground–state and the transition state to promote catalysis. In this case it is the large change in bond angles and lengths about the α-phosphate group as it goes from the four- (ground-state) to the five-coordinate (transition-state) species that the enzyme discriminates.[82] Without these bond angle and bond length

changes, the side-chains would probably interact equally with ATP in its unreacted and transition-state forms giving rise to uniform binding (see above).

enzyme	k_3 (s^{-1}) [reduction]	$K_{tyrosine}$ (μM)	[a]K_{ATP} (μM)
wild-type	38	12	4.7
His45Gly	0.16 [240-fold]	10	1.2
Thr40Ala	0.0055 [7000-fold]	8.0	3.8
His45Gly Thr40Ala	0.00012 [3 x 10^5-fold]	4.5	1.1

Table 1.2 Kinetic consequence of the removal of interactions involved in preferentially stabilizing the transition–state. Data taken from ref. [78, 82]. [a]These values are actual dissociation constants.
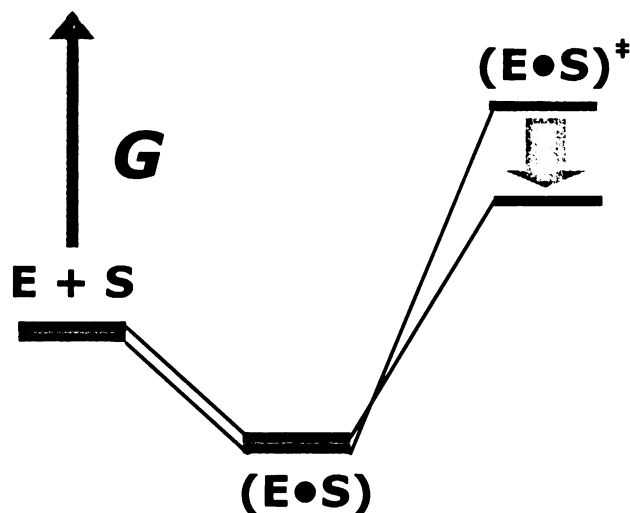
Figure 1.11 Free-energy diagram illustrating the effects of preferential transition-state stabilization. The additional interactions (grey → black) are used only to stabilize $(E \bullet S)^{\ddagger}$, resulting in a decrease in the free-energy difference between $(E \bullet S)$ and $(E \bullet S)^{\ddagger}$. For this reaction, k_{cat}/K_M is increased, K_M is unchanged, and k_{cat} is increased.

Enzyme-Intermediate Complementarity. An important theme that emerged from studies with the tyrosyl-tRNA synthetase is the role of enzyme-intermediate complementarity. This theme is a contradiction to the ideas of both Pauling and Haldane who said that enzyme active sites should be complementary to reaction transition-states.[20,40,41] Transition-state complementarity is always important for catalyzed reactions that have just a single important transition-state and where the substrates and products diffuse into solution. However, it is not surprising that this postulate may not apply to multi-step processes or reactions that generate products or

unstable intermediates that must remain bound to the enzyme for the succeeding step.[4]

The binding interactions involving two residues, Cys35 and His48, were found to be responsible for the enzyme-intermediate complementary in the tyrosyl-tRNA sythetase.[80,83,84] The Cys35 thiol interacts with the 3'-OH of the ribose of ATP, while His48 interacts with the endocyclic oxygen of the ribose (Figure 1.8). The removal of these interactions results in no significant changes in K'_A ($k'_{+[A]}/k'_{-A}$) or K'_T ($k'_{+[T]}/k'_{-T}$) (Figure 1.7), indicating that the binding interactions involving these residues contribute little to the stability of the E•Tyr•ATP ground state complex (Table 1.3). The interactions involving these residues do, however, contribute to decreasing the free-energy *difference* between the E•Tyr•ATP ground state and the [E-Tyr-ATP]‡ transition-state complexes, thus increasing k_3. More importantly, these interactions exert most of their effect by stabilizing the E•Tyr-AMP complex.

The result of this complementarity is two-fold. First, there is an increase in the equilibrium constant ($K_{formation}$) for the reaction on the enzyme (E•Tyr•ATP ↔ E•Tyr-AMP•PP) relative to that in solution (Tyr + ATP ↔ Tyr-AMP + PP), where on the enzyme, $K_{formation}(E)$ = [E•Tyr-AMP•PP]/[E•Tyr•ATP] and in solution, $K_{formation}(soln)$ = [Tyr-AMP][PP]/[Tyr][ATP].[4,83] In solution, the reaction in the forward

direction is very endothermic as indicated by the small formation

constant ($K_{formation}$(soln)) = 3.5 x 10^{-7}). By binding Tyr-AMP far more

tightly than Tyr and ATP, the enzyme increases the equilibrium

constant almost 10^7-fold ($K_{formation}$(E) = 2.3) (Table 1.3).
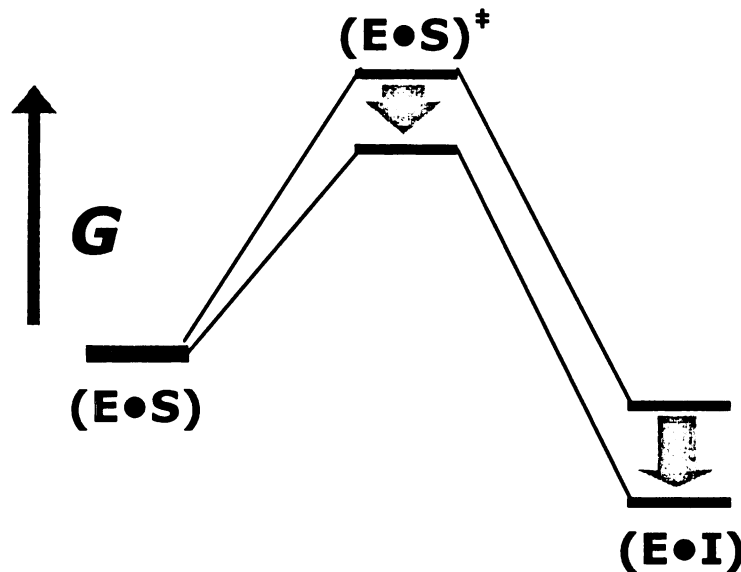
Figure 1.12 Free-energy diagram illustrating the effects of enzyme-intermediate complementarity. The additional interactions (grey → black) are used to stabilize (E•S)‡ and (E•I), resulting in a decrease in the free-energy difference between (E•S) and (E•S)‡ and a favorable free-energy increase for the process, (E•S) ↔ (E•I).

The second result of this complementarity is prevention of

unwanted side reactions.**[4,83]** The tyrosyl adenylate (Tyr-AMP) is a

mixed anhydride that is very susceptible to hydrolysis. In solution the

reaction rate for hydrolysis is 8 x 10^{-2} s^{-1}, whereas in the active site of

the enzyme the rate is reduced to 5 x 10^{-5} s^{-1}. This reduction is a

result of the fact that the enzyme is able to bind more tightly to Tyr-

AMP than to the transition-state of the unwanted hydrolysis reaction. There is a linear free energy relationship between the binding of the unstable E•Tyr-AMP complex and its rate of hydrolysis semi-qualitatively establishing a link between binding and intermediate protection.[83]

Enzyme	k_3 (s^{-1})	k_{-3} (s^{-1})	[a]K'_A (mM) [a]K_T (mM)	[a]K_{eq} (k_3/k_{-3})
wild-type	38	16.6	4.7 12	2.29
Cys35Gly	4.0	31.0	4.5 11	0.12
Cys35Ser	4.7	32.8	4.8 8	0.15
His48Gly	9.9	16.4	9.9 23	0.60

Table 1.3 Kinetic consequence of enzyme–intermediate complementarity. Data taken from ref. [78, 83]. [a]These values are actual dissociation constants.

Enzyme-intermediate complementarity has also been observed in the enzyme triosephosphate isomerase (TIM).[85,86] The results of the complementarity in this system are similar to those in the tyrosyl-tRNA synthetase system. This glycolytic enzyme catalyzes the interconversion of D-glyceraldehyde 3-phosphate (GAP) and dihydroxyacetone phosphate (DHAP) which proceeds through an enediol phosphate intermediate. TIM catalyzes the isomerization of

GAP to DHAP by almost 10 orders of magnitude over the rate

enhancement provided by a simple base such as acetate ion.[73,87]

Removal of intermediate•enzyme binding interactions results in a less

favorable equilibrium formation constant of the enediol (Figure 1.13).

In addition, the intermediate falls off the enzyme much faster than it

partitions to product (in both directions).[85] Tight binding of the

intermediate also disfavors the unwanted elimination reaction that

generates inorganic phosphate and methyl glyoxal by 4 orders of

magnitude.
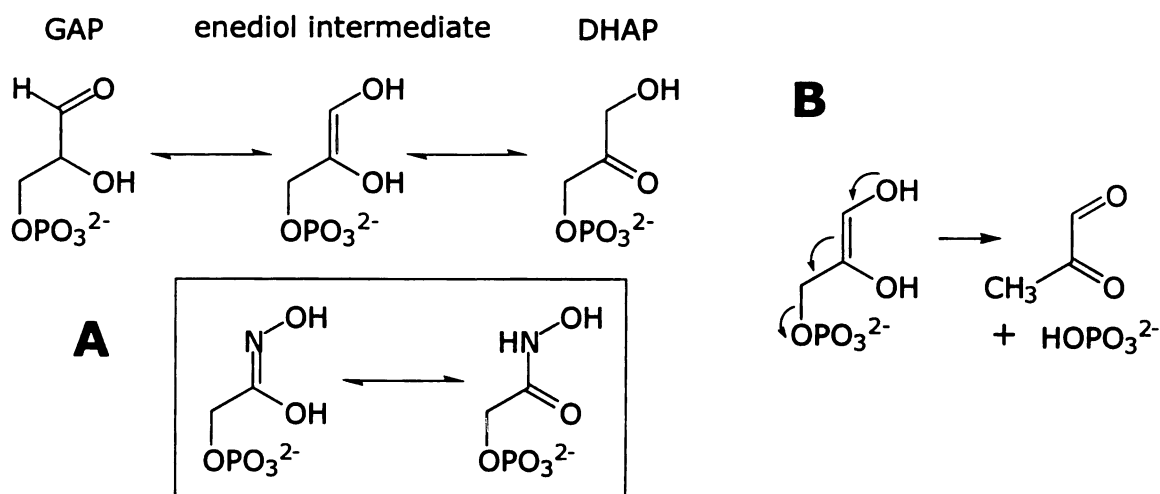
Figure 1.13 A. Reaction catalyzed by triosephosphate isomerase. Key: GAP, D-glyceraldehyde 3-phosphate; DHAP, dihydroxyacetone phosphate. (boxed) The intermediate analog, 2–phosphoglycolohydroxamate (2 tautomers). **B.** Unwanted elimination side reaction of the enediol intermediate that generates methyl glyoxal and phosphate.

```
        ┌──────────┐                            ┌──────────┐
     ┌──┘  G        │                        ┌──┘  GpA₅    │
     │        OH    │                        │             │
     └─────┐ )      │          ──────▶       └─────┐       │
           │ │      │                              │       │
   C C C U C Up A₅  │                      C C C U C U_OH  │
 ┌A G G G A G G -5' │                    ┌A G G G A G G -5'│
 └──────────────────┘                    └─────────────────┘
```
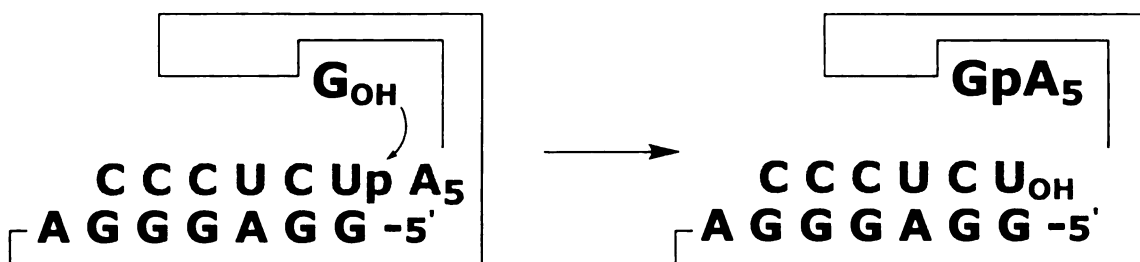
Figure 1.14 Reaction catalyzed by the Tetrahymena ribozyme. The -OH represents the 3' hydroxyl group. The -p represents the phosphate diester group that is bonded to the 5' hydroxyl group of the nucleotide on the right and bonded to the 3' hydroxyl on the left.

Ground–State Destabilization. An illustrative example of the use of remote binding energy to facilitate ground-state destabilization within a catalytic active site emanates from studies of the *Tetrahymena* ribozyme in Daniel Herschlag's laboratory.[88] This ribozyme is derived from the intervening sequence of the *Tetrahymena* pre-ribosomal RNA that catalyzes a site-specific endonuclease reaction analogous to the first step in self-splicing of pre-rRNA (Figure 1.14).[89,90] The catalytic RNA molecule catalyzes the phosphoryl transfer reaction with a rate enhancement of 10^{11}-fold over the uncatalyzed reaction—a rate enhancement that is comparable to those exhibited by many enzymes. In this catalyzed reaction, the oligonucleotide substrate binds to the ribozyme to form the $(E \bullet S)_{open}$ complex which is mostly stabilized by standard Watson-Crick duplex hydrogen bonding interactions.[91] The formation of tertiary non-Watson-Crick hydrogen bonding interactions results in the formation of

the (E•S)$_{closed}$ complex (Figure 1.15).[91,92] It is in this complex

that the phosphoryl transfer reaction can occur.

$$E + S \xrightarrow{K_S^* = K_S \times K_{tertiary}} (E•S)_{closed}$$
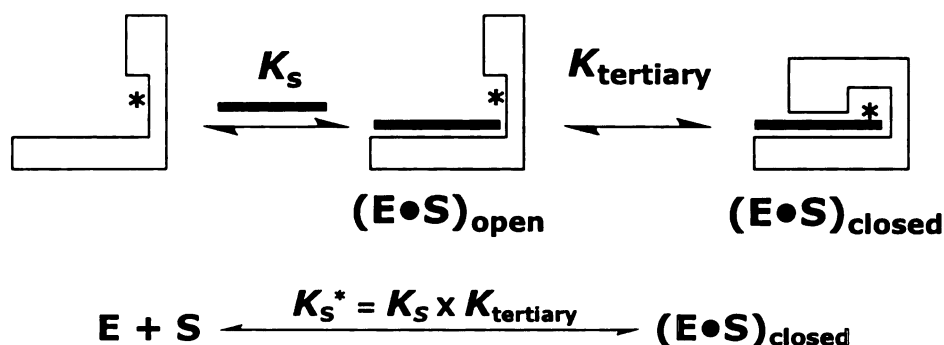
Figure 1.15 Oligonucleotide substrate binding. Thick line represents oligonucleotide substrate. The oligonucleotide substrate of the ribozyme binds in two steps. The substrate base pairs to a region of the ribozyme referred to as the internal guide sequence forming open complex (E•S)$_{open}$. The formation of this complex creates a surface favoring the formation of additional tertiary interactions resulting in the closed complex (E•S)$_{closed}$.
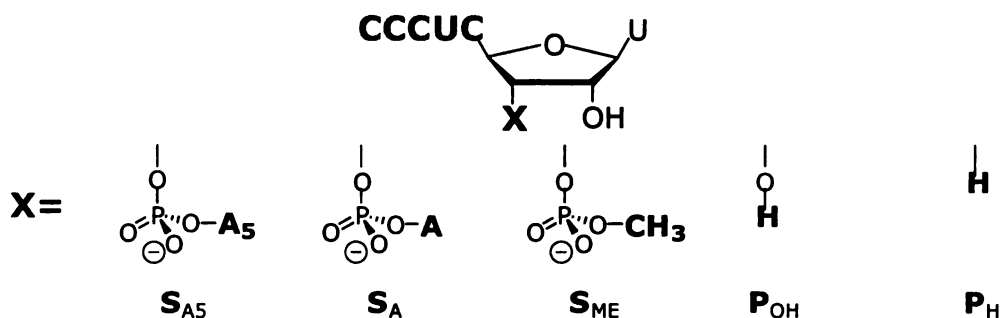
Figure 1.16 Substrate analogs used to study active site interactions in the *Tetrahymena* ribozyme.

Substrate	$K_s^* \times 10^6$ M^{-1}	$K_s \times 10^6$ M^{-1}	$K_{tertiary}$	$\Delta\Delta G_{tert}$ (kcal/mol)
S_{A5}	125	4	30	+ 2.8
P_{OH}	420	0.7	600	+ 0.0
S_A	50	3.1	16	+ 2.2
S_{ME}	13	1.1	12	+ 2.3
P_H	13	0.9	14	+ 2.2

Table 1.4 Thermodynamic consequence of ground–state destabilization. Data taken from ref. [88].
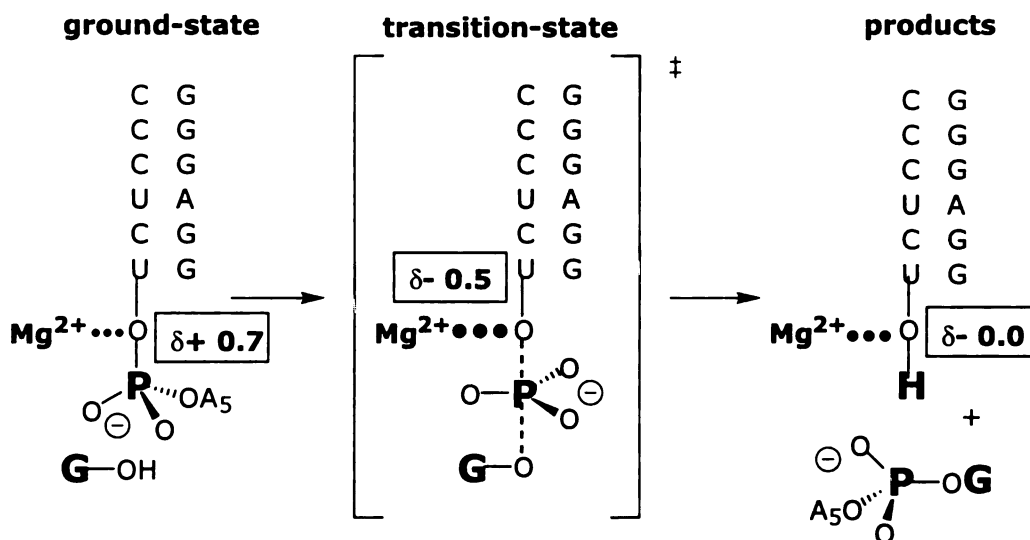
Figure 1.17 Schematic of Mg^{2+} - 3'oxygen interactions during the ribozyme catalyzed phosphoryl transfer reaction. Substrate destabilization is indicated by small dots. In the transition state, the bridging oxygen develops a partial negative charge and interacts strongly with the Mg^{2+} ion, as indicated by the large dots. The boxed numbers indicate the effective charge on the oxygen (as determined from LFER-see text) relative to P_{OH}.

The catalyst uses free energy from remote binding interactions

to juxtapose two electropositive atoms: an electron deficient

phosphoryl oxygen (calculated from LFERs–see below) of the

ribonucleotide substrate S_{A5} (Figure 1.16) and an electropositive Mg^{2+} ion (Figure 1.17).[88] This unfavorable interaction between the two atoms is relieved in the transition-state. The presence of this destabilization was uncovered by the observation that the oligonucleotide substrate, S_{A5} binds $\approx$ 3-fold less tightly to the ribozyme than does the oligonucleotide product, P_{OH} (Figure 1.16, Table 1.4).[89] This result is paradoxical since it is expected that the
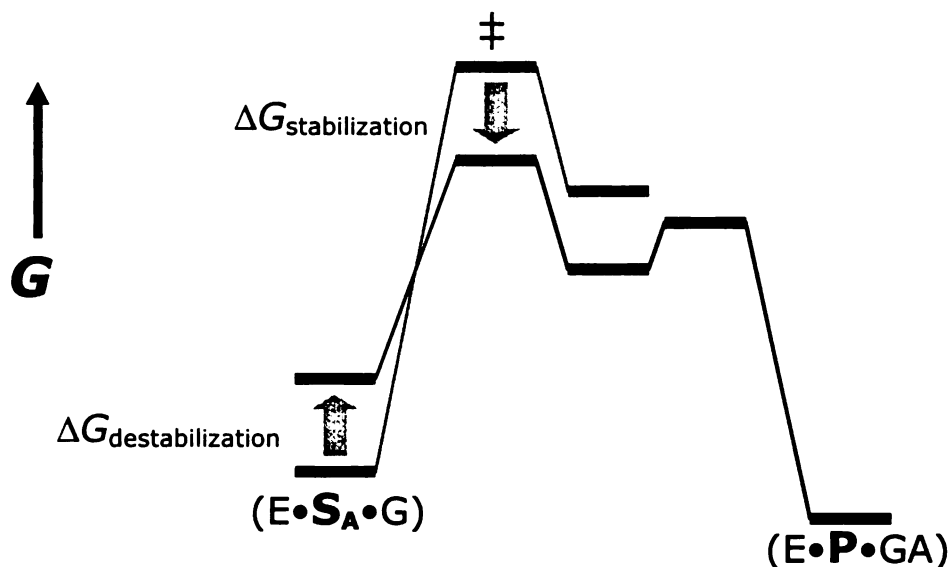
Figure 1.18 Free energy reaction profile demonstrating the effects of the active site Mg^{2+} - 3' oxygen interactions on the ribozyme reaction. The gray profile represents a hypothetical free energy reaction profile in the absence of the active site Mg^{2+}. In the absence of Mg^{2+} it is assumed that the tertiary interactions are the same.

substrate can potentially use the polyA tail to form additional binding interactions with the ribozyme to increase its affinity. The decrease in affinity is shown not to be due to unfavorable interactions with the

polyA tail as its removal (examined with S_A and S_{ME} (Figure 1.16))

does not restore the binding affinity.[88] The S_A and S_{ME} substrates

form tighter open complexes ($(E \cdot S)_{open}$) with the ribozyme than does

P_{OH} indicating that most of the destabilization is associated with the

formation of the tertiary interactions (Table 1.4). The difference in

binding between the oligonucleotides, P_{OH} and P_H (Figure 1.16),

indicates that the interactions involving the 3' oxygen play an

important role in stabilizing the closed complex ($(E \cdot S)_{closed}$). Yet, it is

only when the oxygen is bonded to phosphorus that the interactions

involving this atom become unfavorable.

There is a significant difference in the electronic properties of a

phosphorylated oxygen atom compared to one that is protonated. The

$\beta_{equilibrium}$ (linear free energy relationship (LFER)) value for the

equilibrium, R'O-P + XRO-H $\leftrightarrow$ R'OH + XRO-P, is +0.7 indicating that

the effective charge for the bridging oxygen of a phosphate diester is

+ 0.7 relative to the protonated oxygen.[93] Thus, in solution, a

positively charged Mg^{2+} ion would be predicted to interact more

favorably with an oxygen from water (or the chemically similar 3' OH

of P_{OH}). It is proposed that the ribozyme uses remote binding

interactions to position the electron-deficient phosphorylated oxygen

of S_{A5} (and S_A) adjacent to the Mg^{2+} (Figure 1.17).

27

The destabilizing ground-state interaction is expected to be stabilizing in the transition-state because the oxygen atom develops more negative character in the transition-state of the phosphoryl transfer reaction (Figure 1.17). This substantially more negative character is indicated by the $\beta_{leaving\ group}$ value of -1.2 for the hydrolysis of a series of phosphate diesters.[94] The ribozyme $Mg^{2+} \bullet$oxygen interactions plays a catalytic role by destabilizing the ground state ($E \bullet S_A$) and by stabilizing the transition-state (Figure 1.18). The remote binding interactions provide an anchor so that these interactions may take place and play their roles in catalysis.

Figure 1.19 Reaction catalyzed by 3-oxoacid Coenzyme A transferase.
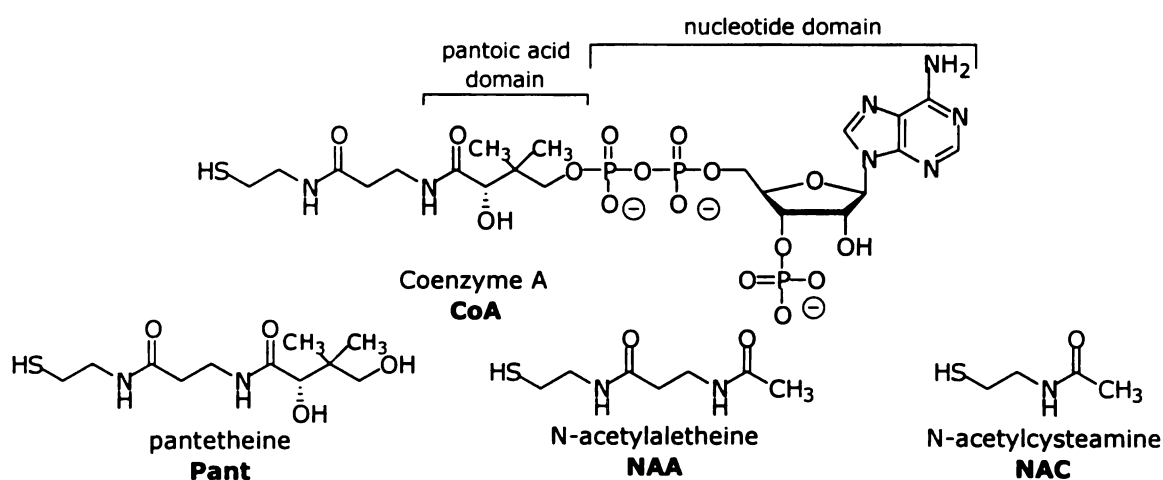
Figure 1.20 Substrate analogs used to study binding energy in the 3-oxoacid Coenzyme A (CoA) transferase.

Destabilizing interactions have also been shown to be important for the catalytic function of 3-oxoacid Coenzyme A (CoA) transferase. This enzyme catalyzes the reversible conversion of succinyl-CoA and acetoacetate into acetoacetyl-CoA and succinate (Figure 1.19).[95,96] It has been estimated that the enzyme uses binding energy from the remote binding interactions with Coenzyme A to bring about an increase in k_{cat}/K_M of about 10^{10}-fold.[97-99] For example, the truncation of CoA to a smaller thiol, methyl mercapto-propionate, decreases k_{cat}/K_M for the reaction with thiol ester substrates by 10^{12} fold.[97] To examine how the enzyme achieves differential binding to effect its catalysis, the transferase reaction was studied with a series of CoA analogs (Figure 1.20).[100]

Jencks *et al.* found that the use of the binding interactions involving the nucleotide and pantoic acid domains play distinct roles in the catalytic process (Figure 1.21).[100] The removal of the nucleotide domain from CoA (to yield pantetheine, Pant (Figure 1.20)), and of the pantoic acid domain from pantetheine (to yield N-acetylaletheine, NAA) results in Michaelis complexes that are less stable by 2.2 and 1.8 kcal/mol, respectively, indicating that the domains interact relatively weakly in the complexes. However, the nucleotide domain plays a much larger role in determining the stability of the E-CoA thioester complex. The removal of the domain (E-CoA →

E-Pant) results in an E-SR complex that is less stable by ~ 7.2

kcal/mol. Interestingly, the removal of the pantoic acid domain (E-

Pant → E-NAA, E-NAC, (Figure 1.20)) results in an E-SR complex that

is more stable by 4.8 kcal/mol, indicating that the pantoic acid domain

actually destabilizes the complex. This result demonstrates that, like

the ribozyme, CoA transferase uses destabilizing interactions in the E-

CoA intermediate that are relieved in the transition-state as a method

to achieve differential binding of the pantoic acid domain. Both

domains are significantly important for stabilizing the transition-states

that flank the thioester complex (Figure 1.21). The nucleotide domain

contributes 9 kcal/mol to the stabilization of the transesterification

transition-states, while the pantoic acid domain contributes 5 kcal/mol.
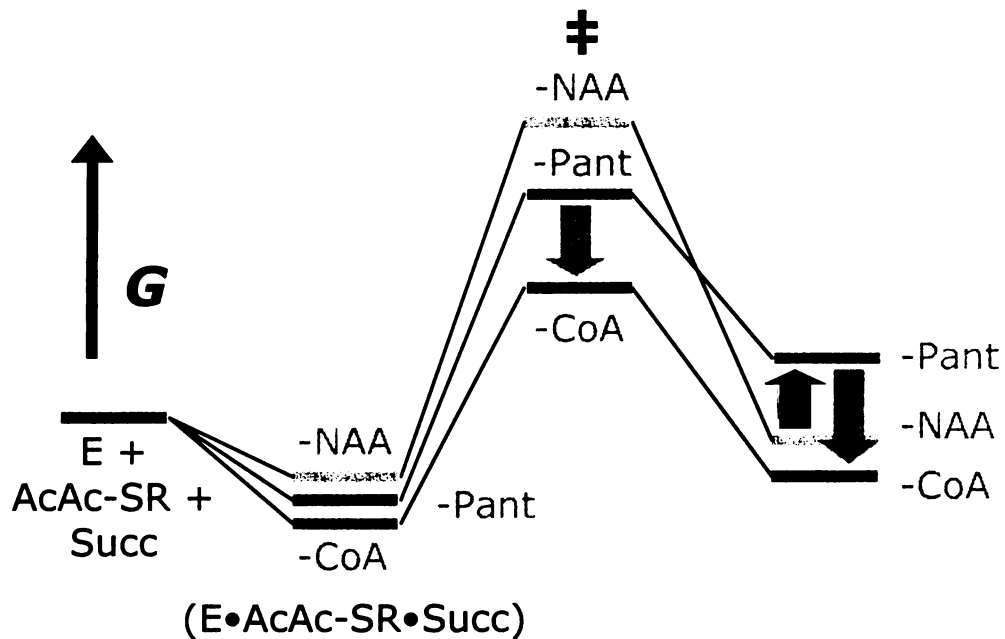
Figure 1.21 Free-energy diagram demonstrating the effects of the nucleotide and pantoic acid domains. The diagram corresponds to the first half reaction, E + AcAc-SR → E-SR + AcAc. Key: AcAc, acetoacetate; E•AcAc-SR•Scc, enzyme-acetoacetylthioester-succinate complex. See Figure 1.19 legend for other abbreviations. The grey arrow shows the stabilizing effect of the nucleotide domain on the transition-state. The black arrow shows the destabilizing effect of the pantoic acid domain on the E-SR complex.

Thesis Overview and Introduction to 17E8

From the above examples, it is obvious that the use of binding energy is important in many aspects of enzyme function. Our desire to understand, dissect, and recapitulate enzyme catalysis has led to the generation of catalytic antibodies.[44,46] The discovery that generating immunoglobulins to haptens that resemble the high energy species of reactions is a nice proof of the principle that tight binding to
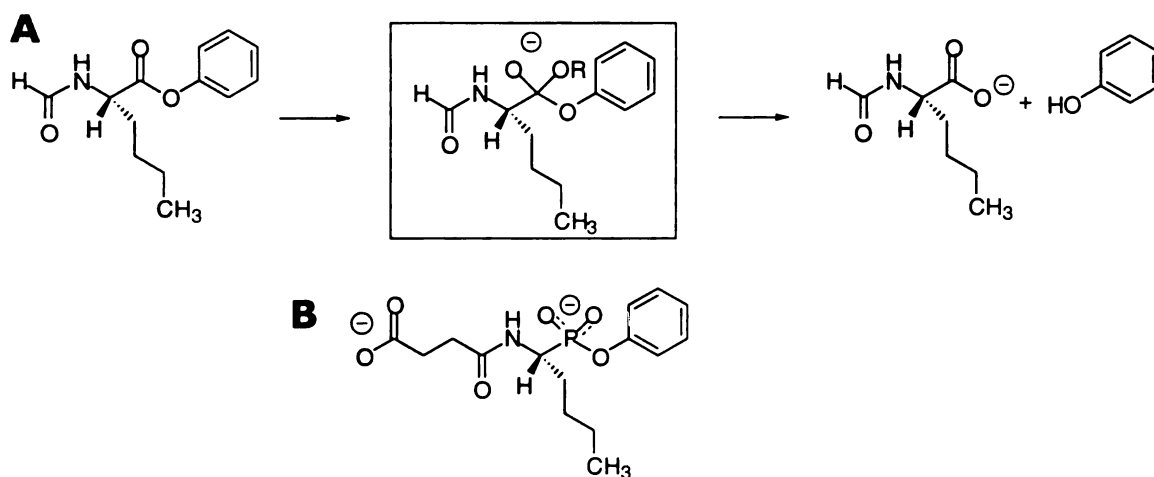
Figure 1.22 A. Reaction catalyzed by 17E8. (boxed) tetrahedral intermediate. B. Phosphonate transition-state analog used to generate 17E8.

such species is a strategy used by enzymes to promote catalysis.[47] Being able to make these catalysts also indicates that this may be a good strategy to generate enzyme-like catalysts.

Haptens used to generate catalytic antibodies are expected to elicit active site-substrate binding interactions that are reminiscent of those found in enzymes.[47,101] How a particular catalytic antibody, 17E8, uses binding interactions programmed by hapten design is the major topic of this thesis. The questions addressed in this thesis include: Which interactions are important for catalysis? (Chapter 2) Are the interactions used just for overall transition-state stabilization? (Chapters 3 and 4) How does the use of the active site interactions compare to the manner in which an evolved enzyme uses analogous interactions? (Chapters 2 and 3) How does the thermodynamic basis of hapten binding translate into catalysis? (Chapter 5)

17E8 is an esterase that catalyzes the enantioselective hydrolysis of N-acyl amino acid phenyl esters that possess the natural S configuration (L) at the α-carbon (Figure 1.20A).[69,102]

Figure 1.23 17E8 Fab fragment with phosphonate bound (see Figure 1.22)

17E8 was raised to a phenyl phosphonate transition-state analog

(Figure 1.20B) and is most active against N-formyl norleucine phenyl esters with k_{cat}, K_M, and k_{cat}/K_M values of 4 s^{-1}, 240 µM, and 1.6 x 10^4 $M^{-1} \cdot s^{-1}$, respectively. The maximum rate acceleration (k_{cat}/k_{uncat}) for this reaction is 2 x 10^4 and this occurs at pH 7.2.[102] Both k_{cat} and k_{cat}/K_M steady state parameters have bell-shaped pH dependence consistent with a mechanistic scheme featuring two ionizable active site residues that mediate catalysis. The maximum values of both parameters occur at approximately pH 9.5. The pK_a values that govern the k_{cat}-pH dependence for the hydrolysis of N-formyl norleucine are 8.9 ± 0.2 and 10.1 ± 0.2; the values for the k_{cat}/K_M-pH dependence are similar (8.4 ± 0.2 and 10.3 ± 0.2). These pK_a values are similar to those associated with the 17E8 mediated hydrolysis of other phenyl ester substrates. Initial mechanistic characterizations including hydroxylamine partitioning studies, suggested that the hydrolytic mechanism included the rate-determining formation of an antibody-acyl intermediate. This was supported by structural studies that showed that 17E8 has an active site that is similar to that of the natural triad hydrolases. Biochemical studies of other catalytic antibodies generated in the same immunization from which 17E8 was obtained offered additional support for this mechanism.[103] However, mutagenesis experiments have suggested that the antibody-acyl intermediate mechanism is probably not operative.[104]

The three dimensional structure of 17E8 complexed with the phenyl phosphonate (Figures 1.23-1.25) was solved to 2.5 Å.[69] The phosphonate binds deeply in a cleft between the light and heavy chain CDR3 loops covering 86% of its accessible surface area. There is good shape complementarity between the surfaces of the hapten and 17E8, with hapten recognition being mediated by positively charged, aromatic, and hydrophobic side-chains. The active site also features well-defined binding pockets for the phenyl

Figure 1.24 Conic representation of the 17E8•hapten complex.
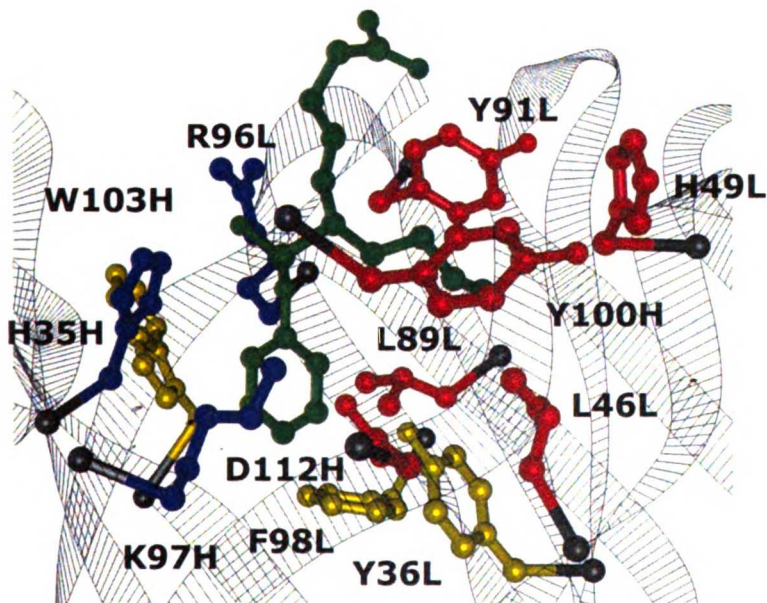
Figure 1.25 Active site interactions in the 17E8•hapten complex. Red residues interact primarily with n-butyl side-chain. Blue residues interact with phosphonate moiety. Yellow residues interact with phenyl group.

group and the n-butyl side-chain of the phosphonate.

The n-butyl side-chain pocket is predominantly formed by hydrophobic side-chains of light chain residues. Mostly aromatic residues, including, Phe98 and Tyr36 from the light chain, and Trp47 and Trp103 from the heavy chain, form the pocket around the phenyl group.

The anionic phosphonate moiety is involved in interactions with side-chains from heavy chain residues including salt-bridges to Lys97H and Arg96L. Arg96L participates in charged hydrogen bonds with the pro-R phosphonyl oxygen atom, and the bridging oxygen atom between the phosphorus atom and the phenyl group of the hapten. A charged hydrogen bond is formed between Lys97H and the pro-S phosphonyl oxygen. These two positively charged residues are believed to form the oxyanion hole that is responsible for stabilizing the anionic transition-state formed by hydroxide attack on the phenyl ester. The interaction with Lys97H is believed to be associated with the basic limb ($pK_a \sim 10$) of the pH profiles for k_{cat} and k_{cat}/K_M. The deprotonation of this residue would remove a stabilizing interaction with the developing oxyanion in the hydrolytic transition-state.

References

(1)   Atkins, P. *Physical Chemistry*; 5th ed.; W.H. Freeman and Company: New York, 1994.

(2)   Leffler, J. E.; Grunwald, E. *Rates and Equilibria of Organic Reactions as Treated by Statistical, Thermodynamic, and Extrathermodynamic Methods*; Dover Publications, Inc.: New York, 1963.

(3)   Jencks, W. P. *Catalysis in Chemistry and Enzymology*; Dover Publications: Mineola, 1969.

(4)   Fersht, A. *Structure and Mechanism in Protein Science: A Guide to Enzyme Catalysis and Protein Folding*; W.H. Freeman and Company: New York, 1999.

(5)   Jencks, W. P. Imidazole and proton transfer in catalysis. *Biochemical Society Symposia* **1970,** *31*, 59-80.

(6)   Jencks, W. P. General acid-base catalysis of complex reactions in water. *Chemical Reviews* **1972,** *72*, 705-755.

(7)   Stefanidis, D.; Jencks, W. P. General base catalysis of ester hydrolysis. *Journal of the American Chemical Society* **1993,** *115*, 6045-6050.

(8)   Kraut, J. How do enzymes work? *Science* **1988,** *242*, 533-40.

(9)   Knowles, J. R. Enzyme catalysis: not different, just better. *Nature* **1991,** *350*, 121-124.

(10)   Walsh, C. *Enzymatic Reaction Mechanisms*; Freeman: San Fransisco, 1979.

(11)   Bruice, T. C. Views on Approximation, orbital steering, and enzymatic and model Reactions. *Cold Spring Harbor Symposia On Quantitative Biology* **1971,** *36*, 21-28.

(12)   Kirby, A. J. Enzyme mechanisms, models, and mimics. *Angewandte Chemie-International Edition in English* **1996,** *35*, 707-724.

(13) Kirby, A. J. Enzyme mimics. *Angew. Chem. Int. Ed. Engl.* **1994,** *33*, 551-553.

(14) Bruice, T. C. Some pertinent aspects of mechanism as determined with small molecules. *Annual Review of Biochemistry* **1976,** *45*, 331-373.

(15) Jencks, W. P.; Gilbert, H. F. General acid-base catalysis of carbonyl and acyl group reactions. *Pure and Applied Chemistry* **1977,** *49*, 1021-1027.

(16) Bearne, S. L.; Wolfenden, R. Mandelate racemase in pieces: Effective concentrations of enzyme functional groups in the transition-state. *Biochemistry* **1997,** *36*, 1646-1656.

(17) Jencks, W. P. Binding-Energy, Specificity, and enzymic catalysis - circe effect. *Advances in Enzymology and Related Areas of Molecular Biology* **1975,** *43*, 219-410.

(18) Jencks, W. P. Economics of enzyme catalysis. *Cold Spring Harbor Symp. Quant. Biol.* **1987,** *LII*, 65-73.

(19) Page, M. I. Entropy, binding energy, and enzymic catalysis. *Angew. Chem. Int. Ed. Engl.* **1977,** *16*, 449-459.

(20) Pauling, L. Molecular architecture and biological reactions. *Chem. Eng. News.* **1946,** *24*, 1375-1377.

(21) Wolfenden, R. Transition-state analog inhibitors and enzyme catalysis. *Annu. Rev. Biophys. Bioeng.* **1976,** *5*, 271-306.

(22) Wolfenden, R. Enzyme catalysis: conflicting requirements of substrate access and transition-state affinity. *Molecular and Cellular Biochemistry* **1974,** *3*, 207-211.

(23) Kaji, A.; Colowick, S. P. Adenosine triphosphate activity of yeast hexokinase and its relation to the mechanism of the hexokinase reaction. *J. Biol. Chem.* **1965,** *240*, 4454-4462.

(24) Spencer, T.; Sturtevant, J. M. The mechanism of chymotrypsin-catalyzed reactions. 3. *J. Amer. Chem. Soc.* **1959,** *81*, 1874-1882.

(25) McConn, J.; Ku, E.; Himoe, A.; Brandt, K. G.; Hess, G. P. Investigations of chymotrypsin-catalyzed hydrolysis of specific substrates. 5. Determination of pre-steady state kinetic parameters for specific substrate esters by stopped flow techniques. *J. Biol. Chem.* **1971,** *246,* 2918-2925.

(26) Neurath, H.; Hartley, B. S. The hydrolysis of peptide and ester bonds. *J. Cell. Comp. Phys.* **1959,** *54,* 179-202.

(27) Gandour, R. D.; Schowen, R. L. *Transition-states of biochemical processes;* Plenum Press: New York, 1978.

(28) Wolfenden, R. Transition-state analogues for enzyme catalysis. *Nature* **1969,** *223,* 704-705.

(29) Lienhard, G. E.; Jencks, W. P. Thiol addition to the carbonyl group. Equilibria and kinetics. *Journal of the American Chemical Society* **1966,** *88,* 3982-94.

(30) Lienhard, G. E.; Secemski, I. I.; Koehler, K. A.; Linquist, R. N. Enzymatic catalysis and the transition-state theory of reaction rates: Transition-state analogs. *Cold Spring Harbor Symp. Quant. Biol.* **1971,** *36,* 45-51.

(31) Kyte, J. *Mechanism in Protein Chemistry;* Garland Publishing: New York, 1995.

(32) Koshland, D. E.; Neet, K. E. The catalytic and regulatory properties of enzymes. *Ann. Rev. Biochem.* **1967,** *37,* 359-410.

(33) Koshland, D. E. Application of a theory of enzyme specifity to protein synthesis. *Proc. Natl. Acad. Sci., USA* **1958,** *44,* 98-104.

(34) Jencks, W. P.; Page, M. I. Orbital steering, entropy, and rate accelerations. *Biochem. and Biophys. Res. Com.* **1974,** *57,* 887-892.

(35) Page, M.; Jencks, W. Entropic contributions to rate accelerations in enzymic and intramolecular reactions and the chelate effect. *Proc. Natl. Acad. Sci.., USA* **1971,** *68,* 1678-1683.

(36) Storm, D. R.; D, E., Koshland Effect of small changes in orientation on reaction rate. *J. Amer. Chem. Soc.* **1972,** *94,* 5815-5824.

(37) Bruice, T. C.; Brown, A.; Harris, D. O. Concept of orbital steering in catalytic reactions. *Proceedings of the National Academy of Sciences of the United States of America* **1971,** *68,* 658-667.

(38) Niemann, C. α-chymotrypsin and the nature of enzyme catalysis. *Science* **1964,** *143,* 1287-1296.

(39) Hamilton, C. L.; Niemann, C.; Hammond, G. S. A quantitative analysis of the binding of n-acyl derivatives of α -amino amides by chymotrypsin. *Proc. Natl. Acad. Sci.* **1966,** *55,* 664-669.

(40) Haldane, B.S. *Enzymes*; Longmans, Green and Co.: London, 1930.

(41) Pauling, L. Nature of forces between large molecules of interest. *Nature* **1948,** *161,* 707-709.

(42) Fersht, A. R. Catalysis, binding, and enzyme-substrate complementarity. *Proc. R. Soc. Lond.B.* **1974,** *187,* 397-407.

(43) Lienhard, G. E. Enzymatic catalysis and transition-state theory. *Science* **1973,** *180,* 149-154.

(44) Pollack, S. J.; Jacobs, J. W.; Schultz, P. G. Selective chemical catalysis by an antibody. *Science* **1986,** *234,* 1570-73.

(45) Jacobs, J. W.; Schultz, P. G.; Sugasawara, R.; Powell, M. Catalytic antibodies. *J. Am. Chem. Soc.* **1987,** *109,* 2174-76.

(46) Tramontano, A.; Janda, K. D.; Lerner, R. A. Catalytic antibodies. *Science* **1986,** *234,* 1566-70.

(47) Lerner, R. A.; Benkovic, S. J.; Schultz, P. G. At the crossroads of chemistry and immunology: catalytic antibodies. *Science* **1991,** *252,* 659-667.

(48) Bender, M. L. Mechanism of catalysis of nucleophilic reactions of carboxylic acid derivatives. *Chem. Rev.* **1960,** *60,* 53-113.

(49) Janda, K. D.; Weinhouse, M., I.; Danon, T.; Pacelli, K. A.; Schloeder, D. M. Antibody bait and switch catalysis: A survey of antigens capable of inducing abzymes with acyl-transer properties. *J. Am. Chem. Soc.* **1991,** *113,* 5427-5434.

(50) Janda, K. D.; Weinhouse, M.; Schloeder, D. M.; Lerner, R. A.; Benkovic, S. J. Bait and switch strategy for obtaining catalytic antibodies with acyl-transfer capabilities. *J. Am. Chem. Soc.* **1990,** *112,* 1274-1275.

(51) Shokat, K. M.; Ko, M. K.; Scanlan, T. S.; Kochersperger, L.; Yonkovich, S.; Thaisrivongs, S.; Schultz, P. G. Catalytic antibodies: a new class of transition-state analogues used to elicit hydrolytic antibodies. *Angew. Chem. Int. Ed. Engl.* **1990,** *29,* 1296-1313.

(52) Gallacher, G.; Jackson, C. S.; Searcey, M.; Goel, R.; Mellor, G. W.; Smith, C. Z.; Brocklehurst, K. Catalytic antibody activity elicited by active immunisation - Evidence for natural variation involving preferential stabilization of the transition-state. *Eur. J. Biochem.* **1993,** *214,* 197-207.

(53) Pollack, S. J.; Schultz, P. G. Antibody catalysis by transition-state stabilization. *Cold Spring Harbor Symp. Quant. Biol.* **1987,** *52,* 97-104.

(54) Jacobs, J. *Catalytic antibodies*; University of California Berkeley, 1989.

(55) Schultz, P. G. Catalytic antibodies. *Acc. Chem. Res.* **1989,** *22,* 287-294.

(56) Bartlett, P. A.; Marlowe, C. K. Phosphonamidates as transition-state analogue inhibitors of thermolysin. *Biochemistry* **1983,** *22,* 4618-4624.

(57) Bartlett, P. A.; Giangiordano, M. A. Transition-state analogy of phosphonic acid inhibitors of pepsin. *J. Org. Chem* **1996,** *61,* 3433-3438.

(58) Morgan, B. P.; Scholtz, J. M.; Ballinger, M. D.; Zipkin, I. D.; Bartlett, P. A. Differential binding energy: a detailed evaluation of the influence of hydrogen-bonding and hydrophobic groups on the inhibition of thermolysin by phosphorous-containing inhibitors. *J. Am. Chem. Soc.* **1991,** *113,* 297-307.

(59) Phillips, M. A.; Kaplan, A. P.; Rutter, W. J.; Bartlett, P. A. Transition-state characterization: a new approach combining

inhibitor analogs and variation in enzyme structure. *Biochemistry* **1992,** *31*, 959-963.

(60) Radkiewicz, J. L.; McAllister, M. A.; Goldstein, E.; Houk, K. N. A theoretical investigation of phosphonamidates and sulfonamides as protease transition-state isostere. *J. Org. Chem.* **1998,** *63*, 1419-1428.

(61) Tantillo, D. J.; Houk, K. N. Fidelity in hapten design: How analogous are phosphonate haptens to the transition-states for alkaline hydrolyses of aryl esters? *J. Org. Chem.* **1999,** *64*, 3066-3076.

(62) Kakinuma, H.; Shimazaki, K.; Takahashi, N.; Takahashi, K.; Niihata, S.; Aoki, Y.; Hamada, K.; Matsushita, H.; Nishi, Y. Comparison of phosphonate transition-state analogs for inducing catalytic antibodies and evaluation of key structural factors by an ab initio study. *Tetrahedron* **1999,** *55*, 2559-2572.

(63) MacBeath, G.; Hilvert, D. Hydrolytic antibodies: variation on a theme. *Chem. & Biol.* **1996,** *3*, 433-445.

(64) Wade, H.; Scanlan, T. S. The structural and functional basis of antibody catalysis. *Ann. Rev. Biophys. Biomol. Struct.* **1997,** *26*, 461-493.

(65) Wedemayer, G.; Wang, L. H.; Patten, P. A.; Schultz, P. G.; Stevens, R. C. Crystal structures of the free and liganded forms of an esterolytic catalytic antibody. *J. Mol. Biol.* **1997,** *268*, 390-400.

(66) Gigant, B.; Charbonnier, J.; Eshhar, Z.; Green, B. S.; Knossow, M. X-ray structures of a hydrolytic antibody and of complexes elucidate catalytic pathway from substrate binding and transition-state stabilization through water attack and product release. *Proc. Natl. Acad. Sci.* **1997,** *94*, 7857-7861.

(67) Charbonnier, J.-B.; Carpenter, E.; Gigant, B.; Golinelli-Pimpaneau, B.; Eshhar, Z.; Green, B. S.; Knossow, M. Crystal structure of the complex of a catalytic antibody Fab fragment with a transition-state analog: Structural similarities in esterase-like catalytic antibodies. *Proc. Natl. Acad. Sci., USA* **1995,** *92*, 11721-11725.

(68) Charbonnier, J.-B.; Golinelli-Pimpanaeu, B.; Gigant, B.; Tawfik, D. S.; Chap, R.; Schindler, D. G.; Kim, S.-H.; Gren, B. S.; Eshhar, Z.; Knossow, M. Structural convergence in the active sites of a family of catalytic antibodies. *Science* **1997**, *275*, 1140-1142.

(69) Zhou, G. W.; Guo, J.; Huang, W.; Fletterick, R. J.; Scanlan, T. S. Crystal structure of a catalytic antibody with a serine protease active site. *Science* **1994**, *265*, 1059-1064.

(70) Fersht, A. R. Dissection of the structure and activity of the tyrosyl-tRNA synthetases by site-directed mutagenesis. *Biochemistry* **1987**, *26*, 8031-8038.

(71) Fersht, A. R.; Leatherbarrow, R. J.; Wells, T. N. C. Binding energy and catalysis: a lesson from protein engineering of the tyrosyl-tRNA synthetase. *Trends. Biochem. Sci.* **1986**, *9*, 321-325.

(72) Fersht, A. R.; Leatherbarrow, R. J.; Wells, T. N. C. Quantitative analysis of structure-activity relationship in engineered protein by linear free-energy relationships. *Nature* **1986**, *322*, 284-286.

(73) Knowles, J. R.; Albery, W. J. Perfection in enzyme catalysis: the energetics of triosephosphate isomerase. *Acc. Chem. Res.* **1977**, *10*, 105-111.

(74) Albery, W. J.; Knowles, J. R. Efficiency and evolution of enzymatic catalysis. *Angew. Chem. Int. Ed. Engl.* **1977**, *16*, 285-293.

(75) Albery, W. J.; Knowles, J. R. Evolution of enzyme function and the development of catalytic efficiency. *Biochemistry* **1976**, *15*, 5631-5640.

(76) Brick, P.; Blow, D. M. Crystal structure of a deletion mutant of a tyrosyl-tRNA synthetase complexed with tyrosine. *J. Mol. Biol.* **1987**, *194*, 287-97.

(77) Brick, P.; Bhat, T. N.; Blow, D. M. Structure of tyrosyl-tRNA synthetase refined at 2.3 A resolution. Interaction of the enzyme with the tyrosyl adenylate intermediate. *J. Mol. Biol.* **1989**, *208*, 83-98.

(78) Fersht, A. R. Relationships between apparent binding energies measured in site-directed mutagenesis experiments and energetics of binding and catalysis. *Biochemistry* **1988,** *27,* 1577-80.

(79) Lowe, D. M.; Winter, G.; Fersht, A. R. Structure-activity relationships in engineered proteins: characterization of disruptive deletions in the α-ammonium group binding site of tyrosyl-tRNA synthetase. *Biochemistry* **1987,** *26,* 6038-6043.

(80) Wells, T. N. C.; Fersht, A. R. Use of binding energy in catalysis analyzed by mutagenesis of the tyrosyl-tRNA synthetase. *Biochemistry* **1986,** *25,* 1881-1886.

(81) Fersht, A. R.; Leatherbarrow, R. J.; Wells, T. C. Structure-activity relationships in engineered proteins: analysis of use of binding energy by linear free energy relationships. *Biochemistry* **1987,** *26,* 6030-6038.

(82) Leatherborrow, R. J.; Fersht, A. R.; Winter, G. Transition-state stabilization in the mechanism of tyrosyl-tRNA synthetase revealed by protein engineering. *Proc. Natl. Acad. Sci., USA* **1985,** *82,* 7840-7844.

(83) Wells, T. N.; Fersht, A. R. Protection of an unstable reaction intermediate examined with linear free energy relationships in tyrosyl-tRNA synthetase. *Biochemistry* **1989,** *28,* 9201-9.

(84) Ho, C. K.; Fersht, A. R. Internal thermodynamics of position 51 mutants and natural variants of tyrosyl-tRNA synthetase. *Biochemistry* **1986,** *25,* 1891-7.

(85) Pompliano, D. L.; Peyman, A.; Knowles, J. R. Stabilization of a reaction intermediate as a catalytic device: definition of the functional role of the flexible loop in triosephosphate isomerase. *Biochemistry* **1990,** *29,* 3186-94.

(86) Sampson, N. S.; Knowles, J. R. Segmental motion in catalysis: investigation of a hydrogen bond critical for loop closure in the reaction of triosephosphate isomerase. *Biochemistry* **1992,** *31,* 8488-94.

(87) Albery, W. J.; Knowles, J. R. Free-energy profile for the reaction catalyzed by triosephosphate isomerase. *Biochemistry* **1976,** *15,* 5627-5631.

(88) Narlikar, G. J.; Gopalakrishnan, V.; McConnell, T. S.; Usman, N.; Herschlag, D. Use of binding energy by RNA enzyme for catalysis by positioning and substrate destabilization. *Proc. Natl. Acad. Sci., USA* **1995,** *92,* 3668-3672.

(89) Herschlag, D.; Cech, T. R. Catalysis of RNA cleavage by the *Tetrahymena* thermophila ribozyme. 1. Kinetic description of the reaction of an RNA substrate complementary to the active site. *Biochemistry* **1990,** *29,* 10159-10171.

(90) Cech, T. R.; Herschlag, D.; Piccirilli, J. A.; Pyle, A. M. Rna Catalysis by a group-I ribozyme - Developing a model For transition-state stabilization. *J. Biol. Chem.* **1992,** *267,* 17479-17482.

(91) Herschlag, D. Evidence For Processivity and 2-step binding of the RNA substrate from studies of $J_{1/2}$ mutants of the *Tetrahymena* Ribozyme. *Biochemistry* **1992,** *31,* 1386-1399.

(92) Herschlag, D.; Eckstein, F.; Cech, T. R. The importance of being ribose At the cleavage site in the tetrahymena ribozyme reaction. *Biochemistry* **1993,** *32,* 8312-8321.

(93) Bourne, N.; Williams, A. Effective charge on oxygen in phosphoryl ($-PO_3^{2-}$) group transfer from an oxygen donor. *J. Org. Chem.* **1984,** *49,* 1200-1204.

(94) Williams, A. *Effective charge and transition-state structure in solution*; Bethell, D., Ed.; Academic Press: New York, 1992; Vol. 27, pp 2-55.

(95) Moore, S. A.; Jencks, W. P. Reactions of acyl phosphates with carboxylate and thiol anions. Model reactions for CoA transferase involving anhydride formation. *J. Biol. Chem.* **1982,** *257,* 10874-10881.

(96) White, H.; Jencks, W. P. Mechanism and specificity and succinyl-CoA:3-ketoacid Coenzyme A transferase. *J. Biol. Chem.* **1976,** *251,* 1688-1699.

(97) Moore, S. A.; Jencks, W. P. Formation of active site thiol ester of CoA transferase and the dependence of catalysis on specific binding interactions. *J. Biol. Chem.* **1982,** *257*, 10893-10907.

(98) Fierke, C. A.; Jencks, W. P. Two functional domains of Coenzyme A activate catalysis Coenzyme A transferase. *J. Biol. Chem.* **1986,** *261*, 7603-7606.

(99) White, H.; Solomon, F.; Jencks, W. P. Utilization of the inactivation rate of coenzyme A transferase by thiol reagents to determine properties of the enzyme-CoA intermediate. *J. Biol. Chem.* **1976,** *251*, 1700-1707.

(100) Whitty, A.; Fierke, C. A.; Jencks, W. P. Role of binding energy with coenzyme A in catalysis by 3-oxoacid coenzyme A transferase. *Biochemistry* **1995,** *34*, 11678-11689.

(101) Mader, M. M.; Bartlett, P. A. Binding energy and catalysis: the implications for transition-state analogs and catalytic antibodies. *Chem. Rev.* **1997,** *97*, 1281-1301.

(102) Guo, J.; Huang, W.; Scanlan, T. S. Kinetic and mechanistic characterization of an efficient hydrolytic antibody: evidence for the formation of an acyl intermediate. *J. Am. Chem. Soc.* **1994,** *116*, 6062-6069.

(103) Guo, J.; Huang, W.; Zhou, W.; Fletterick, R. J.; Scanlan, T. S. Mechanistically different catalytic antibodies obtained from immunization with a single transition-state analog. *Proc. Natl. Acad. Sci., USA* **1995,** *92*, 1694-1698.

(104) Baca, M.; Scanlan, T. S. S.; Stephenson, R. C.; Wells, J. A. Phage display of a catalytic antibody to optimize affinity for transition-state analog binding. *Proc. Natl. Acad. Sci.* **1997,** *94*, 10063-10068.

Chapter 2. 17E8•Substrate Active-site Interactions

Abstract

In this chapter, we investigate how the catalytic antibody 17E8 uses well-defined active site interactions that are removed from the reactive center to promote catalysis. In addition, the enantioselectivity of 17E8 mediated hydrolysis is examined. We find that the antibody is highly active towards substrates, regardless of side-chain length (1 to 4 side-chain carbons), that possess the S configuration (L) at the α-carbon. There is no detectable activity towards those substrates that have the R configuration at the α-carbon or towards substrates that contain substituents larger than a hydrogen atom in the pro-R position at the Cα center. The complete removal of the substrate side-chain results in a loss of detectable catalysis, indicating that the interactions between the side-chain and its recognition pocket play a major role in catalysis. In contrast, the removal of the N-acyl substituent does not result in a substantial loss of activity, indicating that binding interactions with this group play a minor role in catalysis. 17E8's ability to use remote side-chain•pocket binding interactions compares well with a natural enzyme

that contains similar active site interactions. These results suggest

that the immune response elicited by haptens can yield active site

interactions that are remote from the catalytic center that can be used

in a functionally similar manner to evolved enzymes.
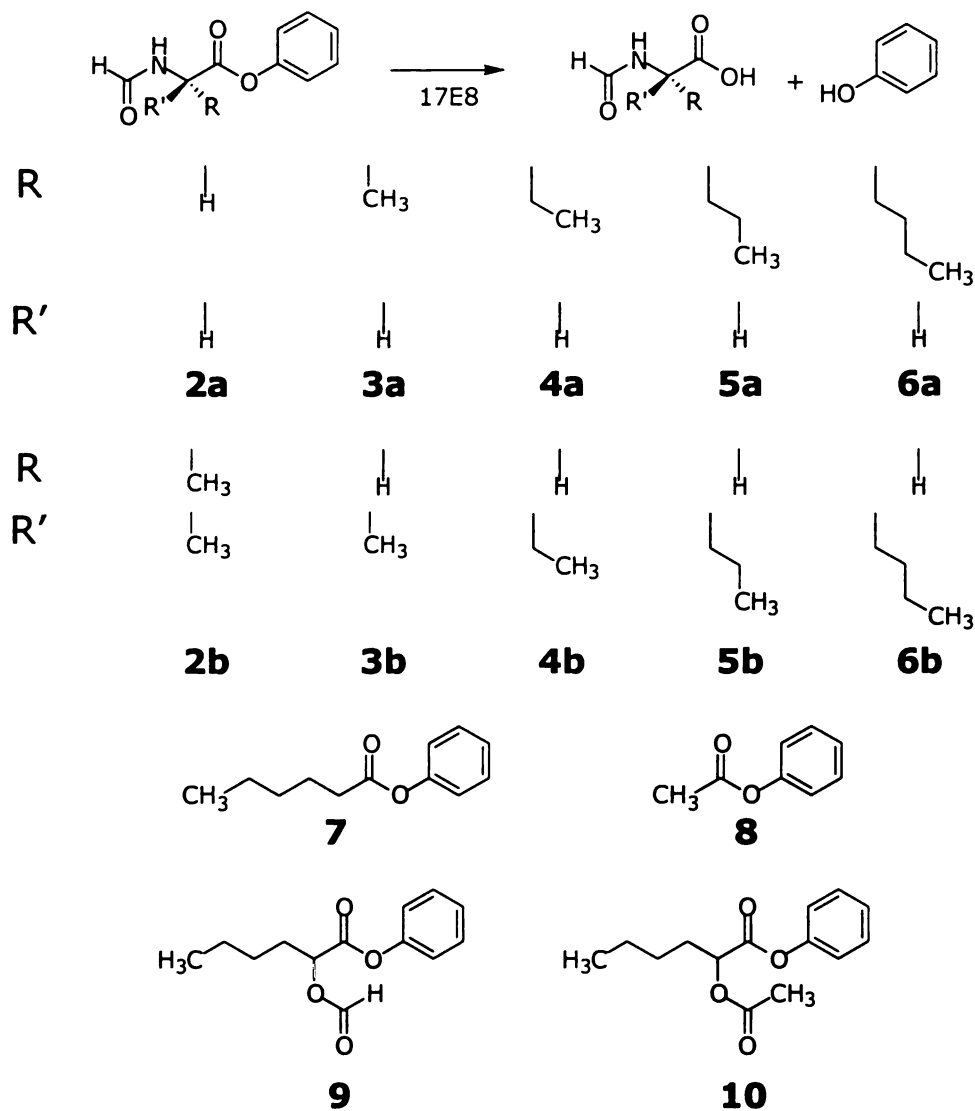
Figure 2.1 Hydrolysis reaction catalyzed by 17E8 (top) and the substrates used to probe the enantioselectivity (bottom). The 'a' group substrates possess the S (L) configuration at the Cα carbon except **2a** which does not contain a stereogenic center. The 'b' group substrates possess the R (D) configuration at the Cα carbon except **2b** which does not contain a stereogenic center. Racemic mixtures of substrates **9** and **10** were used.
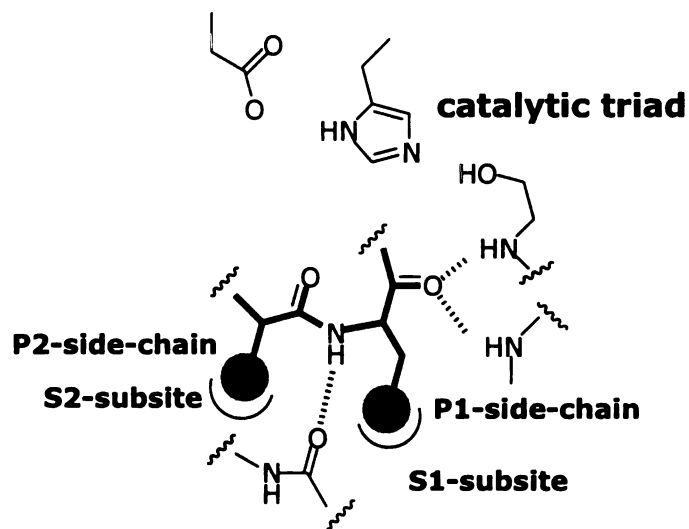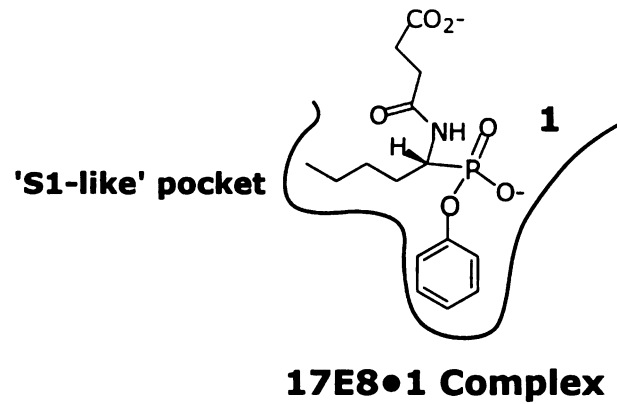
Figure 2.2 (top) Schematic of the 17E8 active site. (bottom) Schematic of important active site interactions in serine proteases. (Nomenclature for the substrate amino acid residues is P_n, ..., P_2, P_1, P_1', P_2', ..., P_n', where P_1-P_1' denotes the hydrolyzed bond. S_n, ..., S_2, S_1, S_1', S_2', ..., S_n' denote the corresponding enzyme binding sites.)

Introduction

The free-energy gained from the formation of active site-substrate binding interactions that are distant from the reactive center can play important roles in enzyme catalysis.[1-4] These interactions govern enzyme specificity, catalytic turnover, and overall transition-state stabilization. Because catalytic antibodies have been generated to mimic enzymes, it is of interest to understand how these 'less-evolved' enzymes use analogous binding interactions in their catalytic mechanisms. Understanding the active sites of the functionally simple antibodies may assist in illuminating the more complex functions in enzyme active sites.

The catalytic antibody 17E8 is an esterase that catalyzes the hydrolysis of N-acyl amino acid phenyl esters (Figure 2.1).[5,6] The structure of the 17E8•hapten complex shows that **1** is buried deeply in the antigen combining site and that there are separate and well-defined binding pockets for the n-butyl side-chain and the phenyl group of the hapten (Figure 2.2).[7] These remote binding interactions between the hapten groups and the antibody are reminiscent of those used by proteolytic enzymes to promote the cleavage of amide bonds.[8-14] The presence of these interactions suggests that this system may serve as a simple model of proteolytic enzymes containing a single, isolated S-subsite pocket for recognition

51

of a P1 hydrophobic side-chain of the amino acid substrate (see Figure

2.2).
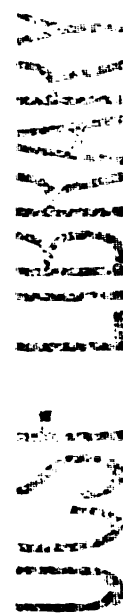
substrate	$C\alpha_{configuration}$	$[\alpha]_D{}^a$	$k_{cat}\ (s^{-1})^b$	$K_M\ (\mu M)^b$
2a	Nonstereogenic	0	N.D.	-
2b	Nonstereogenic	0	N.D.	-
3a	S	- 36.0°	0.9 ± 0.1	4 ± 4
3b	R	+ 35.6°	N.D.	-
3	Racemic	0	0.8 ± 0.1	9 ± 2
4a	S	- 26.6°	0.4 ± 0.1	3 ± 1
4b	R	+ 26.2°	N.D.	-
4	Racemic	0	0.5 ± 0.1	10 ± 3
5a	S	- 22.0°	1.5 ± 0.1	0.18 ± 0.03
5b	R	+ 20.1°	N.D.	-
5	Racemic	0	1.4 ± 0.1	0.33 ± 0.03
6a	S	- 14.0°	2.1 ± 0.1	0.10 ± 0.01
6b	R	+ 13.7°	N.D.	-
6	racemic	0	2.0 ± 0.1	0.18 ± 0.04
6c[c]		- 6.2°	4.4 ± 0.4	0.25 ± 0.04
7[c]	nonstereogenic	0	2.2 ± 0.6	0.6 ± 0.2
8	nonstereogenic	0	-	-
9[c,d]	nonstereogenic	0	*	* 2 x 10⁴
10[c,d]	nonstereogenic	0	*	* 9 x 10³

Table 2.1 Enantioselectivity of 17E8 catalysis. [a]The optical activity of the substrates was determined on a Perkin-Elmer 241 polarimeter (Na beam). All samples were prepared in dichloromethane, and the optical density measurements were made at 25.0°C after zeroing the instrument with dichloromethane. [b]Activity assays were performed in 50 mM borate, 150 mM NaCl, pH 8.7 at 24.5 ± 0.5 °C. Steady-state kinetic constants were obtained from nonlinear fits of v versus [S] data to the Michaelis-Menten equation using the KaliedaGraph program. [c]The kinetic data for these substrates were obtained in 50 mM CHES, 150 mM NaCl, pH 9.5. [d]The k_{cat}/K_M values are reported because accurate k_{cat} and K_M values could not be determined due to the solubility limit of the substrates. These k_{cat}/K_M values can be compared to that of **6c** (8 x 10³) which was determined under the same conditions. N.D. = none detected.
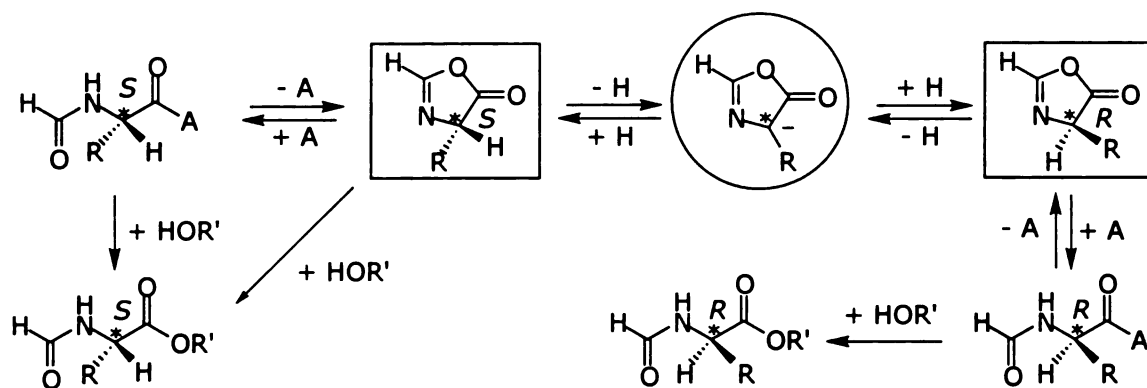
Figure 2.3 Racemization via oxazolone formation. Activation of N-formyl amino acid leads to the cyclization reaction affording the oxazolone (boxed species). Deprotonation of the oxazolone at the Cα (designated by the asterisk) carbon yields the achiral oxazolonium ion (circled) which can be reprotonated on either face at the prochiral position resulting in racemization. The activated amino acid can then be regenerated by the attack by the nucleophilic activating reagent or by the alcohol to yield the desired ester. The stereochemistry at the Cα position is shown in italics.

Results and Discussion

Initial kinetic studies with 17E8 showed that the reaction was catalyzed in an enantioselective manner.[5] However, the method used for the synthesis of the substrates resulted in Cα racemization, preventing the preparation of enantiomerically pure substrates with either the R or S Cα configuration. The synthetic route used involved the esterification of N-formyl amino acids with the coupling reagent, dicyclohexylcarbodiimide (DCC). The use of carboxy-activating reagents such as DCC for acyl substitution reactions with amino acids

bearing an α-N-formyl substituent is plagued by the formation of oxazolones, a side reaction that competes with the direct formation of the ester (Figure 2.3).[15-18] This intermediate contains a labile Cα proton and is able to undergo racemization. Attack of the oxazolone by the nucleophilic activating group or alcohol affords the partially racemized N-formyl amino acid ester (Figure 2.3).

The synthesis nonetheless produced enantiomerically enriched Cα R and S substrates starting from the R and S amino acids, respectively. The S-enriched substrate was found to have a higher specific activity by the expected amount assuming complete S-enantioselectivity for the 17E8-catalyzed reaction.[5] The S-enantioselectivity found in the kinetic experiments is in agreement with the three-dimensional structure of the 17E8•1 complex that shows that the enantiomer of 1 with the same Cα configuration as the S-substrate was bound in the active site although racemic 1 was used in the crystallization experiments.[7] Although these experiments established that 17E8 is more active toward S-substrates, they do not unambiguously establish that 17E8 has no activity (binding or catalysis) towards the corresponding R-esters. In addition, the use of enantiomerically enriched substrates make it difficult to accurately determine the steady-state kinetic parameters for the S and R substrates.

An alternative synthetic route used to prepare the enantiomerically pure substrates is shown in Figure 2.4. This route involves the esterification of N-Boc amino acids.[19] The presence of the tert-butyloxy carbonyl (Boc) protecting group is known to protect against racemization by inhibiting the formation of the oxazolonium ion (Figure 2.3).[15,18] Following the esterification of the N-Boc amino acid, the Boc group is removed and the amino acid is formylated by stardard procedures (Figure 2.4).[20]
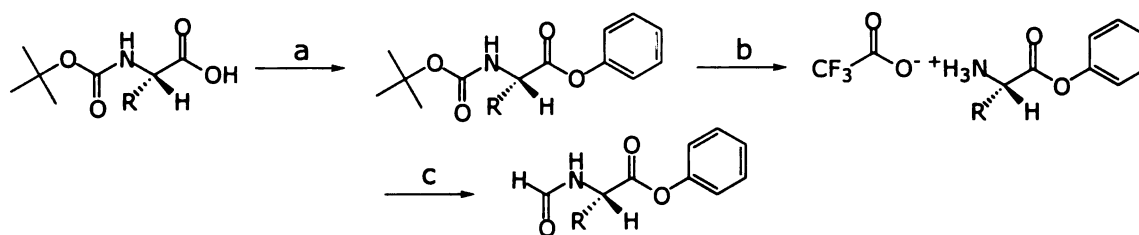
Figure 2.4 Synthesis of enantiomerically pure S-phenyl ester substrates. (a) CH_2Cl_2, phenol, Et_3N, HBTU (2-(1H-benzotriazole-1yl)-1,1,3,3-tetramethyluronium hexafluorophosphate) (b) 50/50 CF_3CO_2H/CH_2Cl2 (c) Ac_2O, HCO_2H

The optical rotations of the substrates are shown in Table 2.1. As expected, the enantiomerically pure *S* and *R* substrates rotate light with similar magnitudes but in opposite directions. The optical activity of the N-formyl norleucine phenyl (**6**) ester substrate prepared from N-formyl-(*S*)-norleucine was smaller in magnitude than that prepared from N-Boc-(*S*)-norleucine suggesting that the new synthetic route afforded greater enantiomeric purity. The optical activity of the phenyl ester substrate prepared from the N-formyl amino acid is close to the

value expected from a mixture containing a 50% enantiomeric excess of the S substrate using the -14.0° value for the enantiomerically pure S substrate and +14.0° value for the R substrate. The racemic phenyl ester substrates were prepared from the racemic N-Boc amino acids.

The enantioselectivity of 17E8 mediated catalysis was examined using the enantiomerically pure S and R substrates and the corresponding racemic mixtures. The esters (**3a-6a**) possessing the S configuration at the Cα carbon were substrates for 17E8. The catalyzed hydrolysis of the esters (**3b-6b**) possessing the R configuration was not detected. The k_{cat} values obtained from kinetic analyses of the racemic mixtures are within experimental error of the value obtained from the steady-state analysis of the enantiomerically pure S substrates, consistent with an S-enantioselective mode of hydrolysis. The K_M values obtained from the kinetic analyses of the racemic mixtures of **5** and **6** are approximately twice that of their enantiomerically pure S counterparts. This suggests that the (R)-substrates do not bind to the active site to act as competitive inhibitors of 17E8 hydrolysis. The high K_M values for **3** and **4** make it technically difficult to obtain precise K_M values for these substrates, thus the 2-fold difference in K_M values between the (S)-**3** and (S)-**4** and racemic (R/S)-**3** and (R/S)-**4** substrates is not as apparent. The presence of high concentrations (>15 mM) of (R)-**3** and (R)-**4** did not increase the

K_M value associated with the hydrolysis of **5a** suggesting that these substrates do not compete with **5a** for the occupancy of the active site.

The serine proteases show similar *S*-enantioselectivity of hydrolysis.**[21-25]** The stereoselectivity of the proteases is relative rather than absolute as substrates possessing the *R* configuration at the $C\alpha$ center are processed albeit much more slowly than their *S* counterparts.**[23,24]** In addition, inhibition experiments have shown that the (*R*)-substrates bind to the enzyme active site.**[23,24]** The explanation to account for the enantioselectivity of the serine protease α-chymotrypsin includes a three-locus model where three non-hydrogen groups attached to the stereogenic α-carbon make stabilizing interactions with specifically oriented active site groups in the Michaelis complex, transition-state complex, and the enzyme-acyl intermediates (see Figure 2.2).**[23]** A hydrogen bond between the NH of the substrate's α-N-acyl group and an active-site hydrogen bond acceptor is one of the critical interactions controlling enantioselectivity. Replacement of the substrate's NH group with an -O- group, which cannot serve as a hydrogen bond donor, results in the relaxation of selectivity as judged by the $(k_{cat})_S/(k_{cat})_R$ and $(k_{cat}/K_M)_S/(k_{cat}/K_M)_R$ ratios.**[23,24]** Interactions involving the P1 side-chain of the substrate are important for selectivity as increasing the number of

58

P1•S1 interactions also improves stereospecificity.[21,23] Substrates possessing a substituent larger than a H atom at the pro-*R* position at the $C\alpha$ position are not cleaved by the enzyme indicating that interactions between this group and the enzyme serve as another stereospecificity sieve.

The binding energy from the three-point locus interactions in α-chymotrypsin also plays an important role in promoting hydrolysis suggesting that the factors controlling enantioselectivity and hydrolysis are linked.[23,24] Replacing the α-NH-acyl group with a hydrogen atom in phenylalanine ester substrates leads to a 4000-fold reduction in k_{cat} and a 9000-fold decrease in k_{cat}/K_M. In contrast, the analogous experiment with 17E8 shows that the substrate N-acyl group is not particularly important for catalysis. In this case, the replacement of the α-NH-acyl group with a hydrogen atom (as demonstrated with substrate **7**) results in negligible reductions in the steady-state kinetic constants (2-fold reduction in k_{cat}, 2-fold increase in K_M, and a 4-fold reduction in k_{cat}/K_M (Table 2.1)). The decreases in k_{cat} and k_{cat}/K_M are mainly due to the differences in inductive effects associated with the $C\alpha$-substituents. In addition, replacing the N-acyl group with an O-acyl group (substrates **9** and **10**) does not result in a significant reduction in the k_{cat}/K_M value (Table 2.1). As with the enzyme, replacing the pro-*R* hydrogen atom with a larger substituent

(demonstrated with substrate **1**) results in a loss of binding and catalysis.

$$E + RCO_2CH_3 \underset{}{\overset{K_S}{\rightleftharpoons}} E{\bullet}RCO_2CH_3 \xrightarrow{k_2} RCO{-}E \xrightarrow{k_3} E + RCO_2H$$
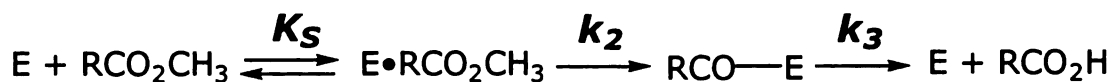
amino acid	k_2 (s^{-1})	k_3 (s^{-1})	K_S (mM)	k_{cat}/K_M $(s^{-1} M^{-1})$ $\Delta\Delta G_b{}^a$ (kcal/mol)
Gly	0.49	0.14	3.38×10^3	0.13 [+6.0]
But	8.8	1.7	417	21 [+2.9]
Nvl	35.6	5.93	100	360 [+1.3]
Nle	103	19	34	3×10^3 [+0.0]
Phe	796	111	7.6	1×10^5 [-2.1]
Tyr	5×10^3	200	17	3×10^5 [-2.7]

Table 2.2 S1-P1 interactions in chymotrypsin catalysis. Data taken from ref 27. Abbreviations for amino acid substrates: Gly: glycine; But: α-amino butyric acid; Nvl: norvaline; Nle: norleucine; Phe: phenylalanine; Tyr: tyrosine. $^a(k_{cat}/K_M)_a/(k_{cat}/K_M)_b=\exp(-\Delta\Delta G_b/RT)$ as defined by Fersht (ref 1).

Studies of the reactions of α-chymotrypsin with alternative substrate esters and amides indicate that the S1-P1 interactions are important for promoting catalysis (Table 2.2).[26-30] The removal of the side-chain pocket interactions result in large reductions in the stability of the Michaelis complex, the rate of enzyme acylation (k_2),

the rate of enzyme deacylation (k_3), and the enzyme's overall

stabilization of the transition-state (k_{cat}/K_M). Similarly, results with the

glycine, alanine, and phenyl acetate (**2a**, **3a**, and **8**) substrates for the

17E8 system indicate that the interactions between the n-butyl side-

chain of **6a** and its recognition pocket are extremely important for

catalysis. The complete removal of the side-chain results in a loss of

detectable catalysis as demonstrated with **2a** and **8**. In addition,

there is a substantial reduction of the 17E8's overall stabilization of the

transition-state with the partial removal of the side-chain

(demonstrated with substrate **3a** and **4a**).

With the available data, a comparison can be made between

chymotrypsin-catalyzed hydrolysis of N-acetyl Tyr (**10**), Phe (**11**), and

Nle (**9**) esters and 17E8-catalyzed hydrolysis of N-formyl Nle (**6a**) and

N-formyl Ala (**3a**) (Table 2.3). Such a comparison is useful for

understanding and evaluating the catalytic response to the n-butyl

side-chain of **1**. The comparisons are made between the enzyme's

'natural' substrate, where P1-S1 interactions are maximized, and an

inferior substrate that has a P1 side-chain that is three carbon atoms

smaller than that of the natural substrate. An assumption in this

comparison is that the P1-S1 interactions are largely hydrophobic even

though the natural P1 chymotrypsin preference is for aromatic amino

acids, whereas the 17E8 side-chain preference is for aliphatic amino

acids. This assumption is supported by P1 specificity studies with α-chymotrypsin using homologous substrate series of Gly, Ala, But, Nvl, Nle, and Phe. A plot of log(k_{cat}/K_M) versus the hydrophobicity parameter, π, yields a linear correlation including the Phe data.[26,29]

catalyst	substrate	no. at P1 C's[a] ΔP1 C's[b]	k_{cat} Δk_{cat}[c] (s^{-1})	K_M ΔK_M[c] (mM)	$\Delta\Delta G_b$ (kcal/ mol)[d]
chymotrypsin	N-Ac-L-Nle-OMe (9)	4	16.1	5.37	
chymotrypsin	N-Ac-L-Tyr-OEt (10)	7	192	0.633	
chymotrypsin	10/9	3[b]	12 fold[c]	8[c]	-2.7
chymotrypsin	N-Ac-L-Phe-OMe (11)	7	97.1	0.93	
chymotrypsin	11/9	3[b]	6 fold[c]	6[c]	-2.1
17E8	(S)-3a	1	0.9	4	
17E8	(S)-6a	4	2.1	0.1	
17E8	6a/3a	3[b]	2 fold[c]	40[c]	-2.2

Table 2.3 Comparison of side-chain catalytic effects between chymotrypsin and 17E8. [a]Refers to the number of carbon atoms contained in the substrate (P1 for chymotrypsin) side-chain. [b]Refers to the difference in the number of carbon atoms between the side-chain of the indicated substrates. [c]Refers to the ratio between steady-state kinetic constants for hydrolysis of the indicated substrates. [d](k_{cat}/K_M)a/(k_{cat}/K_M)b = exp(-$\Delta\Delta G_b$/RT) as defined by Fersht (ref. 1). Kinetic constants for chymotrypsin taken from ref. 26.

The kinetic data show that 17E8 has a specificity that is similar to that of chymotrypsin for the natural substrates over the substrates

with the smaller P1 substituent. The addition of three P1 carbon atoms results in the gain of 2.2 kcal/mol of catalytically productive binding energy ($\Delta\Delta G_b$) for 17E8, whereas 2.1 and 2.7 kcal/mol of binding energy accompanies S1 pocket filling for chymotrypsin with Phe and Tyr substrates, respectively. Interestingly, the isolated effects on k_{cat} and K_M resulting from increased side-chain•pocket binding interactions are markedly different for 17E8 and chymotrypsin. In chymotrypsin catalysis, the increase in binding energy is distributed approximately evenly between the processes associated with k_{cat} and K_M, whereas in 17E8 nearly all of the additional binding energy is used to decrease the value of K_M.

Conclusions

The results from this study suggest that the immune response elicited by the hapten, **1**, produced an antibody active site that contains a specificity pocket that may be functionally similar to those used in the evolved enzyme α-chymotrypsin and other enzymes that contain analogous recognition pockets. Both α-chymotrypsin and 17E8 are able to use hydrophobic binding interactions that are remote from the reaction center to direct enantioselectivity and stabilize the hydrolytic transition-state. The magnitude of transition-state stabilization gained from the hydrophobic side-chain•pocket interactions is similar for the antibody and the enzyme. The precise mechanism by which the binding energy is used to accelerate hydrolysis appears to be different for the natural enzyme and the antibody. 17E8's active site does appear to be less sophisticated than that of α-chymotrypsin in that the natural enzyme uses binding interactions with more substrate groups than does 17E8. The enzyme also uses the binding interactions to increase catalytic turnover whereas 17E8 does not.

References

(1) Fersht, A. *Structure and Mechanism in Protein Science: A Guide to Enzyme Catalysis and Protein Folding*; W.H. Freeman and Company: New York, 1999.

(2) Fersht, A. R. Catalysis, binding, and enzyme-substrate complementarity. *Proc. R. Soc. Lond.B.* **1974,** *187*, 397-407.

(3) Jencks, W. P. *Catalysis in Chemistry and Enzymology*; Dover Publications: Mineola, 1969.

(4) Gandour, R. D.; Schowen, R. L. *Transition states of biochemical processes*; Plenum Press: New York, 1978.

(5) Guo, J.; Huang, W.; Scanlan, T. S. Kinetic and mechanistic characterization of an efficient hydrolytic antibody: evidence for the formation of an acyl intermediate. *J. Am. Chem. Soc.* **1994,** *116*, 6062-6069.

(6) Guo, J.; Huang, W.; Zhou, W.; Fletterick, R. J.; Scanlan, T. S. Mechanistically different catalytic antibodies obtained from immunization with a single transition-state analog. *Proc. Natl. Acad. Sci., USA* **1995,** *92*, 1694-1698.

(7) Zhou, G. W.; Guo, J.; Huang, W.; Fletterick, R. J.; Scanlan, T. S. Crystal structure of a catalytic antibody with a serine protease active site. *Science* **1994,** *265*, 1059-1064.

(8) Bauer, C. A.; Brayer, G. D.; Sielecki, A. R.; James, M. N. Active site of α-lytic protease: enzyme-substrate interactions. *European Journal of Biochemistry* **1981,** *120*, 289-94.

(9) Bauer, C.-A.; Thompson, R. C.; Blout, E. R. The active centers of *Streptomyces griseus* protease 3 and α-chymotrypsin: enzyme-substrate interactions remote from the scissile bond. *Biochemistry* **1976,** *15*, 1291-1296.

(10) Kraut, J. Serine proteases: structure and mechanism of catalysis. *Ann. Rev. Biochem.* **1977,** *46*, 331-358.

(11) Perona, J. J.; Craik, C. S. Structural basis of substrate specificity in the serine proteases. *Prot. Sci.* **1995,** *4*, 337-360.

(12) Perona, J. J.; Craik, C. S. Evolutionary divergence of substrate specificity within the chymotrypsin-like serine protease fold. *J. Biol. Chem.* **1997**, *272*, 29987-29990.

(13) Thompson, R. C. Binding of peptides to elastase: Implication for the mechanism of substrate hydrolysis. *Biochemistry* **1974**, *13*, 5495-5501.

(14) Stroud, R. M. A family of protein-cutting proteins. *Amer. Sci.* **1974**, *231*, 74-88.

(15) Bodansky, M. *Principles of Peptide Synthesis*; second ed.; Springer: New York, 1993.

(16) Goodman, M.; Stueben, K. C. Amino acid active esters. III. Base-catalyzed racemization of peptide active esters. *J. Am. Chem. Soc.* **1962**, *27*, 3409-3416.

(17) Jersey, J. d.; Kortt, A. A.; Zerner, B. On the mechanism of hydrolysis of N-acylamino acid nitrophenyl esters. *Biochem. Biophys. Res. Comm.* **1966**, *23*, 745-750.

(18) Kemp, D. S. *Racemization in peptide synthesis*; Gross, E. and Meienhofer, J., Ed.; Academic Press: New York, 1979; Vol. 1.

(19) Castro, B.; Evin, G.; Claude, S.; Seyer, R. Peptide coupling reagents: VIII. A high yield preparation of phenyl esters of amino acids using benzotriazolyoxytris[dimethylamino]phosphonium hexafluorophosphoate (BOP reagent). *Synthesis* **1977**, , 413.

(20) Sheehan, J. C.; Yang, D.-D. H. The use of N-formylamino acids in peptide synthesis. *J. Am. Chem. Soc.* **1958**, *80*, 1154-58.

(21) Cohen, S. G.; Schultz, R. M.; Weinstein, S. Y. Stereospecificity in hydrolysis by α–chymotrypsin of esters of alpha, alpha-disubstituted acetic and beta, beta-disubstituted propionic acids. *Journal of the American Chemical Society* **1966**, *88*, 5315-5319.

(22) Coletti-Previero, M. A.; Kraicsovits, F.; Previero, A. Stereospecificity of α–chymotrypsin. Changes of substrate configuration during enzymatic hydrolysis. *Febs Letters* **1973**, *37*, 93-96.

(23) Ingles, D. W.; Knowles, J. R. The stereospecificity of α-chymotrypsin. *Biochem. J.* **1968**, *108*, 561-569.

(24) Ingles, D. W.; Knowles, J. R. Specificity and stereospecificity of α-chymotrypsin. *Biochem. J.* **1967,** *104*, 369-377.

(25) Schwartz, H. M.; Wu, W.-S.; W.marr, P.; Jones, J. B. Predicting the enantiomeric selectivity of chymotrypsin. Homologous series of ester substrates. *J. Am. Chem. Soc.* **1978,** *100*, 5199-5203.

(26) Berezin, I. V.; Kazanskaya, N. F.; Klyosov, A. A.; Martinek, K. On the relationship between structure and reactivity of α-chymotrypsin substrates. *FEBS Lett.* **1971,** *15*, 125-128.

(27) Berezin, I. V.; Kazanskaya, N. F.; Klyosov, A. A. Determination of the individual rate constants of α-chymotrypsin-catalyzed hydrolysis with added nucleophilic agent 1,4-butanediol. *FEBS Lett.* **1971,** *15*, 121-124.

(28) Bauer, C. A. Active centers of Streptomyces griseus protease 1, Streptomyces griseus protease 3, and α-chymotrypsin: enzyme-substrate interactions. *Biochemistry* **1978,** *17*, 375-80.

(29) Dorovska, V. N.; Varfolomeyev, S. D.; Kazanskaya, N. F.; Klyosov, A. A.; Martinek, K. The influence of the geometric properties of the active centre on the specificity of α-chymotrypsin catalysis. *FEBS Lett.* **1972,** *23*, 122-124.

(30) Knowles, J. R. Enzyme specificity: α-chymotrypsin. *J. Theoret. Biol.* **1965,** *9*, 213-228.

Chapter 3. Remote Binding Energy in Antibody Catalysis. Studies of a Catalytically Unoptimized Specificity Pocket

Abstract

Binding interactions remote from the hydrolytic reaction center have been probed with substrates and phosphonate transition-state analogs to understand how these types of interactions are used to promote catalysis in the 17E8 system. We find that the hapten-generated recognition pocket in 17E8 has properties that are analogous to specificity pockets in enzymes. We have also found that there are specific requirements to form catalytically productive interactions between the side-chain and recognition pocket including: conformation, size, and geometry. An additional requirement includes favorable simultaneous interactions between the side-chain and binding pocket along with favorable interactions with the oxyanion hole. The 17E8 side-chain recognition pocket seems to be less 'catalytically' efficient than analogous amino acid side-chain pockets in enzymatic systems. The apparent binding energy gained from the methylene•pocket interactions in the 17E8

system is significantly smaller than those observed in natural enzymes. Furthermore, 17E8 does not use specific interactions in the recognition pocket to significantly affect catalytic turnover (k_{cat})–a trait of an un-optimized catalyst. Analysis of the crystal structure of the 17E8•hapten complex, has allowed for the identification of differences between the active sites of 17E8 and several proteases. The identified differences give insight to the sources of the inefficient use of binding energy.

Introduction

The use of binding energy to achieve rate accelerations is one feature that distinguishes enzymes from simple catalysts. This notion of translating binding energy into catalysis has been exploited in the generation the enzyme mimics such as catalytic antibodies. These immunoglobulins have been generated against haptens that are designed to create binding sites that use binding energy to promote catalysis.[1-3] So far, most of the catalytic antibody design efforts have focused on the protein environment proximal to the portion of the substrate that undergoes bond changes. Although there is no doubt that this part of the active site is an essential feature of a catalyst, nature has shown that interactions that occur away from the site of bond cleavage can be used to promote catalysis.[4-6]

Previous studies suggest that binding interactions away from the catalytic center are essential for catalysis by the antibody 17E8.[7] This antibody was generated against a phosphonate monoanion and catalyzes the efficient, enantioselective hydrolysis of the phenyl ester of n-formyl norleucine (Figure 3.1a).[8] The crystal structure of the 17E8•hapten complex indicates that there are several binding interactions that are responsible for 17E8's

70

catalytic properties, including a well defined pocket for the n-butyl

side-chain of the transition-state analog, and presumably the

transition-state of the hydrolytic reaction (Figures 3.2a and 3.2b).

Removal of these side-chain interactions results in a loss of

catalysis, suggesting a role for the 17E8 recognition pocket that is

similar to the role of specificity pockets used by natural enzymes,

especially those that utilize peptides or amino acids as

substrates.[4,6,9-11]

To study this hapten-generated recognition pocket and the

catalytic use of remote binding interactions in the 17E8 mechanism,

a series of α-(formyl-amino)-phenyl esters, all of which contain

different side-chains (Figure 3.3), was synthesized and evaluated

as substrates in the 17E8 catalyzed reaction (Figure 3.1a). In

addition, a series of corresponding α-(formyl-amino)-phosphonates

was synthesized to probe binding interactions that would occur

upon the formation of the hydrolytic transition-state or a nearby

tetrahedral intermediate (Figure 3.4). The results from these

experiments provide a conceptual framework for how these remote

interactions are used in the 17E8 mechanism and how important

these interactions are to 17E8 catalysis.
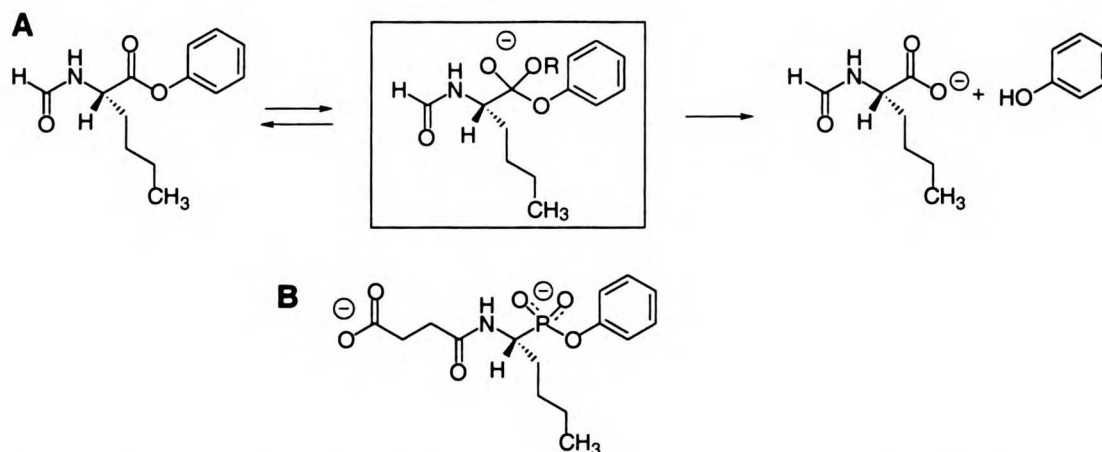
Figure 3.1 A. The esterolytic reaction catalyzed by 17E8. (boxed) The putative high energy tetrahedral intermediate. **B.** The phosphonate anion used to generate 17E8.
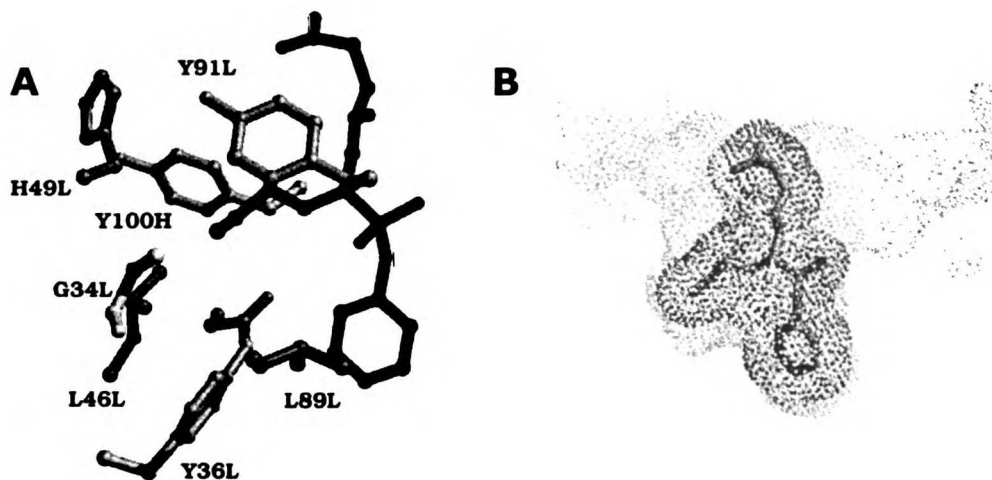
Figure 3.2 A. The active site residues proximal to the n-butyl side-chain of **5p**. The hapten is colored black. **B.** Solvent accessible surface of the 17E8 hapten binding site (light-grey) complexed with **5p** (black). The program MIDAS was used to generate both figures.[12,13]
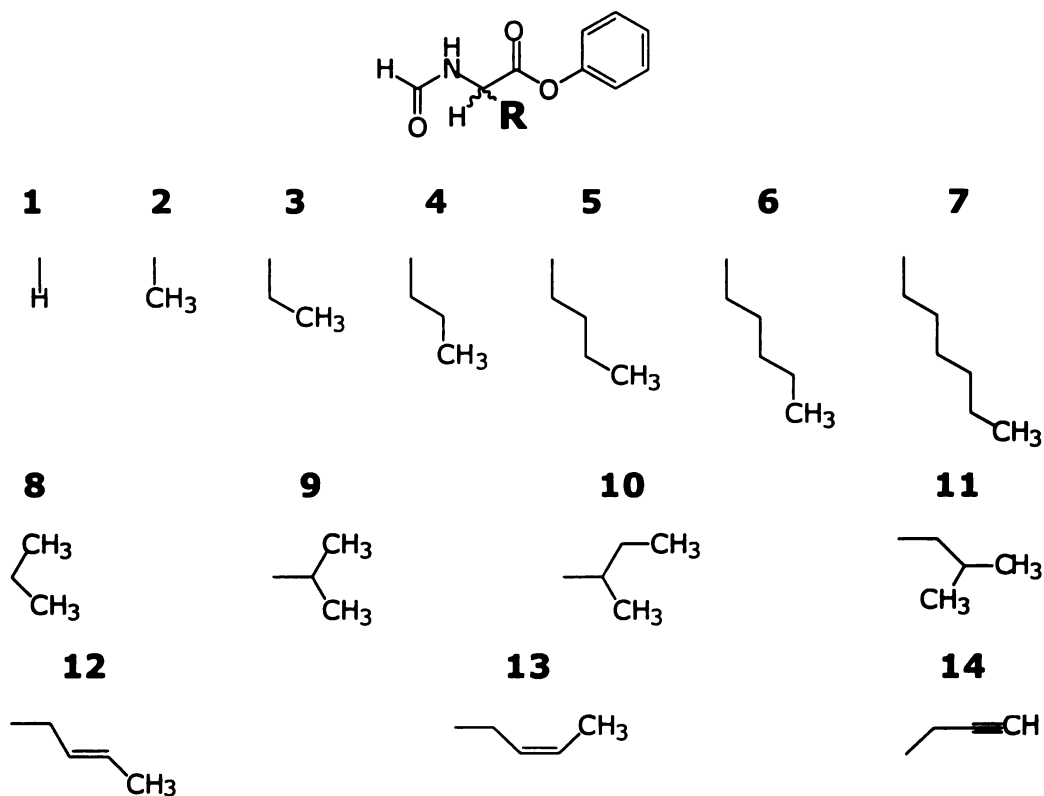
Figure 3.3 The phenyl esters used to probe the catalytic transition state binding interactions in the 17E8 mechanism. (top) Substrate skeleton where R represents the position at which side-chain (bottom) was varied. Substrates with side-chains (**1-7**) correspond to the homologous series, (**8-11**) the branched series, and (**12-14**) the conformationally restricted series.
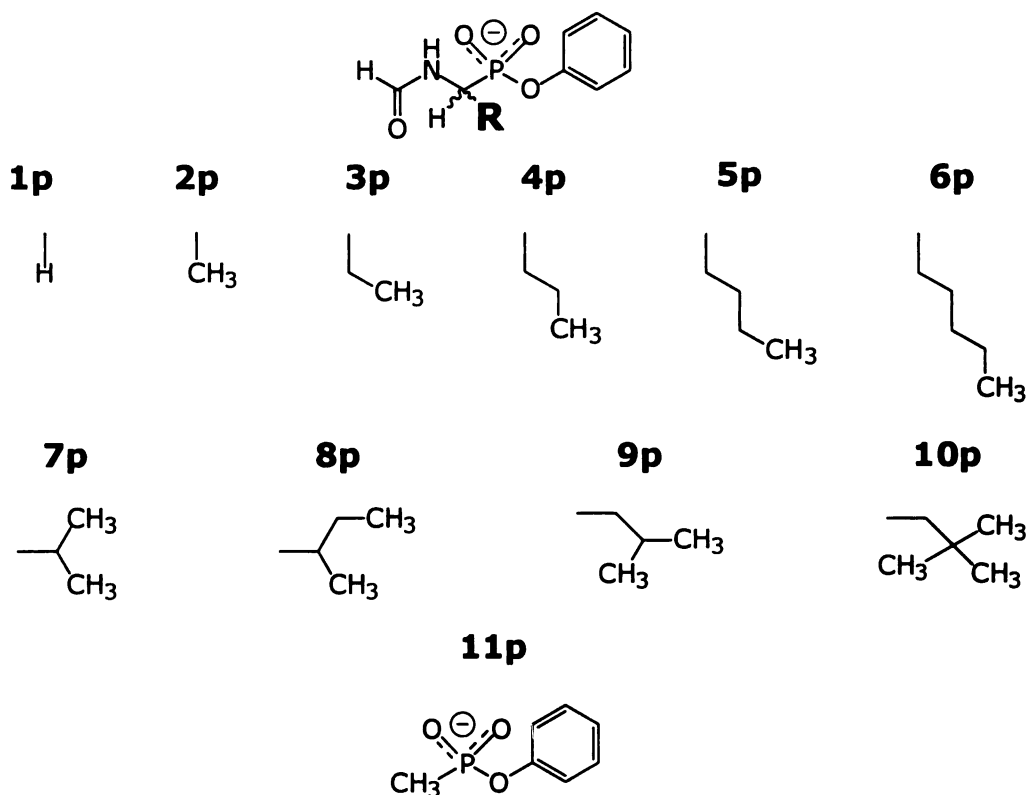
Figure 3.4 The phosphonate phenyl esters. (top) Phosphonate skeleton. (bottom) Side-chains. Side-chains (**1p-6p, 11p**) correspond to the homologous series and (**7p-10p**) the branched series.

Results

Homologous Series. To investigate the use of binding energy for catalysis between the methylene units of the side-chain and the recognition pocket of 17E8, we used a series of phenyl ester substrates and phosphonates that contain aliphatic side-chains of varying lengths (Figure 3.3, **1–7**; Figure 3.4, **1p-6p**). Table 3.1 shows the values of k_{cat}, K_M, k_{cat}/K_M, and the relative transition-state stabilization energies, $\Delta\Delta G_b$ (relative to **5**), for the series of substrates. The k_{cat} and K_M values were affected by changing the number of methylene groups in the side-chain. The magnitude of these effects varied with respect to each of the steady-state constants. The changes in k_{cat} were the smallest of the three values, spanning a range of about five-fold (0.4 s^{-1} to 2.1 s^{-1}). The changes in K_M (0.18 mM to 3.4 mM) and k_{cat}/K_M (180 s^{-1}M^{-1} to 12,000 s^{-1}M^{-1}) are larger, spanning almost two orders of magnitude. The values of k_{cat} and k_{cat}/K_M were the largest for **5** and decreased in the order n-propyl **4** $\approx$ n-pentyl **6** > methyl **2** $\approx$ ethyl **3**. Removing a methylene group from the side-chain decreased $\Delta\Delta G_b$ by as much as 1.9 kcal/mol and as little as 0.3 kcal/mol depending on the position in the side-chain. The substrate with no side-chain, **1**, showed no detectable activity, as did the substrate with the n-hexyl side-chain

7. In addition, neither of these substrates competed effectively with hydrolysis of **5**, as there was no change in the k_{cat} or K_M values (data not shown), at high concentrations (44 mM **1**, and 3 mM **7**).

Similarly, the K_i values of the corresponding phosphonates (**1p-6p**, Figure 3.4) were affected by the changes in the number of methylene units in the side-chain. The K_i values for the phosphonates are shown in Table 3.2. All of the phosphonates were competitive inhibitors of the catalyzed hydrolysis of substrate **5** (data not shown), suggesting that they bind in the active site of the antibody and that the K_i values represent the thermodynamic binding constants K_d for each phosphonate.[70] The K_i values for this series ranged from 1700 μM to 0.47 μM, spanning about four orders of magnitude. The order of increasing affinity of the phosphonates to 17E8 mirrors that of the catalytic specificity of the corresponding substrates. The energetic changes, $\Delta\Delta G_b$, reflected by the K_i values for the side-chain variations are similar to those for the k_{cat}/K_M values for the corresponding substrates.

Two phosphonates (**1p** and **11p**) were used to probe transition-state binding interactions upon complete removal of the side-chain. The corresponding substrates are not cleaved by the antibody. The K_i values of **1p** and **11p** are 1.7 mM ($\Delta\Delta G_b$ = 4.8

kcal/mol) and 53 μM (2.8 kcal/mol), respectively (Table 3.2). **1p** is an obvious candidate because, like the rest of the homologous series, it serves as a probe for the methylene•pocket interactions without changing other substituents on the molecule. However, the absence of a substituent on the α-carbon introduces the additional complexity of conformational freedom. Thus, the $\Delta\Delta G_b$ for **1p** reflects both the lack of side-chain•pocket interactions and the newly introduced rotational entropic requirement for binding the phosphonate.[14,15] **11p** also serves as a probe for investigating the effects of removing the side-chain. In this molecule, extra conformational freedom has not been introduced due to the degenerate conformers upon rotation about the α-C-P bond; however, the interactions between the n-formyl group and the protein are lost. Although these molecules were used to investigate the same problem, they have very different binding affinities. The $\Delta\Delta G_b$ values (relative to **5p**) nevertheless indicate that the side-chain is very important for phosphonate binding. The anomalous tight binding of **11p** could be a result of restriction of conformation due to the bond deletion, the removal of an unfavorable interaction between 17E8 and the n-formyl group, or of changes in the solvation properties of the molecule.

Branched series. We used substrates that were branched at different positions to determine steric and geometric restrictions that govern the interactions between the substrate side-chain and the recognition pocket. The kinetic values for these substrates are shown in Table 3.1. The γ-branched leucine ester (**11**) was a substrate for the antibody, whereas the α- (**8**) and β-branched (**9, 10**) substrates were not hydrolyzed by the antibody. The k_{cat} value of 2.1 s^{-1} for the leucine substrate (**11**) was similar to that of its linear counterpart **5**, whereas the K_M value is 10-fold higher (1.6 mM) resulting in a decreased k_{cat}/K_M (**11** compared to **5**). The presence of high concentrations of **9** (4 mM) and **10** (2 mM) approximately doubled the K_M value of **5** (relative to the value in their absence-data not shown) with no change in k_{cat}. These results yield the approximate K_i values of 4 mM for **9** and **10**. The presence of a high concentration of **8** did not change the K_M (or k_{cat}) value of **5**.

The K_i values of phosphonates that contain branched side-chains (**7p-10p**) were also obtained (Table 3.2). As with the homologous phosphonate series, these were found to be competitive inhibitors of the catalyzed reaction. Phosphonate **9p**, which corresponds to the γ-branched substrate **11** had a K_i value of

18 μM ($\Delta\Delta G_b$ = 2.2 kcal/mol). The β-branched phosphonate, **7p** is a respectable binder to the antibody binding site with a K_i value of 68 μM, whereas the corresponding substrate **9** is not hydrolyzed by 17E8. Its K_i value is similar to that of **2p**, whose corresponding substrate was cleaved by the antibody. We did not use a substrate that corresponded to phosphonate **10p,** but this molecule was of interest because it contained a bulky side-chain which would presumably require large structural changes in the recognition pocket for binding. The K_i of 1.1 mM is much larger than those in the homologous series. The energetic changes for binding these phosphonates, **7p** and **10p,** relative to the phosphonate **5p** are 2.4 kcal/mol and 4.0 kcal/mol respectively.

Figure 3.5 Bound side-chain conformation. (left) Phosphonate hapten shown in bound conformation. (right) Newman projection of n-butyl side-chain (Cβ-Cε). Hapten side-chain dihedral angle in **A** high energy eclipsed conformation and **B** low energy anti conformation.
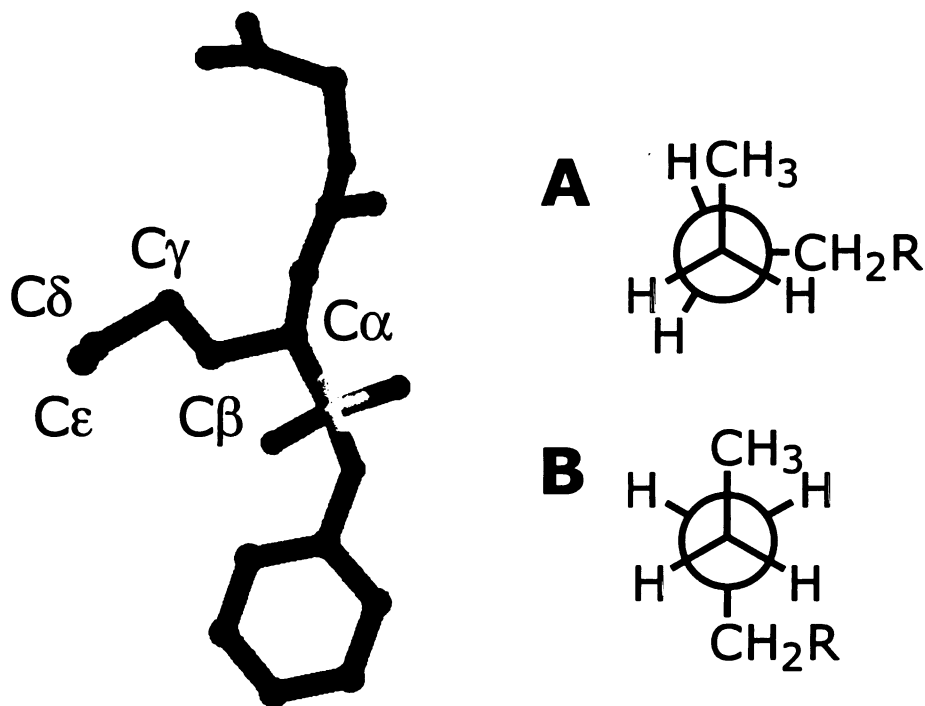
Conformationally restricted substrate series. The conformationally restricted series was used to investigate the effects of side-chain conformation on catalytic activity. The crystal structure of the 17E8•hapten complex suggests the binding of a high energy hapten side-chain rotamer conformation (resembling the conformer in Figure 3.5a) about the dihedral defined by the δ and γ carbons (Figure 3.5). The substrate containing the side-chain

with the cis double bond **13** was an active substrate whereas that containing the trans double bond **12** was not hydrolyzed (Table 3.1). There is a small decrease in the k_{cat} value of **13**, relative to that of the linear substrate **5**, (2.1 s^{-1} to 1.4 s^{-1}) and essentially no change in K_M (0.18 mM to 0.21 mM); the k_{cat}/K_M value was decreased only two fold (12,000 $M^{-1}s^{-1}$ to 6800 $M^{-1}s^{-1}$). The presence of a high concentration of **12** (2.7 mM) approximately tripled the K_M value of **5** (data not shown) with no change in k_{cat}. This result yields an approximate K_i of about 1.6 mM for **12**. The substrate with the alkynyl side-chain, **14**, was also processed by the antibody. Its k_{cat} and K_M values are 1.3-fold and 10-fold higher than the parent substrate **5**, respectively. The increased k_{cat} may be solely due to an electronic effect, since the buffer catalyzed reaction of **14** is increased over that of **5** to the same extent.

Table 3.1 Steady-state kinetic analysis of transition-state binding of the homologous, branched, and conformationally restricted series. All reactions were performed in 50 mM borate, 150 mM NaCl (pH 8.70) at 24.5 ± 1.0°C. The kinetic constants were determined from saturation plots of initial rates versus substrate concentration. Substrate concentrations used are listed in Experimental Section. The errors shown were obtained from calculated fits (KaleidaGraph-Synergy Software) of the data to the Michaelis-Menton equation. The errors in the k_{cat}/K_M values were from the propagation of the fitted k_{cat} and K_M errors. All of the catalyzed reactions were inhibited to background levels with saturating concentrations of **5p** (>25 μM). The $\Delta\Delta G_b$ values were calculated with the equation - $RTln[(k_{cat}/K_M)_X/(k_{cat}/K_M)_5]$ where R is the gas constant and T is the absolute temperature. X corresponds to a substrate to which **5** is being compared. The detection limit that has been estimated for the 17E8 reaction at pH 8.70 is approximately 5-10 M^{-1} s^{-1} for k_{cat}/K_M. This estimate is based on the lowest k_{cat} value detected (**3**) and the highest substrate concentration used 44 mM (**1**). We believe this to represent an lower detection limit as the k_{cat} value for (**3**) could be obtained easily and reproducibly. [a] This substrate was determined by ^{1}H NMR to contain a 50:50 mixture of the cis and trans isomers. The values in brackets are corrected for the actual concentration of the cis isomer. The trans isomer was shown to be inactive as a substrate.

Substrates	k_{cat} (s^{-1})	K_M (mM)	k_{cat}/K_M (s$^{-1} \bullet$M^{-1})	$\Delta\Delta G_b$ (kcal/mol)
Homologous Series				
1	no catalysis	-	-	-
2	1.0 ± 0.1	3.4 ± 0.4	290 ± 40	+ 2.2
3	0.37 ± 0.03	2.1 ± 0.5	180 ± 180	+ 2.5
4	1.4 ± 0.1	0.32 ± 0.04	4500 ± 60	+ 0.6
5	2.1 ± 0.1	0.18 ± 0.03	12000 ± 1400	+ 0.0
6	1.3 ± 0.1	0.88 ± 0.12	1500 ± 20	+ 1.2
7	no catalysis	-	-	-
Branched Series				
8	no catalysis	-	-	-
9	no catalysis	-	-	-
10	no catalysis	-	-	-
11	2.1 ± 0.1	1.6 ± 0.2	1300 ± 200	+ 1.3
Conformationally Restricted Series				
12	no catalysis	-	-	-
13[a]	1.4 ± 0.1	0.42 ± 0.07 [0.21 ± 0.04]	3400 ± 700 [6800 ± 1400]	+ 0.7 [+ 0.3]
14	2.8 ± 0.1	1.5 ± 0.1	1900 ± 200	+ 1.1

Inhibitor	Ki (μM)	$\Delta\Delta G_b$ (kcal/mol)
Homologous Series		
1p	1700	+ 4.8
2p	56	+ 2.9
3p	30	+ 2.5
4p	1.2	+ 0.6
5p	0.47	+ 0.0
6p	5.3	+ 1.4
Branched Series		
7p	68	+ 2.9
8p	7.2	+ 1.6
9p	18	+ 2.2
10p	1100	+ 4.6
11p[a]	53	+ 2.8

Table 3.2 Inhibition constants of the phosphonates. The constants were determined by plotting the slope values obtained from Lineweaver-Burk plots against inhibitor concentration and obtaining the intercept on the [inhibitor] axis which yields -K_i. The slope values are equal to $((K_M(1+[I]/K_i))/V_{max})$. The inhibitor concentrations used to obtain the K_I values in Experimental Section. The $\Delta\Delta G_b$ values were calculated from the equation - RTln[$(K_i)_x/(K_i)_{5p}$]. [a]The hydrolysis of phenyl acetate, the substrate that corresponds to the phosphonate, **11p**, is not catalyzed by 17E8 (data not shown).

Discussion

Nature has evolved many enzymes to use their specificity pockets efficiently. In addition to overall transition-state stabilization, these pockets have been experimentally shown to serve several specific roles for catalysis.[16-22] One role is to assist in the formation of a productive Michaelis complex with the correct substrates and to hinder the formation of incorrect substrates. A second role is to help position precisely the substrate reactive groups relative to those on other substrates or catalytic groups in the enzyme active site. A third role of specificity pockets is to assist in the preferential stabilization of transition-states and high energy intermediates. Although these are separate roles, nature has coupled them to optimize the efficient use of these interactions in catalysis of specific substrates.[20,21,23-26] In this study, we investigate how binding energy in a specificity pocket programmed by hapten design is used in the mechanism of an esterolytic antibody--a protein that has not been optimized by nature to perform catalysis.

Overall Transition-state Stabilization. Alternative substrate and transition-state analogs provide two different probes to investigate how 17E8's specificity pocket interactions affect the

energy of the transition-state. There is a good linear correlation between the $\ln(K_i)$ values of the phosphonates and the $\ln(k_{cat}/K_M)$ values of the corresponding substrates indicating the presence of
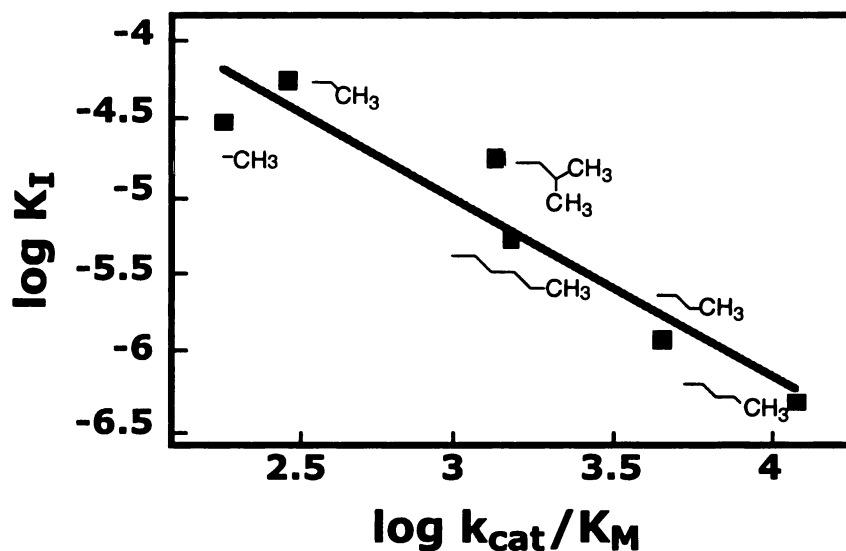
Figure 3.6 Transition state analog binding versus catalytic efficiency. ln K_i vs ln k_{cat}/K_M (slope = -1.13 ± 0.17 R=0.95). The data were fit with the KaleidaGraph curve fitting program (data taken from tables 3.1 and 3.2).

similar binding interactions between 17E8 and both the phosphonate inhibitors and the transition-states of the catalyzed reactions (Figure 3.6), suggesting that the inhibitors are good approximations of the transition-state.[26,27] The analogs contain sufficiently different side-chains, thus the correlation implies that the free-energy modulation of the transition-state complexes is a result

86

of changes in the side-chain•pocket interactions and not a result of changes in the catalytic mechanism with the different substrates.

The 17E8 specificity profile (as defined by the k_{cat}/K_M values for the different substrates) resembles that of natural enzymes that contain similar specificity pockets (e.g. chymotrypsin and methionyl-tRNA synthetase).[10,28-30] Filling the pocket results in higher catalytic activities and overfilling the pocket is detrimental to catalysis. This result is gratifying as this is the first catalytic antibody specificity pocket to be systematically studied. However, the two orders of magnitude range spanned by the substrates' k_{cat}/K_M values is small compared to those of similar substrates with chymotrypsin (four orders of magnitude) and methionyl-tRNA synthetase (seven orders of magnitude). Interestingly, the range of K_i values spanned in the 17E8 system is comparable to ranges seen with thermolysin and α-lytic protease.[19,31]

The parameters that govern specificity with 17E8 are also similar to those that dictate specificity in enzymatic systems, i.e. substrate side-chain size, shape, and geometry. The importance of size is best exemplified by the homologous series results, which indicate that there is an optimal length for a linear side-chain of four carbons. The addition or subtraction of methylene groups to this optimal side-chain results in a loss of transition-state stabilization.

The results with the branched substrates suggest that a linear side-chain structure is not required, but only the γ-branching geometry is allowed. This tolerance for only certain side-chain branching is also observed with several serine proteases as γ-branching is allowed and β-branching is very detrimental.[32,33]

A strict conformational requirement to form catalytically productive side-chain•pocket interactions is illustrated by the results from the conformationally restricted series in which the side-chain with the cis double bond (13) was a substrate and the side-chain with the trans double bond (12) was not. The torsion angle (Cβ-Cε) measured from the refined crystallographic coordinates is approximately 124° (Figure 3.5). The lowest energy conformation for this torsion angle is 180° (Figure 3.5b).[34,35] However, in crystallographic models, dihedral angles are difficult to define unambiguously within less than about 20°, especially in cases where the dihedral in question extends beyond the Cβ-Cγ bond.[36-38] The kinetic results suggest that the bound conformer of the 4-carbon side-chain of 5, resembles a high energy rotamer more closely mimicked by the side-chain of 13 and that the conformer mimicked by 12 is one that cannot bind to the antibody.

However, the energetic cost needed for the antibody to constrain the side-chain is not realized with the fixed rotamer mimic (**13**). This conformer is about 3.5 kcal/mol higher in energy than the staggered, low-energy conformer. Thus structurally constraining the side-chain should allow for this energy to be expressed in greater transition-state stabilization. The decrease in activity (Table 3.1) for **13** compared to **5** is most likely a result of the fact that the cis isomer does not resemble the bound rotamer precisely due to changes in the hybridization at the δ and γ carbons as well as differences in the dihedral angle between **13** and the actual bound rotamer.[34,35] The alkene side-chain is also less hydrophobic (than **5**), thus raising the desolvation cost for binding.[39,40] The fact that **14** was also a substrate suggests that the rotameric requirement is only important for the torsion angle defined by carbons Cβ-Cϵ.

Another parameter that has been shown to affect specificity in analogous enzyme systems is side-chain hydrophobicity. The $\log(K_i)$ and $\log(k_{cat}/K_M)$ values of the phosphonates and substrates correlate to the hydrophobicity parameter, π (Figure 3.7, see legend for definition of π) which suggests that the hydrophobic effect may provide a large contribution to transition-state binding. This result

is supported by the crystal structure of the 17E8•**5p** complex as the majority of atoms within 5Å of the side-chain carbons are from aliphatic and aromatic amino acid residues (see Figure 3.1A).**[41]** In studies with chymotrypsin, the log(k_{cat}/K_M) values of a series of substrates similar to ours correlated linearly to π as did those of another serine protease, subtilisin, which shares a similar specificity to chymotrypsin.**[28,29,42]** The slopes of the log(k_{cat}/K_M) vs hydrophobicity obtained from these enzymatic systems are larger than those obtained from 17E8.

17E8's active site apparent hydrophobicity results in an average free-energy contribution to transition-state stabilization per methylene group of about 0.7 kcal/mol. This value is essentially the same as the 0.5 kcal/mol value obtained from experiments in which small molecules were partitioned between aqueous and organic phase.**[43,44]** The negligible difference between the two values does not reflect the expected more favorable methylene•pocket interactions in the protein•ligand complexes compared to methylene•organic solvent interactions and the advantage of having a preformed pocket.**[4,45]** The $\Delta\Delta G_b$ per methylene group is also significantly smaller than the corresponding values in natural enzymes that contain similar side-chain recognition pockets that have evolved to form efficient binding interactions.**[4-**

90

6,46] For the enzymatic systems, the $\Delta\Delta G_b$ per methylene group

determined from substrate homologous series experiments range

from 1.5 kcal/mol to 3.5 kcal/mol. The smaller average value for

$\Delta\Delta G_b$ per methylene group indicates that 17E8 does not use binding

interactions as efficiently as an evolved enzyme that contains a

similar amino acid side-chain recognition pocket.

Figure 3.7 Hydrophobicity of the substrate and phosphonate side-chains versus the substrate steady-state kinetic constants and phosphonate inhibition constants. The parameter, π, is derived from the equation: log (P/P_o), where (P_o) is the ratio of the solubility of the parent compound (H-X) in an organic phase to that in the aqueous phase, and (P) is that of a compound on which the H- substituent has been exchanged for -R, to give R-X.[39, 40] **A.** In k_{cat}/K_M (slope = 1.1 ± 0.4, R=0.87) **B.** In K_i (slope = -1.4 ± 0.2, R=0.98) **C.** In K_M (slope -0.82 ± 0.20, R=0.93). The substrates **6** and **11** (and phosphonates **6p** and **11p**) were not included in the correlations because we believe that these molecules could not be accommodated without changes in pocket structure or binding mode making the analysis of these compounds ambiguous.
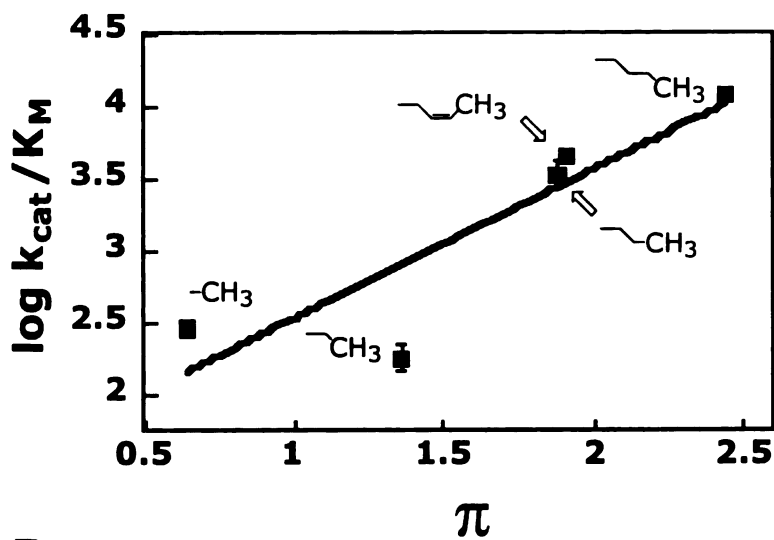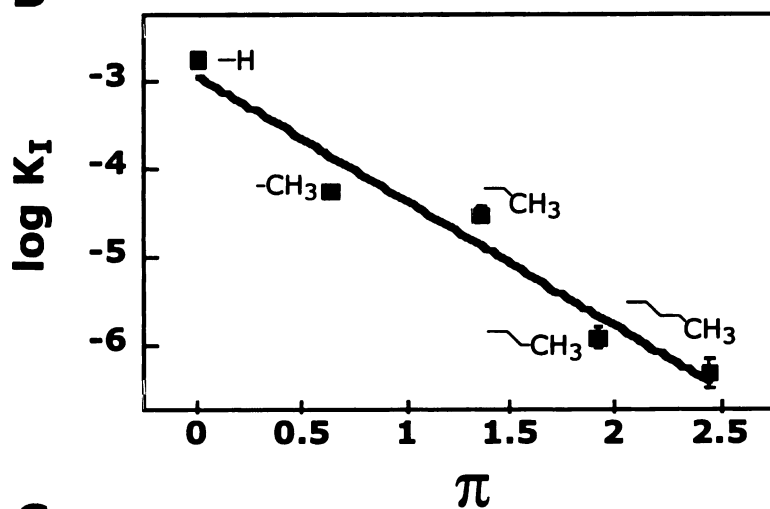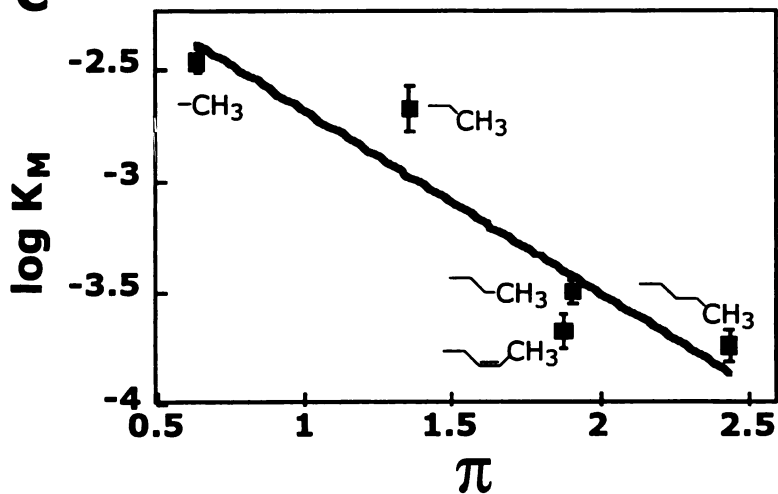
The P1 side-chain is completely buried upon the formation of the transition-state in serine proteases.[4,20,47,48] In contrast, partial solvent accessibility of the hapten side-chain is clearly
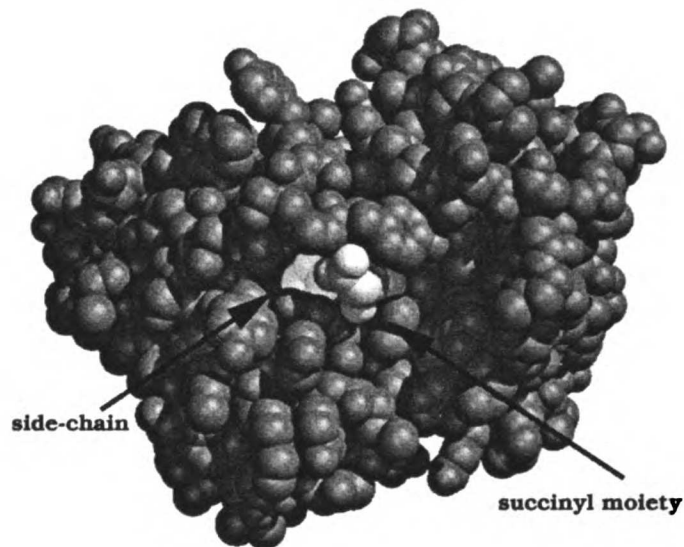
Figure 3.8 The top-view of a space-filling model of the 17E8 (black)•**5p** (light and dark-grey) complex. The model was generated with the MIDAS program.[13]

evident in the structure of the 17E8•hapten complex (Figures 3.2b and 3.8). It has been shown that the partial solvent accessibility of methylene groups in hydrophobic cores results in a reduced contribution to protein stability compared to those that are contained in completely buried cores.[49,50] The reduced contribution results from a reduction in the hydrophobic effect and the number of packing interactions. An extension of this can

93

similarly be drawn to the carbons in the side-chain of **5p** and most likely contributes to the apparent unoptimized nature of the 17E8 recogniton pocket.

Formation of the Michaelis Complex. 17E8 does use the free-energy from the side-chain•pocket interactions to stabilize the Michaelis complex. This use of binding energy is especially apparent for the homologous series of substrates in which the deletion of each methylene group from **5** (to **2**) results in an increase in K_M. As with the transition-state, side-chain size, geometry, conformation, and hydrophobicity (Figure 3.7) affect the free-energy of the 17E8 Michaelis complex, lending further support for the participation of the pocket for substrate binding. The K_M increase for the substrates **6**, **11**, and **14** further demonstrates this sensitivity.

The lack of detectable catalysis for **1**, **7-10**, and **12** does not rigorously prove that the substrates cannot form ground state Michaelis-type complexes with 17E8. To estimate the free-energies of their Michaelis-type complexes, the approximate K_i values of these compounds were obtained. The free-energies for the 17E8 complexes with **9**, **10**, and **12** are 1.4 to 2 kcal/mol greater than 17E8•**5** complex. The K_i values for **1**, **7**, and **8** could not be obtained because of the solubility limits of the compounds; thus, the free energies corresponding to the K_i values of these compounds

must be even greater than those determined. These results lend

further support to the side-chain•pocket interactions being

important for the free-energy of the Michaelis complex.

Destabilizing interactions are introduced in the case of the long (**7**)

and branched (**8-10**) substrates, whereas many of the favorable

interactions are removed with the substrate **1**.

Alignment of catalytic groups. The side-chain•pocket

interactions are used to assist in the alignment of the oxyanionic

intermediate to the stabilizing cationic center on 17E8.

Interestingly, the results from the homologous series indicate that

only one methyl group (substrate **2**) is needed for proper alignment

of the substrate to the 17E8 catalytic machinery. The k_{cat} values do

not increase significantly with the addition of larger side-chain

groups (**2** to **6**). The presence of very short (**1**), long (**7**), α and β-

branched (**8-10**), or conformationally incorrect (**12**) side-chains

results in a loss of detectable catalysis.

One explanation for the lack of catalysis with these substrates

may be the inability of the transition-states to interact productively

with the catalytic center. The high K_i values of the inactive

substrates cannot fully account for the lack of detectable catalysis

as there are active substrates that have similarly high K_M values. To

understand how substrates are discriminated against in the

95

transition-state, the binding of transition-state analogs (phosphonates) corresponding to the several inactive substrates was investigated. The weak binding of **1p,** and correspondingly, transition-state binding, in itself provides a rationale of why the corresponding substrate **1** was not hydrolyzed detectably by 17E8. The transition-state analog, **7p** is a respectable binder (K_d similar to **2p**), although the corresponding substrate **9** was not cleaved detectably by 17E8. The ability of this analog to bind tightly may be due to its potential to bury more hydrophobic surface area (80Å^2, **7p** vs 33Å^2, **2p**). This side-chain burial must be at the expense of forming efficient interactions with the oxyanion center as evident from the loss of catalysis and the similar binding constant to **2p**. The addition of a methylene unit to the side-chain of **7p** results in increased binding affinity (**8p,** 101 Å^2), supporting the idea that the tight binding of **7p** partly results from the burial of hydrophobic surface area. Nevertheless, the decreases in favorable free-energy of the complexes of **7p** and **8p** with 17E8 (+2.9 and +1.6 kcal/mol, respectively, relative to **5p**) indicate the stability of these complexes has somehow been compromised. The anomalous tight binding of transition-state analogs that correspond to substrates that are not turned over or slowly turned over has also been observed and structurally characterized for α-lytic protease.[19] The ability to

96

bury more hydrophobic surface area at the expense of several active site hydrogen bonds is postulated to be one of the reasons for the anomalous binding behavior and loss of catalysis. The prevalence of side-chain•pocket interactions in phosphonate, and presumably transition-state, binding is also demonstrated with **10p**.
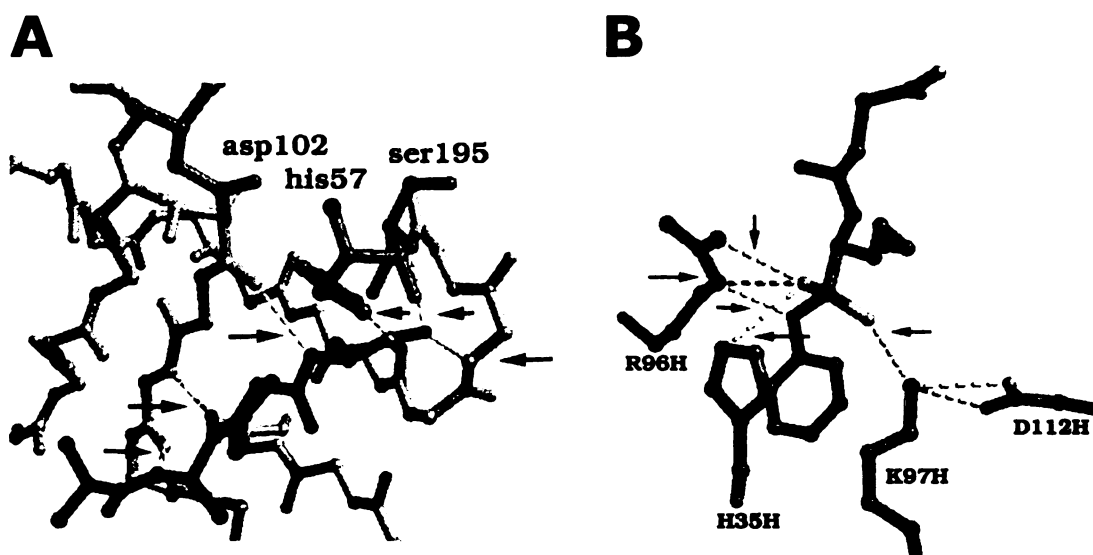
Figure 3.9 Active site interactions of serine proteases and 17E8. **A.** α-lytic protease complexed with methoxysuccinyl-A-A-P-boroAla.**[19] B.** 17E8•**5p** complex. Active site hydrogen bonds are indicated by the arrows. The figures were generated with the MIDAS program.**[13]**

In the serine protease systems, additional subsite binding, active site hydrogen bonds, and the oxyanion hole are used in addition to the interactions in the S1 pocket to obtain the large rate accelerations (Figure 3.9A).**[19-21,47,51,52]** Interestingly, this strategy is used by most proteases regardless of the overall tertiary

protein structure. The energy gained from the noncovalent interactions in the specificity pocket is a function of all of these components, some of which are remote from the specificity pocket.[4,17,23,48,53-56] By coupling the S1-P1 interactions to other machinery in the active site, the proteases have created a cooperative network that increases the apparent energy of S1-P1 interactions.[25] 17E8 does have a network of interactions that can be used in concert with side-chain•pocket interactions. The 17E8 active site contains a center for stabilizing the formation of an oxyanion, but it does not use additional subsite interactions to increase the apparent binding energies from the interactions with oxyanion hole (Figure 3.9b). 17E8 is also missing active site hydrogen bonds that serve as critical kinetic specificity determinants that assist in the more productive use of the side-chain pocket binding energy.[20,47,55]

Preferential Stabilization of the Transition-state. Although overall transition-state stabilization increases as methylene groups are added to the side-chains of substrates **1-5**, the addition of these units did not significantly increase the k_{cat} values indicating that the binding energies from the additional methylene•pocket interactions were not used differentially between binding the ground state Michaelis and the transition-state complexes. This

98

uniform use of binding energy is thought to be characteristic of an evolutionarily un-optimized catalyst.[57-59] There are natural enzymes that use much of the binding energy from side-chain•pocket interactions for substrate binding specificity and not transition-state discrimination.[10,30,46,60] However, in these systems, kinetic specificity determinants (binding interactions that discriminate at the k_{cat} level only) have also been identified-- suggesting that the uniform use of energy from side-chain•specificity pocket interactions is permissible as long as there are other sources of differential binding.[10,30,46,60]

Because they are raised against transition-state analogs, and in most cases have been selected for tight binding to these analogs, catalytic antibodies are usually designed to influence only the $E + S^{\ddagger} \leftrightarrow (E \bullet S)^{\ddagger}$ equilibrium-not the equilibria $E + S \leftrightarrow E \bullet S$ or $E \bullet S \leftrightarrow (E \bullet S)^{\ddagger}$. These generation techniques leave no *a priori* reason for one to expect these proteins to enforce the discriminatory use of remote binding energy between antibody bound species. In fact, the general problem of product inhibition with catalytic antibodies suggests that uniform binding of common moieties on substrates, high energy intermediates, and products may be prevalent.[1,61] This is in contrast to enzymes which have evolved to use binding interactions selectively in their mechanisms and not at only one

location on the reaction coordinate.[5,62-65] Indeed, a more optimized 17E8 might select against Michaelis complexes that use too much side-chain binding energy. In the 17E8 system, the use of the methylene•pocket interactions to increase k_{cat}/K_M and not to increase k_{cat} makes this clearly a case in which ground state interactions are inhibitory to increasing the turnover number.[27]

Conclusions

In this study, we find that 17E8 does use the binding energy between the n-butyl side-chain and its recognition pocket to stabilize the bound transition-state indicating that binding interactions that are remote from the catalytic center can be programmed by hapten design. We also find that this pocket has some characteristics similar to those contained in evolved enzymes, including the mechanisms and molecular forces used for specificity. One side-chain methyl group is sufficient to ensure high turnover and presumably alignment of the carbonyl group on the ester substrate with the oxyanion hole. Additional methylene groups increase the turnover number almost negligibly but contribute substantially to the formation of the Michaelis complex and catalytic efficiency (k_{cat}/K_M) indicating that 17E8 uses these additional side-chain•pocket interactions uniformly in the Michaelis and transition-state complexes. This result substantiates the need for selection techniques other than transition-state analog binding in catalytic antibody screening procedures. Optimistically, this suggests that this selection technique may provide a good starting point for a catalyst and that further protein engineering is needed for optimization. The 17E8 side-chain•pocket interactions are used less

efficiently than those in enzymes as the apparent binding energy gained from the methylene•pocket interactions is significantly smaller in the 17E8 system than is observed in enzymes. Analysis of the 17E8•**5p** complex reveals several possible sources of this reduced apparent binding energy, including incomplete burial of the side-chain upon transition-state formation and the absence of other binding interactions that could be coupled to the side-chain•pocket to preclude wasteful side-chain binding. These features provide at least some insight into how 17E8 might be engineered.

Experimental Section

Synthesis

General Methods and Reagents. Reactions requiring anhydrous conditions were carried out in flame-dried glassware under an atmosphere of argon. Anhydrous solvents were purchased from Aldrich. Chromatography solvents were purchased from Fisher Corp. and were used as received. Reagents were purchased either from Sigma or Aldrich and used as received unless noted otherwise. ^1H NMR and ^{13}C NMR were recorded on a General Electric 300-MHz instrument. The NMR samples were prepared in 5-mm tubes, and the chemical shifts are reported in parts per million (δ) relative to the standards TMS for samples in CDCl$_3$ and TSP (3-(trimethylsilyl)-1-propanesulfonic acid sodium salt) for samples in D$_2$O. Flash chromatography was performed with Merck silica gel 60 (230-400 mesh). Ion exchange chromatography was performed with diethylaminoethyl (DEAE) Sephadex A-25 (anion exchange) and Dowex 50WX2-100 (cation exchange). The resins were washed and prepared according to manufacturers' recommendations.

Synthesis of n-formylated Amino Acid Ester Substrates, 1-14.

Formylation of substrates. The amino acids were formylated in the manner as decribed by Sheehan and Yang.[66] A general procedure for the preparation of the formylated amino acids is as follows: Acetic anhydride (33 mL, 325 mmol) was added dropwise to a solution of d-, l- norleucine (1.3 g, 10 mmol) dissolved in 100 mL of formic acid. After the addition of acetic anhydride, the solution was stirred at room temperature for 3 hours. The mixture was then concentrated by rotary evaporation to yield a white powder. This crude material was carried on directly to the esterification step.

Preparation of phenyl esters. The phenyl esters were prepared from the formylated amino acids as described by Castro *et al*.[67] A general procedure for the esterification of the formylated amino acids is as follows: racemic n-formyl-norleucine (1 g, 6 mmol), phenol (0.6 g, 6 mmol), triethylamine (1.2g, 12 mmol), and HBTU (2-(1H-Benzotriazole-1-yl)-1, 1, 3, 3-tetramethyluronium hexafluorophosphate) (2.3 g, 6 mmol) were dissolved in 50 mL of dichloromethane. The mixture is stirred at room temperature for 3 hours. Saturated aqueous NaCl (50 mL) was added to the solution. The solution was then extracted with ethyl acetate (3 x 30 mL). The organic phase was then washed with 2N HCl (3 x 30 mL), saturated

NaHCO$_3$ (3 x 30 mL), and saturated NaCl (2 x 50 mL). The organic phase was then dried with NaSO$_4$ and the solvent removed by rotary evaporation to yield a yellow oil, which was chromatographed. Elution using a gradient of (1:5 to 1:1) ethyl acetate:hexanes afforded **5** (1.2 g, 86% yield) as a colorless oil.

n-formyl-glycine phenyl ester (1) ^{1}HNMR (300 MHz, CDCl$_3$) δ 8.32 (s, 1H), 7.42 (t, J = 7.5Hz, 2H), 7.25 (t, J = 7.8 Hz, 2H), 7.12 (d, J = 7.8Hz, 1H), 6.29 (br s, 1H), 4.39 (d, J = 5.4 Hz, 2H); ^{13}CNMR δ 161.2, 129.6, 126.4, 121.2, 40.1; MS (EI): 180.1 (MH$^+$), 94.0, 86.0, 65.0, 58.0; HRMS calcd for C$_9$H$_{10}$N$_1$O$_3$ 180.0661 found 180.0662.

n-formyl-alanine phenyl ester (2) Yield 0.73 g (88%) ^{1}HNMR (300 MHz, CDCl$_3$) δ 8.23 (s, 1H), 7.40 (t, J = 7.8 Hz, 2H), 2.23 (t, J = 7.5, 7.2 Hz, 1H), 7.10 (d, J = 8.1 Hz, 2H), 6.35 (br s, 1H), 4.93 (p, J = 7.2 Hz, 1H), 1.62 (d, J = 7.2 Hz, 3H); ^{13}C NMR δ 160.5, 129.5, 126.3, 121.2, 47.0, 18.4; MS (EI): 194.1(MH+), 165.1, 116.1, 100.0, 94.0, 82.9, 72.0, 65.0, 55.0; HRMS calcd for C$_{10}$H$_{21}$N$_1$O$_3$ 193.0739 found 193.0748.

n-formyl-α-amino butyric phenyl ester (3) Yield 0.64 g (80%)

(^{1}HNMR (300 MHz, CDCl$_3$) δ 8.28 (s, 1H), 7.40 (t, J = 7.8 Hz, 2H), 7.26 (t, J = 7.5, 6.9 Hz, 1H), 7.10 (d, J = 8.1 Hz, 2H), 6.29 (br s, 1H), 4.93 (q, J = 6.9 Hz), 2.19-2.05 (m, 1H), 1.97 (h, J = 7.2 Hz, 1H), 1.06 (t, J = 7.5 Hz); ^{13}C NMR δ 160.7, 129.6, 126.3, 121.2, 52.0, 25.7, 9.40; MS (EI): 207.1(M$^+$), 207.1, 179.1, 133.0, 114.1, 94.0, 86.1, 65.0, 58.1; HRMS calcd for C$_{11}$H$_{14}$N$_1$O$_3$ (MH$^+$) 208.0974 found 208.0970.

n-formyl-norvaline phenyl ester (4) Yield 0.69g (90%) ^{1}HNMR (300 MHz, CDCl$_3$) δ 8.26 (s, 1H), 7.39 (t, J = 7.5 Hz, 2H), 7.26 (t, J = 7.5, 7.2 Hz, 1H), 7.06 (d, J = 8.1 Hz), 6.30 (br d, J = 6.0 Hz, 1H), 4.95 (dt, J = 7.5, 5.7 Hz, 1H), 2.09-1.97 (m, 1H), 1.87 (p, J = 6.9-7.5 Hz, 1H), 1.50 (sept, J = 7.2, 7.5 Hz, 2H), 1.01 (t, J = 7.2 Hz, 3H); ^{13}C NMR δ 160.7, 129.5, 126.3, 121.2, 50.8, 34.5, 18.5, 13.6; MS (EI): 222.1 (MH$^+$), 128.1, 100.1, 94.0, 82.9, 65.0, 58.0; HRMS calcd for C$_{12}$H$_{16}$N$_1$O$_3$ 222.1130 (MH$^+$) found 222.1133.

n-formyl-norleucine phenyl ester (5) Yield 1.2g (86%) ^{1}HNMR (300 MHz, CDCl$_3$) δ 8.27 (s, 1H), 7.40 (t, J = 7.8 Hz, 2H), 7.26 (t, J = 7.2, 7.5 Hz, 1H), 7.09 (d, J = 7.8 Hz, 2H), 6.21 (br d, J = 6.0 Hz, 1H), 4.95 (dt, J = 7.5, 5.7 Hz, 1H), 2.16 - 2.00 (m, 1H), 1.90 (m, 1H), 1.42 (m,

4H), 0.94 (t, J = 6.9, 6.6 Hz, 3H); ^{13}C NMR δ 160.7, 129.6, 126.3,

121.2, 51.0, 32.2, 27.2, 22.3, 13.8; MS (EI): 236.1(MH$^+$), 207.1,

142.1, 114.1, 94.0, 82.9, 69.1, 58.0; HRMS calcd for $C_{13}H_{18}N_1O_3$

236.1287 (MH$^+$) found 236.1296.

n-formyl-α-amino heptanoic acid phenyl ester (6) The α-amino

heptanoic acid was synthesized by the method as described by

O'Donnel *et al* using bromopentane.[68] Yield 0.22g (88%) ^{1}HNMR

(300 MHz, CDCl$_3$) δ 8.27 (s, 1H), 7.40 (t, J = 7.5 Hz, 2H), 7.26 (t, J =

7.5, 7.2 Hz, 1H), 7.09 (d, J = 8.1, 2H), 6.19 (d, J = 7.2 Hz, 1H), 4.95

(dt, J = 7.5, 5.4 Hz, 1H), 2.05 (m, 1H), 1.88 (m, 1H), 1.49,1.30 (m,

8H), 0.89 (t, J = 6.6 Hz, 3H); ^{13}CNMR δ 160.5, 129.5, 126.3, 121.2,

51.0, 32.5, 31.3, 24.8, 22.4, 13.9; MS (EI): 250.1 (MH$^+$), 156.1,

128.1, 94.0, 83.1, 58.0; HRMS calcd for $C_{14}H_{20}N_1O_3$ (MH$^+$) 250.1443

found 250.1440.

n-formyl-α-amino octanoic acid phenyl ester (7) Yield 0.62g

(88%)^{1}HNMR (300 MHz, CDCl$_3$) δ 8.33 (s, 1H), 7.42 (t, J = 7.5 Hz,

2H), 7.26 (t, J =7.2 Hz, 1H), 7.10 (d, 7.8 Hz, 2H), 6.19 (br d, J = 6.3

Hz, 1H), 4.9 (dt, J = 6.9, 6.3 Hz, 1H), 2.05 (m, Hz, 1H), 1.87 (m, 1H),

1.41, 1.31 (m, 8H), 0.90 (t, J = 5.7 Hz, 3H); ^{13}C NMR δ 160.6, 129.6,

126.3, 121.2, 51.0, 32.5, 31.5, 28.8, 25.1, 22.5, 14.0; MS(EI): 264.2

(MH$^+$), 235.2, 170.1, 142.1, 114.1, 94.0, 77.0; HRMS calcd for

$C_{15}H_{22}NO_3$ (MH$^+$) 264.1600 found 264.1598.

n-formyl-α-amino isobutyric acid phenyl ester (8) Yield 0.47g

(60%) ^{1}HNMR (300 MHz, CDCl$_3$) δ 8.16 (s, 1H), 7.39 (t, J = 7.5, 7.8,

2H), 7.24 (t, J = 6.9, 7.2, 1H), 7.10 (d, J = 7.8, 2H), 6.25 (br s, 1H),

1.75 (s, 6H); ^{13}C NMR δ 160.5, 129.5, 126.0, 121.3, 56.2, 24.8 MS

(EI): 208.1 (MH$^+$), 179.1, 147.0, 114.1, 94.0, 86.1, 65.0, 58.1; HRMS

calcd for $C_{11}H_{13}NO_3$ (MH$^+$) 208.0974 found 208.0983.

n-formyl-valine phenyl ester (9) Yield 0.58g (75%) ^{1}HNMR (300

MHz, CDCl$_3$) δ 8.38 (s, 1H), 7.46 (t, J = 7.5, 7.8 Hz, 2H), 7.32 (t, J =

6.6 Hz, 1H), 7.15 (d, 7.8 Hz, 2H), 6.21 (br d, J = 6.0 Hz, 1H), 4.99

(dd, J = 9.0, 4.5 Hz, 1H), 2.46 (h, J = 6.9 Hz, 1H), 1.15, 1.12 (d, J =

6.9 Hz, d J = 7.2 Hz, 6H); ^{13}C NMR δ 170.3, 160.9, 150.3, 129.6,

126.3, 121.3, 55.7, 31.4, 19.0, 17.7; MS (EI): 222.2(MH$^+$), 128.1,

100.1, 94.0, 85.0, 72.1, 65.0; HRMS calcd for (MH$^+$) 222.1130 found

222.1135.

n-formyl-isoleucine phenyl ester (10) Yield 0.66g (89%) ^{1}HNMR

(300 MHz, CDCl$_3$) δ 8.24 (s, 1H), 7.39 (t, J = 7.5, 7.8 Hz, 2H), 7.25 (t,

J = 7.2 Hz, 1H), 7.10 (d, J = 8.1 Hz, 2H), 6.30 (br d, J = 7.5 Hz, 1H),

4.99 - 4.92 (m, 1H), 1.90 - 1.67 (m, 3H), 1.02 (d, J = 5.7, 6H); ^{13}C

NMR δ 171.3, 160.8, 129.5, 126.2, 121.2, 49.5, 41.5, 24.9, 22.8,

21.9; MS (EI): 236.1(MH$^+$), 207.1, 149.0, 142.1, 133.0, 114.1, 94.0

86.1, 77.0, 69.1; HRMS calcd for (MH$^+$) 236.1290 found 236.1295.

n-formyl-leucine phenyl ester (11) Yield 0.52g (75%) ^{1}HNMR (300

MHz, CDCl$_3$) δ 8.32, 8.30 (s, 1H), 7.40 (t, J = 7.5, 7.8 Hz, 2H), 7.26 (t,

J = 7.2, 7.5 Hz, 1H), 7.09 (d, J = 8.1 Hz, 2H), 6.21, 6.15 (br d, br d, J

= 6.9 Hz, 1H), 5.07, 4.96 (dd, dd, J = 9.0, 3.6 Hz, J = 8.7, 4.5 Hz,

1H), 2.17 (m, 1H), 1.57 (m, 1H), 1.34 (m, 1H), 1.06, 1.00 (m, 6H); ^{13}C

NMR δ 160.9, 160.7, 129.6, 126.3, 121.2, 55.1, 53.9, 38.2, 37.8,

15.6, 14.6, 11.6, 11.7 MS (EI): 236.1 (MH$^+$), 142.1, 114.1, 94.0,

82.9, 69.1, 58.0; HRMS calcd for (MH$^+$) 236.1287 found 236.1290.

n-formyl-*trans*-crotyl glycine phenyl ester (12) Yield 0.66g (89%)

^{1}HNMR (300 MHz, CDCl$_3$) δ 8.26 (s, 1H), 7.39 (t, J = 7.5, 7.8 Hz, 2H),

7.28 (t, J = 6.9, 7.8 Hz, 1H), 7.08 (d, J = 7.8 Hz, 2H), 6.17 (br s, 1H),

5.67 (d qt, J = 15.0, 6.3Hz, 1H), 5.42 (dt, J = 15.0, 6.9 Hz, 1H), 4.96

(dt, J = 7.8, 5.7 Hz, 1H), 2.71 (t, J = 6.3 Hz, 2H), 1.72 (d, J = 6.3 Hz,

3H); ^{13}C NMR δ 160.4, 130.9, 126.3, 123.8, 121.2, 50.8, 35.3, 18.0;

MS (EI): 233.1 (M$^+$) 140.1, 112.1, 94.0, 82.9, 67.1; HRMS calcd for

$C_{13}H_{15}N_1O_3$ (M$^+$) 233.1049 found 233.1052.

n-formyl-*cis*-crotyl glycine phenyl ester (13) The α-amino-*cis*-4-

hexenoic acid was synthesized by the method as described by

O'Donnel *et al* using cis-crotyl bromide.[68] Yield 0.32g (85%)

^{1}HNMR (300 MHz, CDCl$_3$) δ 8.25 (s, 1H), 7.41 (t, J = 7.5, 7.8 Hz, 2H),

7.32 (t, J = 7.5 Hz, 1H), 7.20 (d, J = 7.8 Hz, 2H), 6.17 (br s, 1H), 5.70

(m, 1H), 5.43 (q, J = 7.5 Hz, 1H), 4.97 (m, 1H), 2.80 (m, 1H), 2.70 (t,

J = 6.6 Hz, 1H), 1.70 (d, J = 7.2 Hz, 1H); ^{13}C NMR δ 160.6, 129.5,

129.1, 126.2, 122.8, 121.2, 50.6, 29.5, 13.0; MS (EI): 234.1 (MH$^+$)

188.1, 154.1, 140.1, 112.1, 94.0, 84.1, 77.0, 67.1; HRMS calcd for

$C_{13}H_{15}NO_3$ (M$^+$) 234.1130 found 234.1129.

1-amino-*cis*-4-hexenoic acid ^{1}HNMR (300 MHz, CDCl$_3$) δ 5.80 (m,

1H), 5.40 (m, 1H), 3.80 (p, J = 6.3 Hz, 1H), 2.68 (m, 1H), 2.58 (t, J

=6.6 Hz, 1H), 1.70 (d, J =6.9Hz, 1H), 1.67 (d, J = 6.9 Hz, 1H); ^{13}CNMR

δ 174.0, 131.8, 130.0, 122.8, 121.9, 53.9, 54.0, 32.3, 27.5, 16.9,

11.9; MS (EI): 129.1(M$^+$), 129.1, 84.1, 74.1, 67.1, 55.1; HRMS calcd for $C_6H_{11}N_1O_2$ (M+) 129.0790 found 129.0794.

n-formyl-propargyl glycine phenyl ester (14) Yield 0.68g (88%)

^{1}HNMR (300 MHz, CDCl$_3$) δ 8.25 (s, 1H), 7.39 (t, J = 7.5 Hz, 2H), 7.26 (t, J = 7.2 Hz, 1H), 7.11 (d, J = 7.8 Hz, 2H), 6.84 (br s, 1H), 5.08 (dt, J = 7.8, 5.0 Hz, 1H), 2.96 (m, 2H), 2.80 (s, 1H); ^{13}C NMR δ 168.7, 160.7, 129.5, 126.4, 121.2, 72.2, 49.4, 38.5, 22.5; MS (EI): 235.2(M$^+$), 170.1, 142.1, 114.1, 94.0; HRMS calcd for $C_{13}H_{18}N_1O_3$ (MH$^+$) 236.1287 found 236.1291.
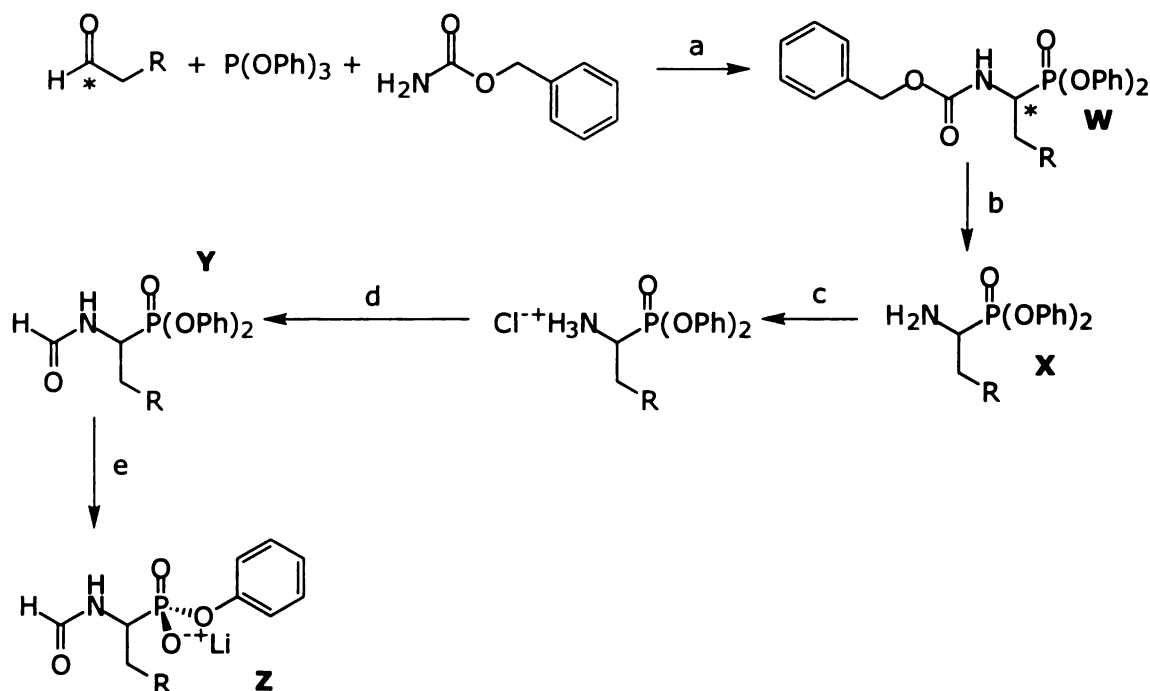
Figure 3.10 Phosphonate synthesis. (a) AcOH (b) 30% HBr/AcOH (c) HCl (aq) (d) EDC (1-(3-Dimethylaminopropyl)-3-ethylcarbodiimide hydrochloride), HCO_2H, **X** (as the hydrochloride), N-methylmorpholine, CH_2Cl_2) (e) NaOH (aq)

Synthesis of n-formylated phenyl phosphonates, 1p-10p

The phosphonates were prepared by the route similar to that described by Guo *et al.*[8] The use of aldehydes with different side-chains yielded the series. A general procedure for the preparation of the phosphonates is as follows: Triphenyl phosphite (10.0 g, 32 mmol), n-pentanal (4.0 g, 48.5 mmol), and benzyl carbamate (4.9 g, 32 mmol) were dissolved in 20 mL of glacial acetic acid. The solution was stirred at 50°C for 2 hours and then stirred at room

temperature for an additional 2 hours. The solution was then concentrated by rotary evaporation to yield an viscous, yellow liquid. The liquid was dissolved in 120 mL of methanol and left at 4°C overnight to yield white crystals (**W**) (9.7 g 65% yield).

The above condensation product (**W**) (5 g, 11 mmol) was dissolved in a solution of 30% HBr in acetic acid (5 mL), and stirred for 1.5 hours at room temperature. Water (100 mL) and ethyl ether (100 mL) were added to the reaction and the resulting mixture was stirred at room temperature for 10 min. Sodium hydroxide (10 M) was added until the aqueous phase reached pH 9. The organic phase was then washed twice with water (50 mL). The addition of 4M HCl (5 mL) resulted in the precipitation of diphenyl α-amino alkyl phosphonate (**X**-HCl) (3.5 g, 89% yield).

The amino hydrochloride salts (**X**-HCl) were formylated as described by Chen *et al.*[**69**] Briefly, EDC (1-(3-Dimethylaminopropyl)-3-ethylcarbodiimide hydrochloride) (2.1g, 11 mmol) was added to a solution of formic acid (1.0 g, 22 mmol) in dichloromethane (30 mL) at 0°C and stirred for 15 min. A solution containing the hydrochloride salt (2.0g, 6 mmol) and N-methylmorpholine (1.1 g, 11 mmol) in dichloromethane (30 mL) was added. The mixture was stirred at 0°C for 8 hours, then at 20 °C for 10 hours. The mixture was then washed with 1N HCl (2x 20 mL),

saturated $NaHCO_3$ (2x 20mL), and saturated NaCl (1x20mL). After drying the organic phase with $NaSO_4$, the solvent was removed by rotary evaporation to yield a yellow oil (**Y**) (1.5 g, 78% yield) which was carried on directly to the next step.

To a solution containing 4.5 mmol NaOH, water (10 mL), and dioxane (10 mL), diphenyl n-formyl alkyl phosphonate (1.5g, 4.3 mmol) from the previous step was dissolved and stirred at room temperature overnight. The reaction mixture was then washed with ethyl ether (10 mL), and the aqueous layer was dried by rotary evaporation. The remaining residue was dissolved in 5 mL of water, brought to pH 8.5 with 2N NaOH, and filtered through a 0.45 μm filter. The solution was chromatographed on a DEAE column by eluting with a linear gradient of 0 N to 0.5 N $(Et)_3N \cdot H_2CO_3$. The collected fractions were concentrated by rotary evaporation and redissolved in water (3mL). The product was converted to the lithium salt by cation exchange chromatography (Dowex-Li^+ form). The collected fractions were lyophilized, yielding **5p** (Li^+salt) (0.79 g, 63% yield (29% overall)) as a white powder (**Z**).

Phenyl [1-(1-N-Formylamino)alkyl]phosphonates

methyl (1p) Yield 0.38 g (25 %) ^1H NMR (300 MHz, D_2O) δ 8.10 (s, 1H), 7.39 (t, J = 7.8 Hz, 2H), 7.21 (t, J = 7.5 Hz, 1H), 7.16 (d, J = 7.8

Hz, 2H), 3.62 (d, J = 12.6 Hz, 2H); ^{13}CNMR δ 166.1 (d, 5.6 Hz), 132.0,

126.7, 123.0, 37.0 (d, J = 151.2 Hz), 17.8; LSIMS-MS(-) 214.1 m/z

(MH$^-$-HCl).

N-Cbz-aminomethyl phosphonic acid ^{1}H NMR (300 MHz, D$_2$O) δ 7.32

(m, 5H), 5.08 (s, 2H), 3.45 (d, J = 11.4 Hz, 2H); ^{13}CNMR δ 137.7,

129.5, 129.1, 128.8, 67.9, 39.3 (d, J = 151.5 Hz) MS (EI): 244.0 (M-

H)$^+$, 228.0, 197.1, 138.0, 108.1, 90.0, 79.1; HRMS calcd for

C$_9$H$_{12}$N$_1$O$_5$P$_1$ (M$^+$) 245.0453 found 245.0459.

diphenyl N-t-boc-aminomethyl phosphonate ^{1}H NMR (300 MHz,

CHCD$_3$) δ 7.18 (m, 5H), 7.06 (m, 10H), 4.97 (s, 2H), 3.82 (dd, J =

10.5, 6.0 Hz, 2H); ^{13}CNMR δ 129.8, 128.6, 128.3, 128.2, 125.5,

120.5, 67.5 MS (EI): 397.1 (M$^+$), 304.1, 289.1, 256.1, 233.0, 215.0,

184.1, 170.1, 140.0, 107.0, 91.1, 77.0; HRMS calcd for C$_{21}$H$_{20}$N$_1$O$_4$P$_1$

(M$^+$) 397.1079 found 397.1065.

ethyl (2p) Yield 0.27g (32%) ^{1}H NMR (300 MHz, D$_2$O) δ 8.05 (s, 1H),

7.38 (t, J = 7.8 Hz, 2H), 7.20 (t, J = 7.2 Hz, 1H), 7.15 (, J = 7.8 Hz,

2H), 4.47 (st, J =7.5 Hz, 1H), 1.55 (dd, J = 15.9, 7.2 Hz, 3H); ^{13}CNMR

δ 165.7 (d, 5.5 Hz), 132.2, 126.7, 123.2, 43.9 (d, J = 153.2 Hz), 17.8; LSIMS-MS(-) 228.2 m/z (MH$^-$-HCl).

propyl (3p) Yield 0.59 g (44%) ^{1}H NMR (300 MHz, D$_2$O) δ 8.16 (s, 1H), 7.39 (t, J = 7.5 Hz, 2H), 7.20 (t, J = 7.2 Hz, 1H), 7.18 (d, J =8.1 Hz, 2H), 4.15 (ddd, J =14.7, 7.8, 7.2 Hz, 1H), 1.96 (m, 1H), 1.64 (m, 1H), 0.96 (t, J = 7.2Hz); ^{13}CNMR δ 166.6 (d, 5.3 Hz), 132.3, 126.9, 123.4, 50.4 (d, J = 152.0 Hz) 25.5, 13.0; LSIMS-MS(-) 242.0 (MH$^-$-HCl).

butyl (4p) Yield 0.24 g (30%) ^{1}H NMR (300 MHz, D$_2$O) δ 8.16 (s, 1H), 7.41 (t, J = 7.5 Hz, 2H), 7.22 (t, J = 7.5 Hz, 1H), 7.15 (d, J =7.5 Hz, 2H), 4.28 (ddd, J =14.7, 8.4, 7.2 Hz, 1H), 1.87 (m., 1H), 1.71 (m, 1H), 1.50 (m, 1H), 1.36 (m, 1H), 0.98 (t, J =7.2 Hz, 3H); ^{13}CNMR δ 166.2 (d, 5.0 Hz), 132.2, 126.7, 123.2, 48.2 (d, J =152.3 Hz), 33.8, 21.4, 15.2 LSIMS-MS(-) 256.3 m/z (MH$^-$-HCl).

pentyl (5p) Yield 0.79 g (29%) ^{1}H NMR (300 MHz, D$_2$O) d 8.02 (s, 1H), 7.37 (t, J = 7.8 Hz, 2H), 7.18 (t, J = 6.3 Hz, 1H), 7.15 (d, J = 7.8 Hz, 2H), 4.22 (ddd, J = 12.0, 8.4, 7.2Hz, 1H), 1.91 (m, 1H), 1.65 (m, 1H), 1.31 (m, 4H), 0.98 (t, J = 6.0 Hz, 3H); ^{13}CNMR δ 166.2 (d, J = 5.1

Hz), 132.1, 126.7, 123.1, 48.4 (d, J =152.2 Hz), 31.3, 30.1 (d, J = 12.6 Hz), 23.9, 15.6; LSIMS-MS(-) 270.3 (MH$^-$-Li).

hexyl (6p) Yield 0.47g (44%) ^{1}H NMR (300 MHz, D$_2$O) δ 8.14 (s, 1H), 7.40 (t, J = 7.8 Hz, 2H), 7.21 (t, J = 7.5 Hz, 1H), 7.17 (d, J = 7.8 Hz, 2H), 4.35 (dd, J = 16.8, 10.5 Hz, 1H), 1.91(m, 1H), 1.66 (m, 1H), 1.44 (m, 1H), 1.10 (m, 5H), 0.87 (t, J = 7.2, 3H); ^{13}CNMR δ 164.1 (d, 4.2 Hz), 132.1, 126.6, 123.1, 48.4 (d, J = 152.8 Hz), 28.8, 27.5, 23.5, 20.2, 11.7 LSIMS-MS(-) LSIMS-MS(-) 284.1 m/z (MH$^-$-HCl).

2-methyl-propyl (7p) Yield 0.25g (27%) ^{1}H NMR (300 MHz, D$_2$O) δ 8.17 (s, 1H), 7.39 (t, J = 7.5 Hz, 2H), 7.20 (t, J = 7.5 Hz, 1H), 7.16 (d, J =8.4 Hz, 2H), 4.19 (dd, J = 17.7, 4.0 Hz, 1H), 2.27 (m, 1H), 1.03 (d, J = 6.9 Hz, 3H), 0.99 (d, J = 6.6 Hz 3H); ^{13}CNMR δ 166.7 (d, J = 6.1 Hz), 132.4, 126.9, 123.5, 53.7 (d, J = 149.5 Hz), 31.2, 19.9; LSIMS-MS(-) 256.1 m/z (MH$^-$-HCl).

2-methyl-butyl (8p) Yield 0.36g (20%) ^{1}H NMR (300 MHz, D$_2$O) δ 8.17,8.15 (s, 1H), 7.40 (t, J = 7.5 Hz, 2H), 7.20 (t, J = 7.8 Hz, 1H), 7.17 (d, J = 7.5 Hz, 2H), 4.39,4.02 (dd, J = 18.0, 4.8 Hz, 1H), 1.97 (m, 1H), 1.76 (m, 1H), 1.05, 1.01(d, J = 6.9 Hz), 0.91 (t, J = 7.2 Hz,

3H); ^{13}CNMR δ 166.3 (d, J = 4.9 Hz), 132.1, 126.6, 123.2, 53.4 (d, J = 149.1 Hz), 50.1 (d, J = 150.2 Hz), 38.0, 37.6, 29.5, 26.8, 18.6, 17.0, 13.5, 13.3; LSIMS-MS(-) 270.0 m/z (MH⁻-HCl).

3-methyl-butyl (9p) Yield 0.73g (36%)^{1}H NMR (300 MHz, D$_2$O) δ 8.13 (s, 1H), 7.40 (t, J = 7.8 Hz, 2H), 7.26 (d. J = 7.5 Hz, 1H), 7.18 (d, J = 7.8 Hz, 2H), 4.54 (dd, J = 15.6, 10.8 Hz), 1.66 (m, 2H), 0.96 (d, J = 5.4 Hz, 3H), 0.90 (d, J = 5.4 Hz, 3H); ^{13}CNMR δ 166.4 (d, 5.0 Hz), 132.4, 126.9, 123.4, 47.2 (d, J = 152.8 Hz), 40.7, 27.0, 25.4, 23.0; LSIMS-MS(-) 270.0 m/z (MH⁻-HCl).

3,3-dimethyl-butyl (10p) Yield 0.37g (22%) ^{1}H NMR (300 MHz, D$_2$O) δ 8.12 (s, 1H), 7.39 (t, J = 7.8 Hz, 2H), 7.20 (t, J = 7.5 Hz, 1H), 7.15 (d, J = 7.8 Hz, 2H), 4.35 (dd, J = 16.8, 10.5 Hz, 1H), 1.85 (dd, J = 14.7, 10.8 Hz, 1H), 1.58 (dd, J = 13.8, 11.1 Hz, 1H), 0.91 (s, 9H); ^{13}CNMR δ 166.0, 132.4, 126.8, 123.4, 46.5 (d, J = 152.8 Hz), 45.0, 31.4; LSIMS-MS(-) 242.0 m/z (MH⁻-HCl).

diphenyl methyl phosphonate Yield ^{1}HNMR δ 7.34 (t, J = 7.8 Hz, 4H), 7.20 (m, 6H), 1.80 (d, J = 17.7 Hz, 3H); ^{13}CNMR δ 150.2 (d J = 8.1 Hz), 129.7, 125.1, 120.4, 11.4 (d, J = 143.2 Hz); MS (EI): 248.1,

170.1, 155.0, 94.0, 77.0, 65.0; HRMS calcd for $C_{13}H_{13}O_3P_1$ 248.0602 found 248.0607.

phenyl methylphosphonate (11p) Yield 0.44g (80%)^{1}H NMR (300 MHz, D_2O) δ 7.43 (t, J = 7.5 Hz, 2H), 7.22 (t, J = 7.8 Hz, 1H), 7.18 (d, J =7.5Hz, 2H), 1.42 (d, J =16.5 Hz, 3H); ^{13}CNMR δ 154.2 (d, J =6.9 Hz), 132.6, 127.1, 123.8, 14.7 (d, J =138 Hz); LSIMS-MS(-) 171.0 (MH⁻ - Li).

Antibody preparation and purification. 17E8 was isolated from ascites fluid and purified by affinity chromatography (protein A) as described by Guo *et al.*[8]

Steady-State Kinetics of the Phenyl Esters. Michaelis-Menton parameters for the substrates were determined by continuous measurement at 270 nm (phenol release ε= 1400 $M^{-1}cm^{-1}$) using a Uvikon 930 (Kontron Instrument) UV-vis spectrophotometer. All assays were performed with cuvette holders thermostated at 24.5 ± 0.5°C with a Lauda RM6 temperature control unit. Cells of 1 cm pathlength (0.5 mL) were used in each experiment. The buffer used in all kinetic experiments was 50 mM sodium borate-150 mM NaCl,

pH 8.7. The antibody concentrations used in the experiments ranged from 0.2 µM to 1.4 µM. The concentration ranges of the substrates were as follows: (**2, 3**) 600 µM to 30 mM; (**4, 5, 6, 7, 11, 12, 13, 14**) 30 mM to 2.0 µM. All substrates were soluble at these substrate concentrations. The reactions were initiated by adding 20 µL of substrate stock in DMSO, to solution of 13-25 µL of IgG (in PBS) and 455-467 µL of pH 8.7 borate buffer. In the background reactions, the IgG was replaced with PBS. All catalyzed assays were performed in triplicate. The background reactions were performed in duplicate. The catalyzed rate was obtained by substracting the average of the background reaction rate from the rate of the catalyzed reaction. The data (v vs [S]) from the experiments were fit with the KaleidaGraph (Synergy Software) curve fitting program using the Michaelis-Menton equation.

Inhibition by the Phosphonates. The phosphonate inhibition experiments were performed by obtaining the steady-state kinetic constants, in an analogous manner as described above, in the presence of fixed concentrations of the phosphonates. In these experiments, the borate buffer contained the phosphonates. Hydrolysis of the phosphonates in the buffer was not detected

spectrophotometrically. The background rate constants were identical within error to those measured with the phosphonate containing buffer. The phosphonate concentrations ranged from (**1p, 10p**) 7 mM to 140 μM (**2p, 3p, 9p**) 300 μM to 30 μM (**4p, 5p, 6p**) 30 μM to 1 μM (**7p, 8p**) 600 μM to 120 μM. The antibody concentration was 0.2 μM. The phosphonate solutions were either used upon preparation or were immediately stored at -20°C. The norleucine substrate, **5**, was used in all of the inhibition experiments. The kinetic data were analyzed with the use of Lineweaver-Burk plots. The inhibition constant was obtained by plotting the slope $[(K_m/V_{max})(1 + [I]/K_i))]$ from the Lineweaver-Burk plots against inhibitor concentration and obtaining the intercept on the [I] axis ($-K_i$).**[70]**

Inhibition by Inactive Substrates These inhibition experiments were performed by obtaining the steady-state kinetic constants, in an analogous manner as described above, in the presence of fixed concentrations of an inactive substrate. The norleucine substrate, **5**, was used in all of the inhibition experiments. In these experiments, the DMSO/substrate stock solutions contain a fixed amount of inactive substrate. The approximate inhibition constant

was obtained from the equation $K_{mapp} = K_{Mo}(1+[I]/K_i)$, where K_{Mapp} was the experimental K_M obtained in the presence of inactive substrate and K_{Mo} is the K_M obtained in the absence of the inactive substrate. In these experiments it was assumed that the inactive substrates were competitive inhibitors. This assumption is substantiated by the fact there was no change in k_{cat} for norleucine in the presence of these inhibitors.[70]

Bibliography

(1) Benkovic, S. J. Catalytic antibodies. *Ann. Rev. Biochem.* **1992**, *61*, 29-54.

(2) Shokat, K. M.; Schultz, P. G. Catalytic antibodies. *Ann. Rev. Immunol.* **1990**, *8*, 335-363.

(3) Wade, H.; Scanlan, T. S. The structural and functional basis of antibody catalysis. *Ann. Rev. Biophys. Biomol. Struct.* **1997**, *26*, 461-493.

(4) Fersht, A. *Enzyme Structure and Mechanism*; 2nd ed.; W.H. Freeman & Co.: New York, 1985.

(5) Jencks, W. P. Economics of enzyme catalysis. *Cold Spring Harbor Symp. Quant. Biol.* **1987**, *LII*, 65-73.

(6) Jencks, W. P. *Catalysis in Chemistry and Enzymology*; Dover Publications: Mineola, 1969.

(7) Wade, H.; Scanlan, T. S. P1-S1 interactions control the enantioselectivity and hydrolytic activity of the norleucine phenylesterase catalytic antibody 17E8. *J. Am. Chem. Soc.* **1996**, *118*, 6510-6511.

(8) Guo, J.; Huang, W.; Scanlan, T. S. Kinetic and mechanistic characterization of an efficient hydrolytic antibody: Evidence for the formation of an acyl intermediate. *J. Am. Chem. Soc.* **1994**, *116*, 6062-6069.

(9) Fersht, A. R. Catalysis, binding, and enzyme-substrate complementarity. *Proc. R. Soc. Lond.B.* **1974**, *187*, 397-407.

(10) Fersht, A. R.; Dingwall, C. An editing mechanism for the methionyl-tRNA synthetase in the selection of amino acid in protein synthesis. *Biochemistry* **1979**, *18*, 1250-1255.

(11) Page, M. I. Entropy, binding energy, and enzymic catalysis. *Angew. Chem. Int. Ed. Engl.* **1977**, *16*, 449-459.

(12) Bash, P. A.; Pattabiraman, N.; Huang, C. C.; Ferrin, T. E.; Langridge, R. Van der Waals surfaces in molecular modeling: implementation with real-time computer graphics. *Science* **1983**, *222*, 1325-1327.

(13) Ferrin, T. E.; Huang, C. C.; Jarvis, L. E.; Langridge, R. The MIDAS display system. *J. Mol. Graphics* **1988**, *6*, 13-27.

(14) Ramachandran, G. N.; Sasisekharan, V. Conformation of polypeptides and proteins. *Adv. Prot. Chem.* **1968**, *23*, 283-437.

(15) Ramakrishnan, C.; Ramachandran, G. N. Stereochemical criterial for polypeptide and protein chain conformation. *Biophys. J.* **1965**, *5*, 909-933.

(16) Knowles, J. R. Enzyme specificity: α-chymotrypsin. *J. Theoret. Biol.* **1965**, *9*, 213-228.

(17) Hedstrom, L.; Farr-Jones, S.; Kettner, C. A.; Rutter, W. J. Converting trypsin to chymotrypsin: Ground-state binding does not determine substrate specificity. *Biochemistry* **1994**, *33*, 8764-8769.

(18) Hedstrom, L.; Perona, J. J.; Rutter, W. J. Converting trypsin to chymotrypsin: residue 172 is a substrate specificity determinant. *Biochemistry* **1994**, *33*, 8757-8763.

(19) Bone, R.; Frank, D.; Kettner, C. A.; Agard, D. A. Structural analysis of specificity: α-lytic protease complexes with analogues of reaction intermediates. *Biochemistry* **1989**, *28*, 7600-7609.

(20) Perona, J. J.; Craik, C. S. Structural basis of substrate specificity in the serine proteases. *Prot. Sci.* **1995**, *4*, 337-360.

(21) Perona, J. J.; Craik, C. S. Evolutionary divergence of substrate specificity within the chymotrypsin-like serine protease fold. *J. Biol. Chem.* **1997**, *272*, 29987-29990.

(22) Thompson, R. C. Binding of peptides to elastase: Implication for the mechanism of substrate hydrolysis. *Biochemistry* **1974**, *13*, 5495-5501.

(23) Gron, H.; Breddam, K. Interdependency of the binding subsites in subtilisin. *Biochemistry* **1992**, *31*, 8967-8971.

(24) Bone, R.; Shenvi, A. B.; Kettner, C. A.; Agard, D. A. Serine protease mechanism: structure of an inhibitory complex of α-lytic protease and a tightly bound peptide boronic acid. *Biochemistry* **1987**, *26*, 7609-7614.

(25) Jencks, W. P. On the attribution and additivity of binding energies. *Proc. Natl. Acad. Sci., USA* **1981**, *78*, 4046-4050.

(26) Wolfenden, R. Transition-state analog inhibitors and enzyme catalysis. *Annu. Rev. Biophys. Bioeng.* **1976**, *5*, 271-306.

(27) Gandour, R. D.; Schowen, R. L. *Transition-states of biochemical processes*; Plenum Press: New York, 1978.

(28) Dorovska, V. N.; Varfolomeyev, S. D.; Kazanskaya, N. F.; Klyosov, A. A.; Martinek, K. The influence of the geometric properties of the active centre on the specificity of α-chymotrypsin catalysis. *FEBS Lett.* **1972**, *23*, 122-124.

(29) Berezin, I. V.; Kazanskaya, N. F.; Klyosov, A. A.; Martinek, K. On the relationship between structure and reactivity of α-chymotrypsin substrates. *FEBS Lett.* **1971**, *15*, 125-128.

(30) Fersht, A. R.; Dingwall, C. Cysteinyl-tRNA synthetase from *Escherichia coli* does not need an editing mechansim to reject serine and alanine. High binding energy of small groups in specific groups in specific molecular interactions. *Biochemistry* **1979**, *18*, 1245-1249.

(31) Bartlett, P. A.; Marlowe, C. K. Phosphonamidates as Transition-State Analogue Inhibitors of Thermolysin. *Biochemistry* **1983**, *22*, 4618-4624.

(32) Bigler, T. L.; Lu, W.; Park, S. J.; Tashiro, M.; Wieczorek, M.; Wynn, R.; Michael Laskowski, J. Binding of amino acid side-chains to preformed cavities: interactions of serine proteinases with turkey ovomucoid third domains with coded and noncoded P_1 residues. *Prot. Sci.* **1993**, *2*, 786-799.

(33) Lu, W.; Apostol, I.; Qasim, M. A.; Warne, N.; Wynn, R.; Zhang, W. L.; Anderson, S.; Chiang, Y. W.; Ogin, E.; Rothberg, I.; Ryan, K.; Laskowski, M. Binding of amino acid side-chains to S_1 cavities of serine proteinases. *J. Mol. Biol.* **1997**, *266*, 441-461.

(34) Compton, D. A. C.; Montero, S.; Murphy, W. F. Low-frequency raman spectrum and asymmetric potential function for internal rotation of gaseous n-butane. *J. Phys. Chem.* **1980**, *84*, 3587-3591.

(35) Allinger, N. L.; Yuh, Y. H.; Lii, J.-H. Molecular mechanics. The MM3 force field for hydrocarbons. 1. *J. Am. Chem. Soc.* **1989**, *111*, 8551-8559.

(36) Janin, J.; Wodak, S.; Levitt, M.; Maigret, B. Conformation of amino acid side-chains in proteins. *J. Mol. Biol.* **1978**, *125*, 357-386.

(37) Pickett, S. D.; Sternberg, M. J. E. Empirical scale of side-chain conformational entropy in protein folding. *J. Mol. Biol.* **1993**, *231*, 825-839.

(38) Schrauber, H.; Eisenhaber, F.; Argos, P. Rotamers: to be or not to be? An analysis of amino acid side-chain conformations in globular proteins. *J. Mol. Biol.* **1993**, *230*, 592-612.

(39) Hansch, C.; Leo, A.; Hoekman, D. *Exploring QSAR: Hydrophobic, Electronic, and Steric Constants*; American Chemical Society: Washington, D.C., 1995.

(40) Hansch, C.; Coats, E. a-chymotrypsin: a case study of substituent constants and regression analysis in enzymatic structure-activity relationships. *J. Pharm. Sci.* **1970**, *59*, 731-743.

(41) Zhou, G. W.; Guo, J.; Huang, W.; Fletterick, R. J.; Scanlan, T. S. Crystal structure of a catalytic antibody with a serine protease active site. *Science* **1994**, *265*, 1059-1064.

(42) Estell, D. A.; Graycar, T. P.; Miller, J. V.; Powers, D. B.; Burnier, J. P.; Ng, P. G.; Wells, J. A. Probing steric and hydrophobic

effects on enzyme-substrate interactions by protein engineering. *Science* **1986**, *233*, 659–661.

(43) Rose, G. D.; Wolfenden, R. Hydrogen bonding, hydrophobicity, packing, and protein folding. *Ann. Rev. Biophys. Biomol. Struct.* **1993**, *22*, 381-415.

(44) Pace, C. N. *Evaluating contribution of hydrogen bonding and hydrophobic bonding to protein folding*; First ed.; Johnson, M. L. and Ackers, G. K., Ed.; Academic Press: San Diego, 1995; Vol. 259, pp 761.

(45) Richards, F. M. Areas, volumes, packing, and protein structure. *Ann. Rev. Biophys. Bioeng.* **1977**, *6*, 151-176.

(46) Fersht, A. R.; Shindler, J. S.; Tsui, W.-C. Probing the limits of protein-amino acid side-chain recognition with the aminoacyl-tRNA synthetases. Descrimination against phenylalanine by tyrosyl-tRNA synthetases. *Biochemistry* **1980**, *19*, 5520-5524.

(47) Perona, J. J.; Hedstrom, L.; Rutter, W. J.; Fletterick, R. J. Structural origins of substrate discrimination in trypsin and chymotrypsin. *Biochemistry* **1995**, *34*, 1489-1499.

(48) Bode, W.; Huber, R. Natural protein proteinase inhibitors and their interactions with proteinases. *Eur. J. Biochem.* **1992**, *204*, 433-451.

(49) Jackson, S. E.; Moracci, M.; elMasry, N.; Johnson, C. M.; Fersht, A. R. Effect of cavity-creating mutation in the hydrophobic core of chymotrypsin inhibitor 2. *Biochemistry* **1993**, *32*, 11259-11269.

(50) Otzen, D. E.; Rhiennecker, M.; Fersht, A. R. Structural factors contributing to the hydrophobic effect: the partly exposed hydrophobic minicore in chymotrypsin inhibitor 2. *Biochemistry* **1995**, *34*, 13051-13058.

(51) Bone, R.; Silen, J. L.; Agard, D. A. Structural plasticity broadens the specificity of an engineered protease. *Nature* **1989**, *339*, 191-195.

(52) Hedstrom, L.; Szilagyi, L.; Rutter, W. J. Converting trypsin to chymotrypsin-the role of surface loops. *Science* 1992, *255*, 1249-1253.

(53) Berti, P. J.; Fearman, C. H.; Storer, A. C. Cooperativity of papain-substrate interaction energies in the S_2 to S'_2 subsites. *Biochemistry* **1991**, *30*, 1394-1402.

(54) Ingles, D. W.; Knowles, J. R. Specificity and stereospecificity of α-chymotrypsin. *Biochem. J.* **1967**, *104*, 369-377.

(55) Ingles, D. W.; Knowles, J. R. The stereospecificity of α-chymotrypsin. *Biochem. J.* **1968**, *108*, 561-569.

(56) Gron, H.; Meldal, M.; Breddam, K. Extensive comparison of the substrate preferences of two subtilisins as determined with peptide substrates which are based on the principle of intramolecular quenching. *Biochemistry* **1992**, *31*, 6011-6018.

(57) Albery, W. J.; Knowles, J. R. Evolution of enzyme function and the development of catalytic efficiency. *Biochemistry* **1976**, *15*, 5631-5640.

(58) Albery, W. J.; Knowles, J. R. Efficiency and evolution of enzymatic catalysis. *Angew. Chem. Int. Ed. Engl.* **1977**, *16*, 285-293.

(59) Albery, W. J.; Knowles, J. R. Free-energy profile for the reaction catalyzed by triosephosphate isomerase. *Biochemistry* **1976**, *15*, 5627-5631.

(60) Fersht, A. R.; Kaethner, M. M. Enzyme hyperspecifity. Rejection of threonine by the valyl-tRNA synthetase by misacylation and hydrolytic editing. *Biochemistry* **1976**, *15*, 3342-3346.

(61) Lerner, R. A.; Benkovic, S. J.; Schultz, P. G. At the crossroads of chemistry and immunology: catalytic antibodies. *Science* **1991**, *252*, 659-667.

(62) Fersht, A. R. Dissection of the structure and activity of the tyrosyl-tRNA synthetases by site-directed mutagenesis. *Biochemistry* **1987**, *26*, 8031-8038.

(63) Narlikar, G. L.; Herschlag, D. Direct demonstration of the catalytic role of binding interactions in an enzymatic reaction. *Biochemistry* **1998**, *37*, 9902-9911.

(64) Avis, J. M.; Fersht, A. R. Use of binding energy in catalysis: optimization of rate in a multistep reaction. *Biochemistry* **1993**, *32*, 5321-5326.

(65) Whitty, A.; Fierke, C. A.; Jencks, W. P. Role of binding energy with coenzyme A in catalysis by 3-oxoacid coenzyme A transferase. *Biochemistry* **1995**, *34*, 11678-11689.

(66) Sheehan, J. C.; Yang, D.-D. H. The use of N-formylamino acids in peptide synthesis. *J. Am. Chem. Soc.* **1958**, *80*, 1154-58.

(67) Castro, B.; Evin, G.; Claude, S.; Seyer, R. Peptide coupling reagents; VIII. A high yield preparation of phenyl esters of amino acids using benzotriazolyoxytris-[dimethylamino]phosphonium hexafluorophosphoate (BOP reagent). *Synthesis* **1977**, 413.

(68) O'Donnell, M. J.; Wojchiechowski, K. Alkylation of protected a-amino acid derivatives in the presence of potassium carbonate. *Synthesis* **1984**, 313-315.

(69) Chen, F. M. F.; Benoiton, N. L. A general method for formylating sensitive amino acids esters. *Synthesis* **1979**, 709-710.

(70) Segel, I. H. *Enzyme Kinetics*; John Wiley and Sons: New York, 1975.

Chapter 4. Use of Binding Energy Along an Antibody Reaction Coordinate

Reproduced in part with permission from [Wade, H.; Scanlan T.S. *Expression of binding energy on an antibody reaction coordinate J. Am. Chem. Soc.* **1999**, *121*, 11935–11941.] Copyright 1999 American Chemical Society

Abstract

In this chapter, the investigation of how the catalytic antibody 17E8 uses remote binding energy along the catalyzed hydrolytic reaction coordinate is reported. With the use of alternative substrate analogs, we have determined that 17E8 can use free-energy from binding interactions between the substrate side-chain and antibody recognition pocket to equally stabilize the transition-state and the Michaelis complex. In these cases, the interactions are not used to increase k_{cat}. Substrates for which the interactions are used to preferentially stabilize the transition-state over the Michaelis complex have also been identified. In these cases, the interactions are used to increase k_{cat}. Mechanistic studies support the idea that the differences in the substrates' kinetic activities result from differences in the expression of side-chain•pocket binding energy along their respective reaction coordinates. These results suggest that generating catalytic antibodies to transition-

state analogs may be limited because the selective use of remote

binding energy cannot be programmed into transition-state

analogs.

Introduction

Enzymes use binding energy to place substrates in a precise position relative to catalytic groups in enzyme active sites. In addition, they are able to use binding energy gained from interactions with non-reacting portions of the substrate to stabilize the transition-state of the reaction.[1-5] However, stabilization of the transition-state (obtaining a large k_{cat}/K_M) is not the sole requirement for efficient catalysis; ensuring rapid turnover (obtaining a large k_{cat}) by decreasing the free energy difference between transition-state complex, $(E\bullet S)^{\ddagger}$, and the ground state Michaelis complex, $(E\bullet S)$ is also necessary.[6-8] Enzymes achieve this by expressing binding energy selectively along the reaction coordinate. By using the free energy from binding interactions that either exclusively stabilize the $(E\bullet S)^{\ddagger}$ or that stabilize the $(E\bullet S)^{\ddagger}$ more than the $(E\bullet S)$, enzymes achieve fast turnover and avoid the unproductive over-stabilization of ground state species.[1-4]

Structural and functional studies of catalytic antibodies have shown that the bulk of catalytic power results directly from the use of binding energy from interactions that are proximal to and remote from the catalytic center.[9-13] Indeed, the catalytic antibody 17E8 uses the energy from noncovalent interactions between the

amino acid side-chain of substrates and a side-chain recognition pocket, which are removed from the reactive center, to promote ester hydrolysis (Figure 4.1).[9,14] These interactions are analogous to those in natural enzymes such as proteases and tRNA synthetases that also use binding interactions between amino acid side-chains and recognition pockets.[15-22]
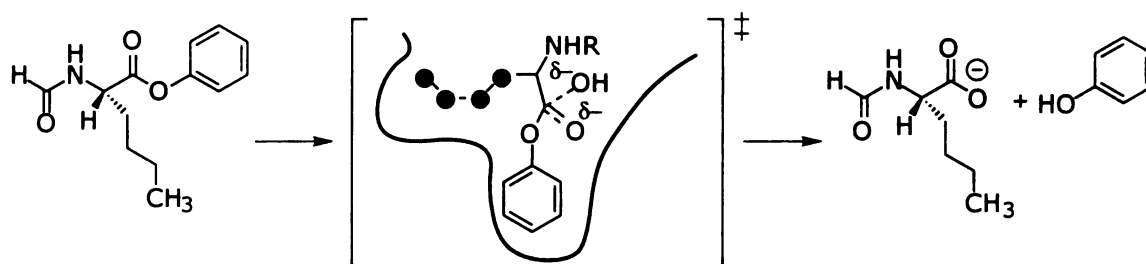
Figure 4.1 Hydrolytic reaction catalyzed by 17E8 and transition-state formed by hydroxide attack.

The removal of the methylene groups from **2** to yield **1** (Figure 4.2) results in an increase in the free-energy of the 17E8•transition-state complex, indicating that 17E8 uses the side-chain•pocket interactions for overall transition-state stabilization (Table 4.1).[9,14] The removal of the interactions also results in a similar decrease in the stability of the Michaelis complex, indicating that 17E8 uses the side-chain•pocket interactions in a manner that has been termed *uniform binding*.[1-4] With *uniform binding*, the binding interactions are used to equally stabilize both the Michaelis and the transition-state complexes (Figure 4.3). Because the

additional side-chain•pocket interactions are not used to decrease the free energy difference between the (IgG•S) and the (IgG•S)[‡] complexes, which would result in an increased k_{cat} value, *uniform binding* can be viewed as a wasteful use of binding energy and a trait of a primitive catalyst.[2,3]

Alternative substrates for which the binding energy between the amino acid side-chain and recognition pocket is used to increase the catalytic turnover number have been identified (Figure 4.2). In this study, we show that the differences in the kinetic activities of these substrates are due to differences in the expression of binding energy along the catalytic reaction coordinate.
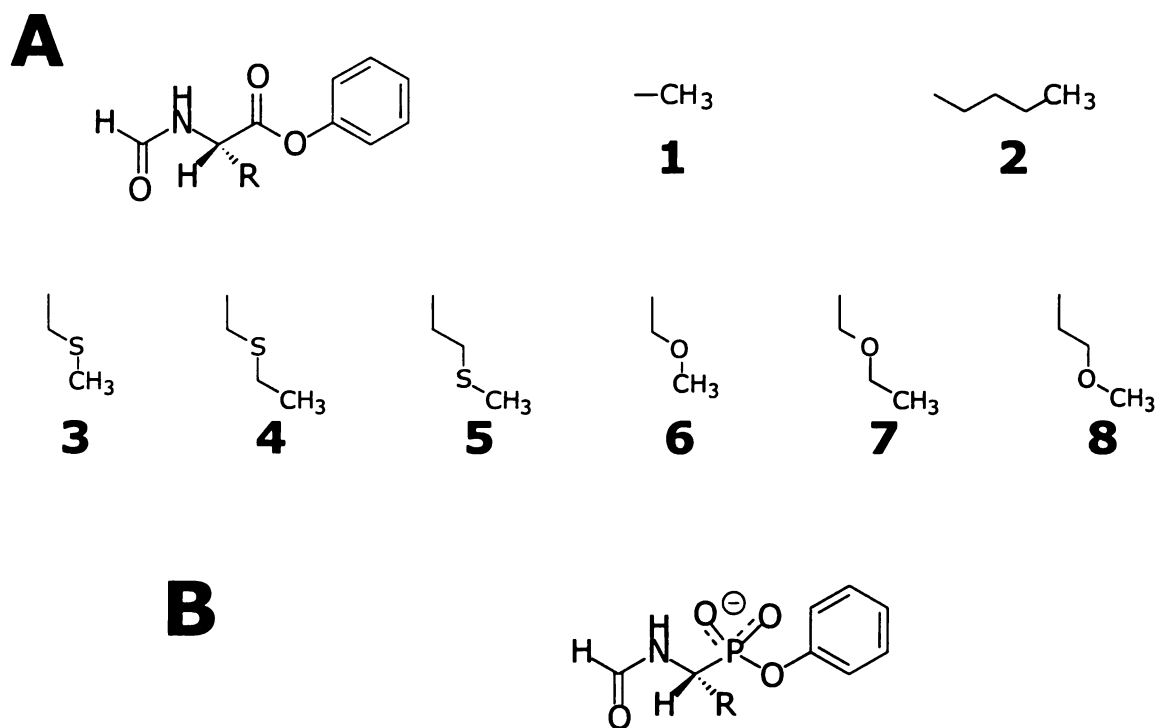
Figure 4.2 **A.** Substrates used to study side-chain•pocket interactions. N-formyl phenyl ester skeleton is shown above side-chains which are designated by R. **B.** N-formyl phenyl phosphonate skeleton of the transition-state analogs used in this study.
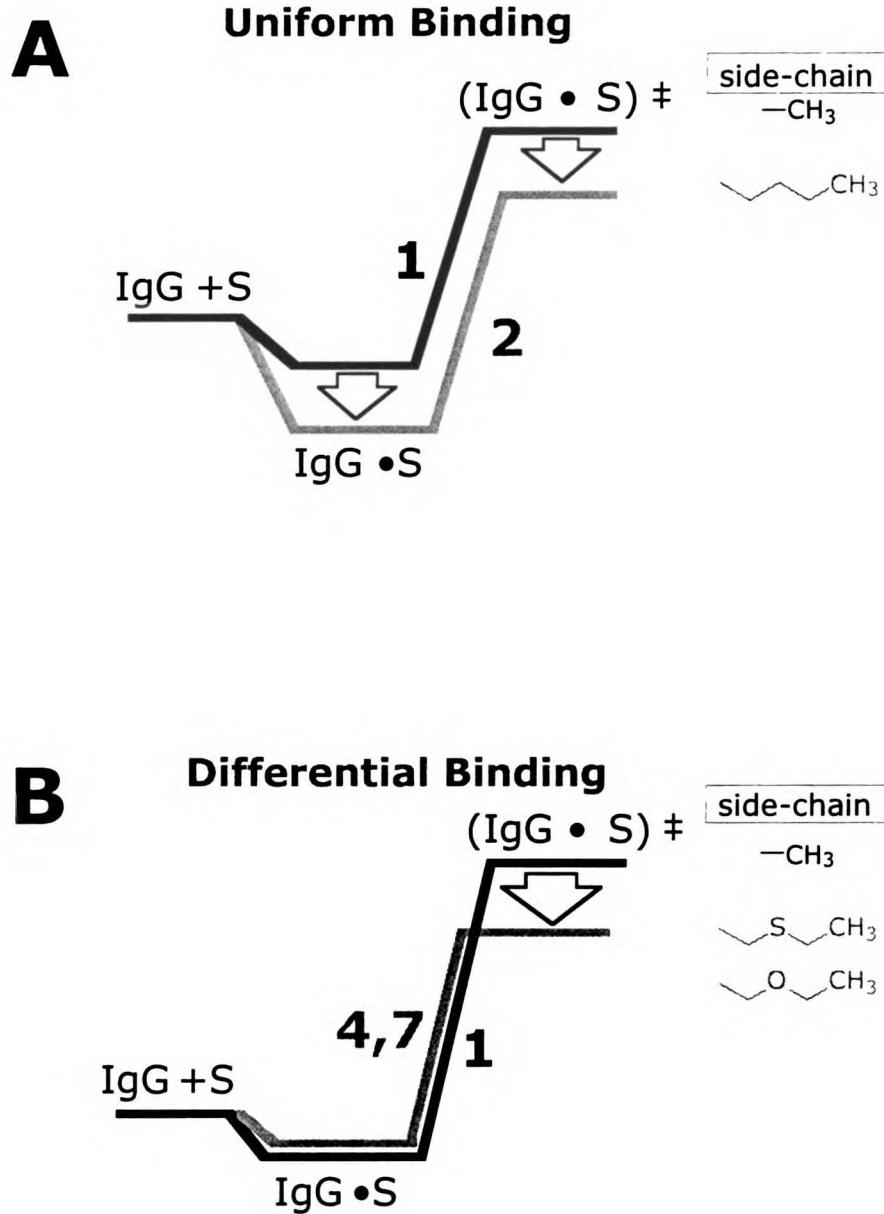
Figure 4.3 Free energy diagrams representing binding energy use and catalysis. **A.** 17E8 catalyzed reaction with **1** (black) and **2** (grey) **B.** 17E8 catalyzed reaction with **1** (black) and **4** & **7** (grey). Both IgG and S represent unbound antibody and substrate respectively. (IgG•S) and (IgG•S)‡ represent the Michaelis and transition-state complexes, respectively.

Results and Discussion

To make 17E8 behave in a more catalytically optimized manner than that demonstrated with the substrates **1** and **2**, we attempted to circumvent the uniform use of the side-chain•pocket binding energy by destabilizing the (IgG•S) complex. This destabilization would leave some of the binding energy to be used to decrease the free energy difference between the (IgG•S) and the (IgG•S)‡ complexes and increase k_{cat}. We decided to exploit the correlation between the stability of the (IgG•S) complex, log K_M, and the hydrophobicity parameter, log P, for the substrate side-chains (Figure 4.4). The relationship suggests that the Michaelis complex can be destabilized by using substrates with side-chains that are less hydrophobic than **2**. There is also a modest correlation between log(k_{cat}/K_M) and log P.[9] It is unclear if either correlation is due to the removal of side-chain•pocket contacts or to side-chain hydrophobicity—factors which are inextricably linked. Therefore, the hydrophobicity of the side-chain was changed while maintaining the maximum number of heavy-atom•pocket contacts. By replacing methylene groups in the side-chain with sulfur and oxygen atoms the hydrophobicity of the side-chain is substantially altered as indicated by the changes in the log P values (Figure 4.4) which are

correlated directly to the free-energy of transfer from octanol to

water for model compounds.[23]
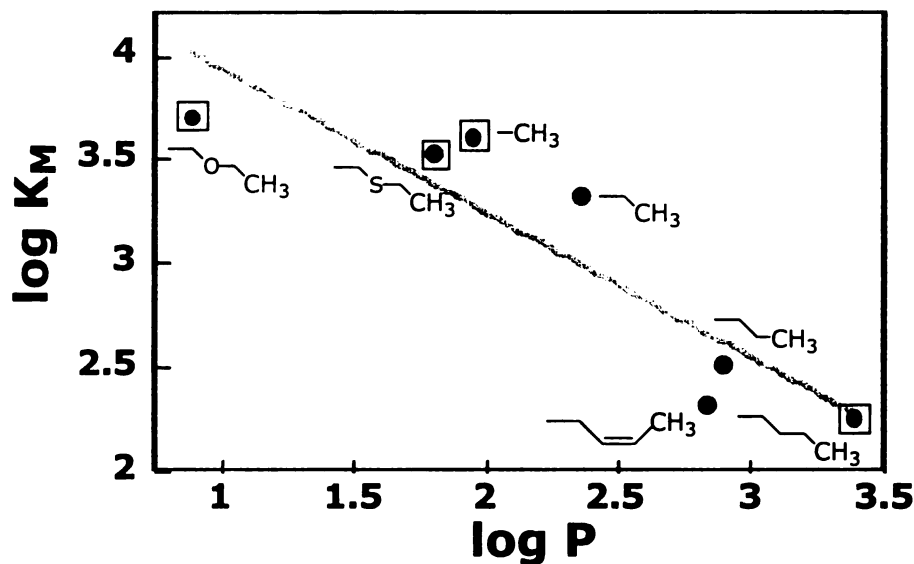
Figure 4.4 Correlation between log P and log K_M values of the substrates used in the 17E8 catalyzed reaction. The K_M values for the substrates that are not discussed in this paper were taken from ref. 9. The K_M values are in the concentration unit of μM. The log P values correspond to those of model compounds that are analogous to the side-chains of the phenyl ester substrates: pentane, log P=3.39, **2**; cis 3-pentene, 2.83; butane, 2.89; propane, 2.36; ethane, 1.81, **1**; diethyl sulfide, 1.95, **4**; diethyl ether, 0.89, **7**. The values were taken from ref. 23. The boxed data designate the substrates that are discussed in this paper. The slope of the line without **4**, and **7** is -0.9 ± 0.2, R=0.93; with **4** and **7** included slope is - 0.7 ± 0.2, R=0.90.

	K_M (μM) [$\Delta\Delta G_s$ (kcal/mol)]	k_{cat} (s^{-1}) [$\Delta\Delta G^{\ddagger}$ (kcal/mol)]	k_{cat}/K_M ($M\bullet s$)$^{-1}$ [$\Delta\Delta G_b$ (kcal/mol)]
1	3400 ± 400	1.0 ± 0.1	290 ± 40
	[0.0]	[0.0]	[0.0]
2	180 ± 30	2.1 ± 0.1	12000 ± 1400
	[-1.7]	[-0.4]	[-2.1]
3	2600 ± 100	18 ± 1	7000 ± 100
	[-0.1]	[-1.7]	[-1.8]
4	4000 ± 200	43 ± 2	11000 ± 700
	[+0.1]	[-2.1]	[-2.0]
5	3400 ± 900	3.3 ± 0.5	970 ± 300
	[0.0]	[-0.7]	[-0.6]
6	4600 ± 200	12 ± 1	2600 ± 100
	[+0.1]	[-1.4]	[-1.2]
7	5000 ± 700	27 ± 2	5400 ± 800
	[+0.3]	[-1.9]	[-1.6]
8	ND	ND	ND

Table 4.1 Steady-state kinetic analysis of substrates. The $\Delta\Delta G_b$ values were calculated with the equation: $-RT\ln[(k_{cat}/K_M)_x/(k_{cat}/K_M)_1]$, where R is the gas constant and T is the absolute temperature. The $\Delta\Delta G_s$ values were calculated from the equation $-RT\ln[(K_M)_x/(K_M)_1]$, $\Delta\Delta G^{\ddagger}$ values were calculated from the equation $-RT\ln[(k_{cat})_x/(k_{cat})_1]$, where X corresponds to a substrate to which **1** is being compared. N.D. = not detected.

The steady state kinetic parameters for the substrates are shown in Table 4.1. As predicted by the log P-log K_M correlation for the homologous aliphatic side-chain series, the heteroatom replacement results in destabilization of the (IgG•S) as indicated by the large increases in K_M and the unfavorable $\Delta\Delta G_s$ values which are as large as 2 kcal/mol (relative to **2**). The K_M values for the substrates with the oxygen replacements (**6-8**) are larger than those with the sulfur replacements (**3-5**) further substantiating the log P-log K_M trend. The inclusion of these substrates on the log K_M-log P plot maintains the linear relationship between the two parameters (Figure 4.4). The heteroatom replacements do not result in significant changes in the k_{cat}/K_M values (compare **4**, **5**, and **7** to **2**) which is in contrast to the result of deleting methylene groups (compare **1** and **2**). The heteroatom replacements do result in increased k_{cat} values for the 17E8 catalyzed reactions. The k_{cat} increase is as high as 20-fold (**4**) and is dependent on the heteroatom position in the side-chain. The γ-replacements (**3,4** and **6,7**) had much larger increases than the δ-replacements (**5 & 8**).

The kinetic behavior of these alternative substrates suggests that the side-chain•pocket binding energy is being used *differentially* between the (IgG•S) and the (IgG•S)‡ complexes (see Figure

4.3).[1,2,4] When the additional binding groups are added to **1** to

yield **3-7**, the (IgG•S) complex is not further stabilized, in contrast

to the **1** to **2** side-chain change. However, the additional groups do

significantly stabilize the (IgG•S)‡ complex as shown by the

negative $\Delta\Delta G_b$ values that are more favorable by as much as 2

kcal/mol. These increases in k_{cat} values for substrates **3-7** suggest

that the additional interactions are used to decrease the free-

energy difference between the (IgG•S) and (IgG•S)‡ complexes.

The $\Delta\Delta G^{\ddagger}$ value (relative to **1**) is decreased by as much as 2.1

kcal/mol (Table 4.1).
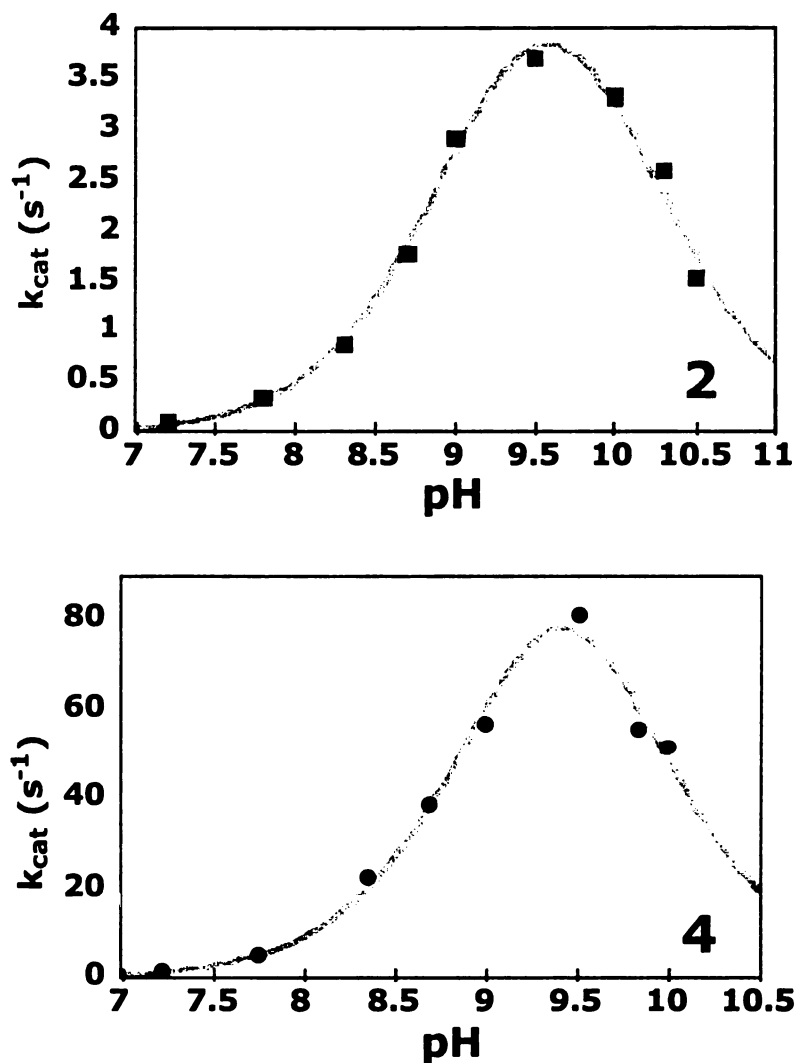
Figure 4.5 pH-k_{cat} profile for 17E8 catalyzed hydrolysis of **2** (top) and **4** (bottom). The pK$_a$ values obtained from the fit to following equation:

$$k_{cat(obs)} = \frac{k_o}{10^{pK_{a1} - pH} + 1 + 10^{pH - pK_{a2}}},$$

where $k_{cat(obs)}$ is the observed k_{cat} value and k_o is the pH independent k_{cat} value. The equation was derived from a scheme based on two ionizable antibody residues (for model see figure 4.6). The pK$_{a1}$ and pK$_{a2}$ values obtained for the substrates are 9.2 ± 0.2 and 9.7 ± 0.2; R =0.993 (**4**) and 9.0 ± 0.1 and 10.0 ± 0.1; R=0.994 (**2**).

Figure 4.6 Model used to fit the pH dependence of 17E8 hydrolysis. The turnover of the (IgGH•S) complex is assumed to be significantly greater than the (IgGH$_2$•S) and the (Ig•S) complexes.

$$\text{IgGH}_2\text{•S}$$

$$\updownarrow K_{a1}$$

$$\text{IgGH•S} \xrightarrow{\;k_{cat}\;} \text{IgGH•P}$$

$$\updownarrow K_{a2}$$

$$\text{IgG•S}$$
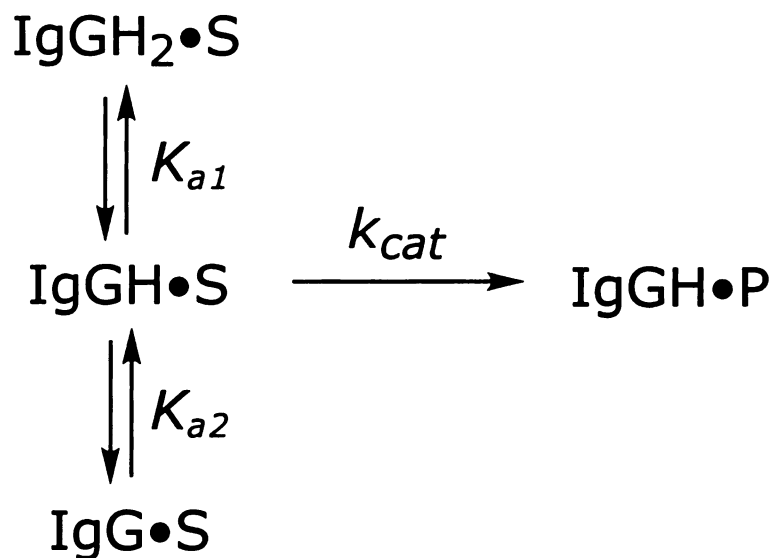
pH	K_M (μM)	k_{cat} (s^{-1})	k_{cat}/K_M (M•s)$^{-1}$
7.22	1400 ± 120	2.1 ± 0.1	1600 ± 100
7.75	2500 ± 240	5.7 ± 0.2	2300 ± 200
8.35	3100 ± 140	23 ± 1	7400 ± 100
8.68	3700 ± 280	39 ± 1	10600 ± 300
9.00	5200 ± 430	57 ± 2	11000 ± 400
9.50	5500 ± 400	82 ± 2	15000 ± 400
9.83	3400 ± 800	56 ± 4	16300 ± 800
10.0	2700 ± 870	52 ± 3	19600 ± 1000

Table 4.2 pH dependence data for the hydrolysis of **4**. See Experimental Section for experimental details.

To ensure that the changes in the kinetic parameters were due to differential binding and not a change in the catalytic mechanism, we performed a pH-rate study for substrate **4**, which is the substrate that has the highest increase in turnover number (Figure 4.5 and Table 4.2). The shape of the plot and the two pK_a
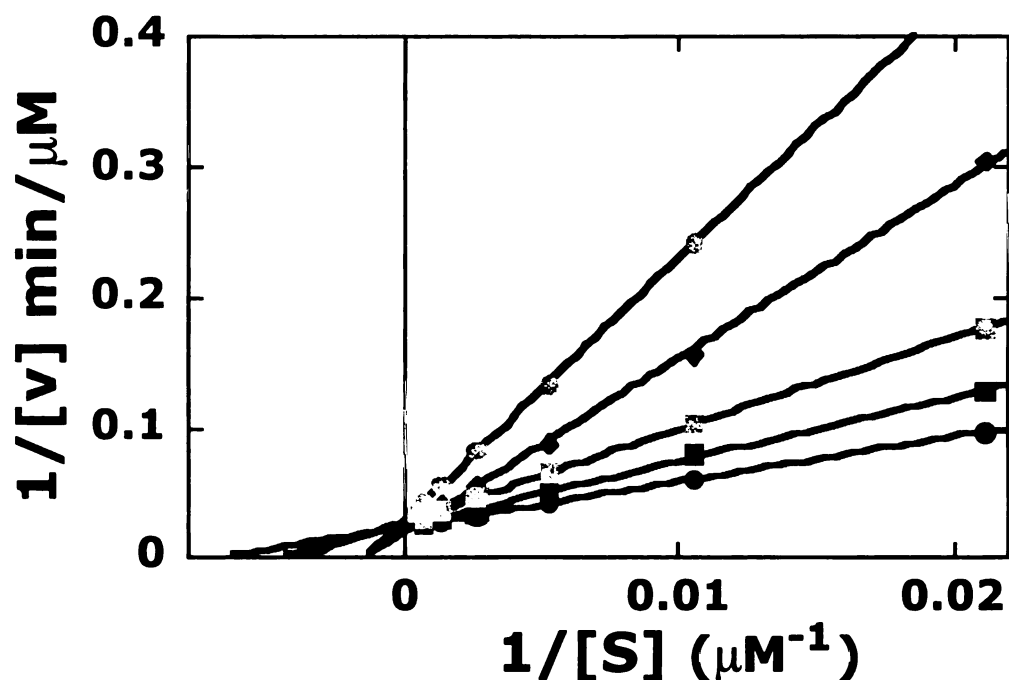
Figure 4.7 Competitive inhibition of 17E8 catalysis by the phosphonate corresponding to substrate **4**. The inhibitor concentrations were -●- (0.0 mM), -■- (0.4 μM), - - (0.8 μM), -◆- (2.3 μM), and -●- (3.9 μM).

values obtained for **4** are similar to those for **2** suggesting that the same residues participate in the rate-determining step for the catalyzed hydrolysis of **2** and **4.[24-26]**
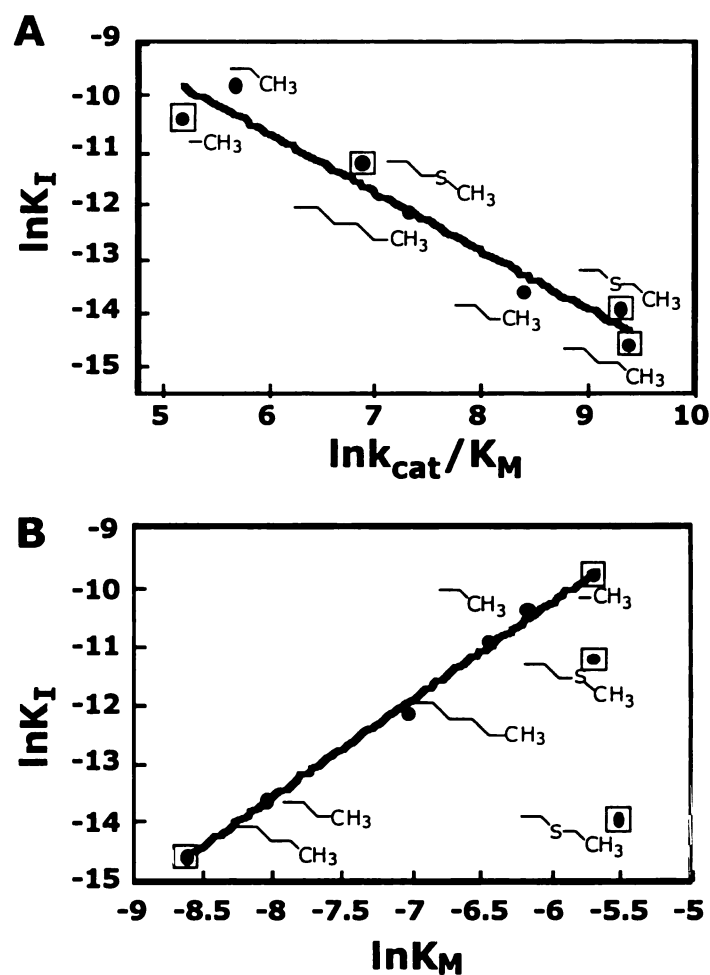
Figure 4.8 Transition-state versus substrate complementarity. **A.** In K_I vs In k_{cat}/K_M (slope = -1.08 ± 0.11 R = 0.973). **B.** In K_I vs In K_M (slope = 1.64 ± 0.05 R = 0.999). The data used in the plots were obtained using various phenyl ester substrates and phosphonates. The substrate and phosphonate skeletons are shown in figure 4.2 The side-chains are shown next to the data points. The data were fit with the KaleidaGraph curve fitting program (data taken from refs. 9 and 14 and table 4.1).

The phosphonate transition-state analog corresponding to substrate **4** was also synthesized and tested for its binding and inhibition activity of the 17E8 catalyzed reaction (see Figure 4.2 for structure). The phosphonate is a competitive inhibitor of the 17E8

145

reaction (Figure 4.7) with a K_i value of 0.8 μM, which is similar to that of the phosphonate corresponding to **2** (0.6 μM). The ln K_I and ln(k_{cat}/K_M) relationship for the substrates and their corresponding transition-state analogs is also maintained with the inclusion of substrates **3** and **4**, supporting the similarity in transition-state structure for **2, 3** and **4** hydrolysis (Figure 4.8a).[27-30] In contrast, the K_I values do not correlate with the K_M values for **3** and **4** (Figure 4.8b). These results support the kinetic evidence that points to differential binding as the cause for the increase in turnover rate. The tight binding of the transition-state analog also discounts the possibility that the increase in turnover rate is solely due to an increase in the intrinsic reactivity of the ester with the replacement of the heteroatom. The larger k_{cat} value for **4** (compared to **7**) also suggests that an increase in the intrinsic reactivity of the carbonyl due to the heteroatom replacement is not a large factor as the oxygen replacement should render the carbonyl group more reactive than the sulfur atom replacement.

To obtain further insight into the mechanistic differences in the catalyzed hydrolysis of substrates **1, 2** and **4**, the temperature dependence of 17E8 catalysis with each of the substrates was studied. The temperature dependence of the steady state parameters K_M, k_{cat}, and k_{cat}/K_M are shown in Tables 4.3-4.5 (Table

146

4.3 for **1**; 4.4 for **2**; 4.5 for **4**). Their temperature dependencies yielded the thermodynamic quantities shown in Table 4.6. There is a pH-rate dependence for the catalyzed reaction; therefore, it is likely that the parameters obtained from the temperature dependence ($\Delta H^\ddagger$, ΔH_{KM}, $\Delta S^\ddagger$, and ΔS_{KM}) include contributions from the protonation and deprotonation of active site residues. For the present discussion, the *differences* in the obtained parameters for the substrates are emphasized. The contributions from the protonation and deprotonation of the active site residues are most likely the same for the substrates as they are cleaved by the same mechanism, with the participation of the same active site residues, and have similar transition state structures.

The ΔH_{KM} values obtained for substrate binding are −2.8, -7.0, and -2.9 kcal/mol for **1**, **2**, and **4**, respectively. The ΔS_{KM} values are 0.5, 6.4, -1.4 cal/(mol•K). In this study, we assume that K_M is approximately equal to K_S (dissociation constant associated with substrate binding). We believe this assumption to be valid for several reasons. The turnover rate for 17E8 is not fast enough to warrant the suggestion that $k_{off} < k_{cat}$, thus leaving the term K_M devoid of chemical steps. The existence of additional unimolecular non-chemical steps (i.e. protein conformational changes) which would precede the rate-determining chemical step is unlikely due to

147

the simple catalytic mechanisms elicited by phosphonate haptens. The rate-determining nature of the hydrolysis of the phenyl ester has been determined in other mechanistic studies.[26] Although the ΔS_{KM} may seem anomalous for a binding event, these types of values (obtained by kinetic and thermodynamic methods) have been noted for the binding of substrates in other enzymatic systems.[31-35] These positive and near zero values for the association of the substrate with 17E8 are consistent with the release of bound water from the 17E8 active site and from the substrate's hydrophobic moieties (phenyl group and side-chain).[26]

Temp (°C), [K]	K_M (μM)	k_{cat} (s^{-1})	k_{cat}/K_M ($M \bullet s)^{-1}$
5 [278]	7500 ± 700	0.12 ± 0.01	17 ± 2
10 [283]	8300 ± 1000	0.15 ± 0.01	18 ± 2
15 [288]	9100 ± 900	0.23 ± 0.01	24 ± 2
20 [293]	9300 ± 1300	0.28 ± 0.02	30 ± 5
25 [298]	11000 ± 1700	0.41 ± 0.03	37 ± 6
30 [303]	11200 ± 2100	0.52 ± 0.04	46 ± 10
35 [308]	12500 ± 1900	0.55 ± 0.04	44 ± 7

Table 4.3 Temperature dependence of the steady-state kinetic parameters for the catalyzed hydrolysis of **1**.

Temp (°C), [K]	K_M (μM)	k_{cat} (s^{-1})	k_{cat}/K_M (M•s)$^{-1}$
10 [283]	79 ± 10	0.29 ± 0.01	3700 ± 530
15 [288]	75 ± 8	0.35 ± 0.01	4600 ± 520
20 [293]	75 ± 7	0.52 ± 0.01	7000 ± 700
25 [298]	97 ± 7	0.69 ± 0.01	7100 ± 500
30 [303]	130 ± 10	0.98 ± 0.03	7400 ± 600
35 [308]	170 ± 14	1.2 ± 0.04	7100 ± 600
40 [313]	270 ± 40	1.8 ± 0.1	6600 ± 1100

Table 4.4 Temperature dependence of the steady-state kinetic parameters for the catalyzed hydrolysis of **2**.

Temp (°C), [K]	K_M (μM)	k_{cat} (s^{-1})	k_{cat}/K_M $(M \bullet s)^{-1}$
5 [278]	2200 ± 100	6.9 ± 0.2	3100 ± 200
10 [283]	2400 ± 400	9.6 ± 0.6	4100 ± 700
15 [288]	2700 ± 70	12 ± 1	4500 ± 100
20 [293]	2800 ± 200	14 ± 1	5200 ± 400
25 [298]	3100 ± 200	17 ± 1	5500 ± 700
30 [303]	3400 ± 200	21 ± 1	6300 ± 400
35 [308]	3700 ± 300	24 ± 1	6500 ± 500

Table 4.5 Temperature dependence of the steady-state kinetic parameters for the catalyzed hydrolysis of **4**.
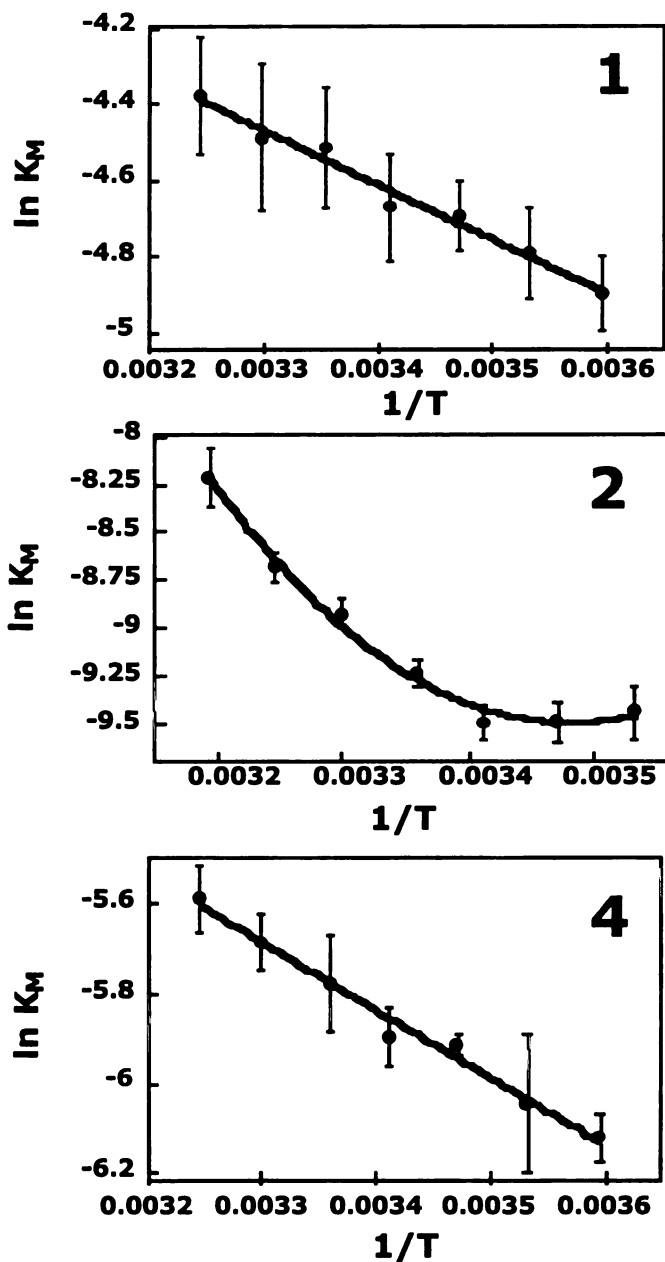
Figure 4.9 Temperature dependence of K_M for **1**, **2**, and **4**. The K_M data for **1** and **4** were fit to the equation:

$$\ln K_M = \frac{\Delta H^o}{RT} - \frac{\Delta S^o}{R}.$$

The K_M data for **2** was fit to the equation:

$$\ln K_M = \frac{\Delta H^o_{T(0)}}{RT} - \left(\frac{\Delta S^o_{T(0)} - \Delta Cp^o}{R} \right) - \frac{\Delta Cp^o \ln T}{R},$$

where $\Delta H^o_{T(0)}$ and $\Delta S^o_{T(0)}$ are the enthalpy and entropy change at 0 K.

152
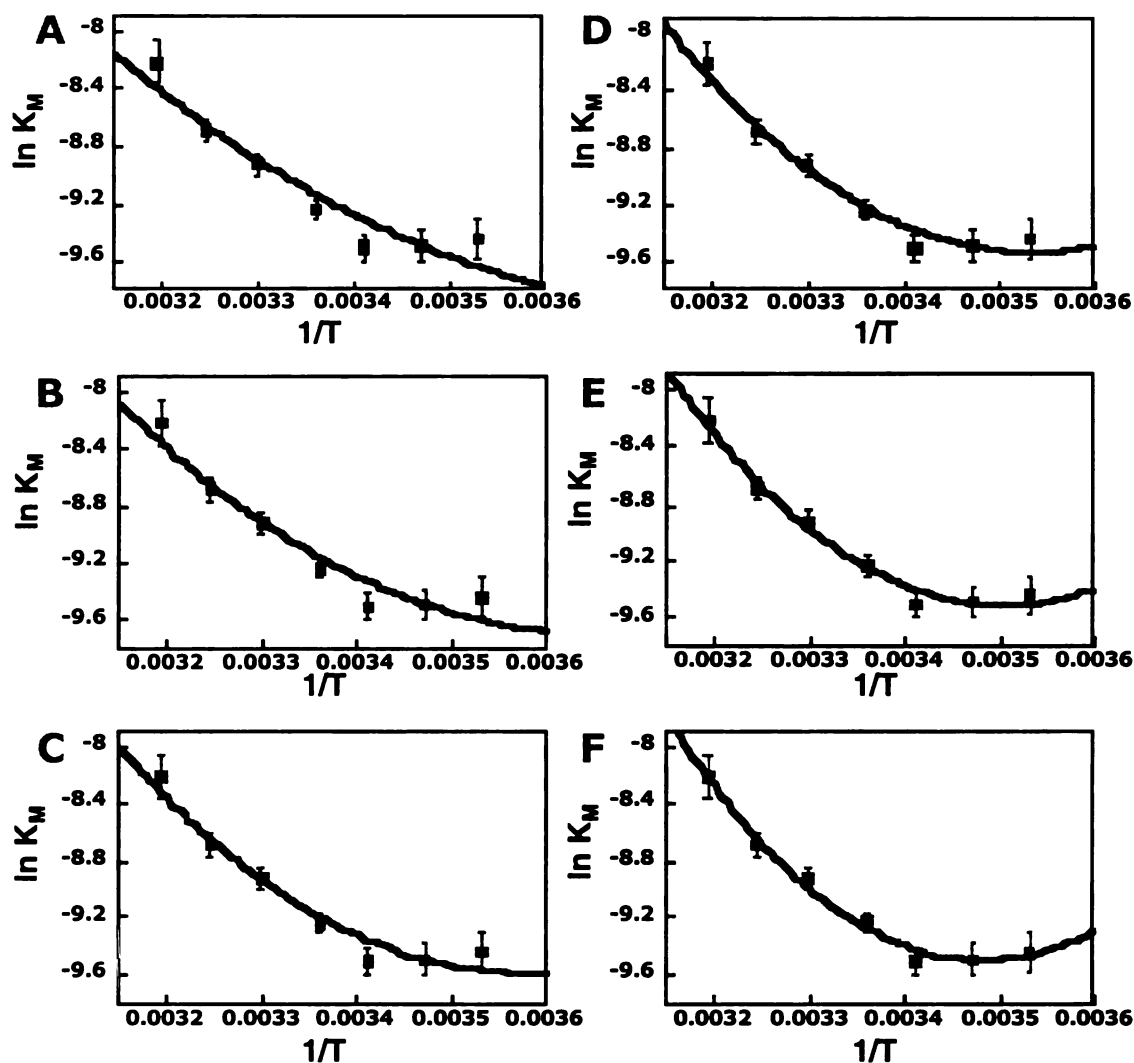
Figure 4.10 van't Hoff curves of K_M (substrate **2**) with fixed ΔCp values. The data were fit to the equation described in the legend of figure 4.9 (for **2**) with the ΔCp parameter held constant at several values. **A.** $\Delta Cp = -200$ cal/(mol•K)$^{-1}$, $\Delta H_{298} = -7.2$ kcal/mol, $\Delta S_{298} = -2.1$ cal/mol, R = 0.956; **B.** $\Delta Cp = -300$ cal/(mol•K)$^{-1}$, $\Delta H_{298} = -7.4$ kcal/mol, $\Delta S_{298} = -6.4$ cal/(mol•K)$^{-1}$, R = 0.971; **C.** $\Delta Cp = -400$ cal/(mol•K)$^{-1}$, $\Delta H_{298} = -7.3$ kcal/mol, $\Delta S_{298} = -4.2$ cal/(mol•K)$^{-1}$, R = 0.981; **D.** $\Delta Cp = -500$ cal/(mol•K)$^{-1}$, $\Delta H_{298} = -7.6$ kcal/mol, $\Delta S_{298} = -8.7$ cal/mol, R = 0.989; **E.** $\Delta Cp = -600$ cal/(mol•K)$^{-1}$, $\Delta H_{298} = -7.5$ kcal/mol, $\Delta S_{298} = -7.0$ cal/mol, R = 0.993; **F.** $\Delta Cp = -700$ cal/(mol•K)$^{-1}$, $\Delta H_{298} = -7.6$ kcal/mol, $\Delta S_{298} = -7.2$ cal/mol, R = 0.995. The given thermodynamic values are associated with $1/K_M$ which formally represents the association constant for the Michaelis complex. (as are those in table 4.6). The ΔH_{298} and ΔS_{298} values associated with the fits were calculated using the equation in the legend of table 4.6.

153
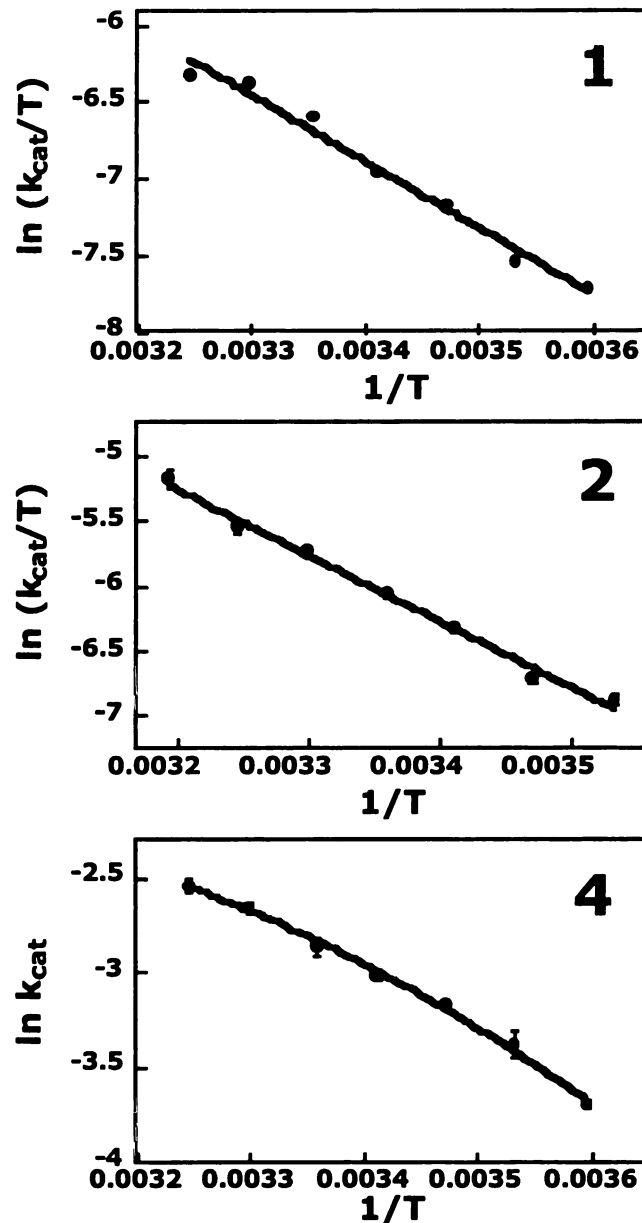
Figure 4.11 Temperature dependence of k_{cat} for **1**, **2**, and **4**. The k_{cat} data for **1** and **2** were fit to the equation:

$$\ln\left(\frac{k_{cat}}{T}\right) = \ln\left(\frac{k_b}{h}\right) + \frac{\Delta S^{\ddagger}}{R} - \frac{\Delta H^{\ddagger}}{RT}.$$

The k_{cat} data for **4** were fit to the equation:

$$\ln k_{cat} = \ln\left(\frac{k_b}{h}\right) - \frac{\Delta H^{\ddagger}_{T(0)}}{RT} + \left(1 + \frac{\Delta Cp^{\ddagger}}{R}\right)\ln T + \frac{\Delta S^{\ddagger}_{T(0)} - \Delta Cp^{\ddagger}}{R},$$

where $\Delta H^{\ddagger}_{T(0)}$ and $\Delta S^{\ddagger}_{T(0)}$ are the enthalpy and entropy of activation at 0 K.
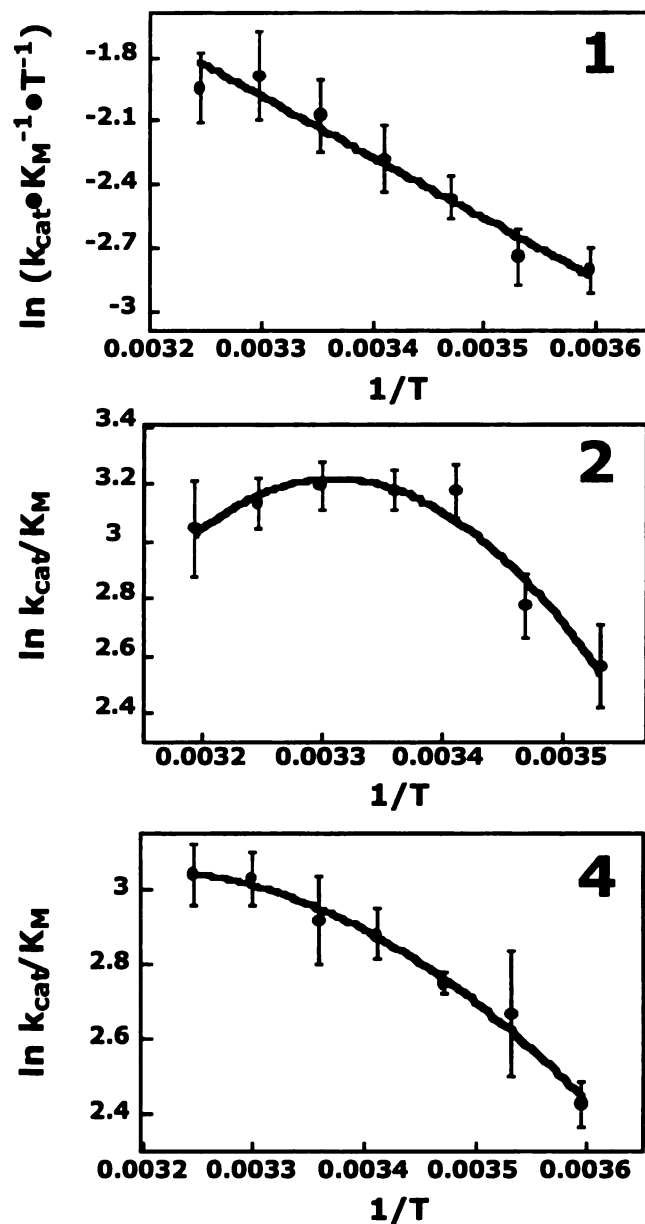
Figure 4.12 Temperature dependence of k_{cat}/K_M for **1**, **2**, and **4**. The k_{cat}/K_M data for **1** was fit to the equation:

$$\ln\left(\frac{k_{cat}}{K_M T}\right) = \ln\left(\frac{k_b}{h}\right) + \frac{\Delta S^{\ddagger}}{R} - \frac{\Delta H^{\ddagger}}{RT}.$$

The k_{cat}/K_M data for **2** and **4** were fit to the equation:

$$\ln\left(\frac{k_{cat}}{K_M}\right) = \ln\left(\frac{k_b}{h}\right) - \frac{\Delta H^{\ddagger}_{T(0)}}{RT} + \left(1 + \frac{\Delta Cp^{\ddagger}}{R}\right)\ln T + \frac{\Delta S^{\ddagger}_{T(0)} - \Delta Cp^{\ddagger}}{R}.$$

155

The van't Hoff plot for substrate **2** results in curved data fit which suggests that the ΔH_{KM} and ΔS_{KM} values are not constant with temperature and that a ΔCp_{KM} term must be included in the van't Hoff equation (Figure 4.9). The curvature of the $\ln K_M$-$1/T$ plot could also arise because of a shift in equilibrium between several (17E8•substrate) complexes or the involvement of chemical rate constants in the Michaelis constant. The involvement of several Michaelis complex forms seems unlikely due the absence of curvature seen in the $\ln K_M$-$1/T$ plots with substrates **1** and **4**. If there was an obligatory isomerization of the Michaelis complex for 17E8 catalysis, one would expect to see the same with other substrates that are processed by the catalyst. The linear nature of the $\ln(k_{cat}/T)$-$1/T$ plot is also consistent with the nonexistence of several Michaelis-like complexes. The "well-behaved" nature of the plot also suggests that there is no equilibrium shift in the ground state for 17E8 catalysis (see below). The ΔCp_{KM} value obtained from the fit is 700 cal/(mol•K). We believe this ΔCp value to be an overestimate. One reason is the inherent difficulty in obtaining accurate heat capacity changes from van't Hoff plots. Another reason is that the heat capacity of binding of the phosphonates that correspond to **1**, **2**, and **4** obtained by calorimetric experiments

are much smaller (>2 fold) than the ΔCp_{KM} and $\Delta Cp^{\ddagger}$ obtained by the

temperature dependence of the kinetic constants. The heat

capacity changes for phosphonate binding are probably

underestimates as the contributions of charged moieties to heat

capacity are opposite in magnitude to those of hydrophobic

moieties. The fit obtained from the Figure 4.9 (and 4.12) is not very

sensitive to the ΔCp variable. Changing the ΔCp from 700 to 300

cal/(mol•K) resulted in a very small change in the ΔH_{KM} (7.0 and 6.8

kcal/mol) and ΔS_{KM} (-6.4 and -6.6 cal/(mol•K)) values (see Figure

4.10). The respective correlation coefficients for the fits with the

above ΔCp values are 0.995 and 0.971, respectively. There is no

observed curvature in the ln K_M-1/T plot with substrates **1** and **4**

(Figure 4.9).

1/K_M			
Substrate	ΔH_{KM} kcal/mol	ΔS_{KM} cal/(mol•K)	ΔCp_{KM} cal/(mol•K)
[1]	-2.8 ± 0.2	0.5 ± 0.6	
[2]	-7.0 ± 0.9	6.4 ± 0.7	-700 ± 80
[4]	-2.9 ± 0.2	-1.4 ± 0.6	

k_{cat}			
Substrate	$\Delta H^{\ddagger}_{kcat}$ kcal/mol	$\Delta S^{\ddagger}_{kcat}$ cal/(mol•K)	$\Delta Cp^{\ddagger}_{kcat}$ cal/(mol•K)
[1]	8.6 ± 0.5	-32 ± 2	
[2]	10.1 ± 0.4	-26 ± 1	
[4]	5.6 ± 0.7	-34 ± 5	-140 ± 50

k_{cat}/K_M			
Substrate	$\Delta H^{\ddagger}_{TS}$ kcal/mol	$\Delta S^{\ddagger}_{TS}$ cal/(mol•K)	$\Delta Cp^{\ddagger}_{TS}$ cal/(mol•K)
[1]	5.8 ± 0.6	-32 ± 2	
[2]	2.0 ± 0.3	-32 ± 1	-620 ± 110
[4]	2.1 ± 0.5	-33 ± 4	-170 ± 50

Table 4.6 The thermodynamic quantities obtained from the temperature dependence of k_{cat}, K_M, and k_{cat}/K_M. The values of $1/K_M$ are shown so that the values represent those for formation of the Michaelis complex as K_M formally represents a dissociation constant. The ΔH_{KM} and ΔS_{KM} values at 298 K values for 2 were calculated from the fit in figures 4.9, 4.11, and 4.12 using the equations:

$$\Delta H^{o}_{298K} = \Delta H^{o}_{T(0)} + T\Delta Cp^{o} \quad \text{and} \quad \Delta S^{o}_{298K} = \Delta S^{o}_{T(0)} + \Delta Cp^{o} \ln T.$$

The $\Delta H^{\ddagger}_{kcat}$ and $\Delta S^{\ddagger}_{kcat}$ values at 298 K values for 2 were calculated from the fit in figures 4.9, 4.11, and 4.12 using the equations:

$$\Delta H^{\ddagger}_{298K} = \Delta H^{\ddagger}_{T(0)} + T\Delta Cp^{\ddagger} \quad \text{and} \quad \Delta S^{\ddagger}_{298K} = \Delta S^{\ddagger}_{T(0)} + \Delta Cp^{\ddagger} \ln T.$$

The data for the k_{cat} dependence on temperature yields $\Delta H^{\ddagger}_{kcat}$

values of 8.6, 10.1, and 5.6 kcal/mol and $\Delta S^{\ddagger}_{kcat}$ values of -32, -26,

and -34 cal/(mol•K) for **1**, **2**, and **4** respectively. The plot of $\ln(k_{cat}/T)$

vs $1/T$ for **4** suggests that $\Delta H^{\ddagger}_{kcat}$ and $\Delta S^{\ddagger}_{kcat}$ values are not constant

with temperature for the reaction with **4** (Figure 4.11). The data can

also be fit to the linear Eyring equation (no $\Delta Cp^{\ddagger}$ included). This

yields $\Delta H^{\ddagger}$ and $\Delta S^{\ddagger}$ values of 6.3 kcal/mol and -32 cal/(mol•K),

respectively. The R value for the fit to the linear equation is 0.993.

The R value for the fit that includes a $\Delta Cp^{\ddagger}$ contribution is 0.998.

The $\Delta Cp^{\ddagger}_{kcat}$ value obtained from the fit is 140 cal/(mol•K). No

curvature is seen in the $\ln(k_{cat}/T)$ vs $1/T$ plots for **1** and **2** (Figure

4.11). The k_{cat}/K_M temperature dependence data yield $\Delta H^{\ddagger}_{TS}$ values

of 5.8, 2.0, and 2.1 kcal/mol and $\Delta S^{\ddagger}_{TS}$ values of -32, -32, and -33

cal/(mol•K) for **1**, **2** and, **4** respectively. The curved $\ln(k_{cat}/K_M)$ vs $1/T$

plot yields $\Delta Cp^{\ddagger}_{TS}$ values of -620 and -170 cal/(mol•K) for **2** and **4**

respectively.

From these thermodynamic quantities, a model for the use of

side-chain•pocket interactions along 17E8's hydrolytic reaction

coordinate can be postulated. The more favorable ΔH_{KM} for **2**

suggests that more interactions are formed in the (**2**•17E8) complex

than in the (S•17E8) complexes with **1** and **4**. The $\Delta\Delta H_{KM}$ of binding

between **1** and **3** is essentially zero, suggesting that a similar number of interactions are formed in the (**1**•17E8) and (**4**•17E8) complexes. The large ΔCp_{KM} value suggests that the interactions formed in the (**2**•17E8) complex are hydrophobic in nature, which is expected due to the structure of the n-butyl moiety and the residues that surround the side-chain in the transition-state•17E8 complex.**[34-37]** In addition to the hydrophobic effect, it has been noted that the existence of a heat capacity change may also result from the contributions of intramolecular vibrations, electrostatic charges, hydrogen bonds, conformational entropy, and possible changes in equilibria.**[35]** The contribution from electrostatic charges and hydrogen bonds is thought to be small due to the small net change in electrostatic interactions and hydrogen bonds upon binding.**[35]** No correction has been made for conformational entropy and internal vibrational contributions to the heat capacity change. The likelihood of possible changes in equilibria has been discussed above. The lack of an observable ΔCp_{KM} and the enthalpic similarity between (**1**•17E8) and (**4**•17E8) suggests that the side-chain does not make substantial contact with the recognition pocket in the Michaelis complex of 17E8 and **4**.

The $\Delta H^{\ddagger}_{kcat}$ is most favorable for **4**, suggesting that more binding interactions are used in the transformation of (IgG•**4**) to (IgG•**4**)‡ than with **1** and **2**. The curvature in the ln(k_{cat}/T)-1/T plot suggests that the hydrophobic effect is playing a role in the turnover of the (IgG•**4**) complex. The $\Delta Cp^{\ddagger}$ (**4**) value is smaller than the ΔCp_{KM} (**2**) value. This is expected as the group contribution of -S- to ΔCp is smaller than that of a -CH$_2$- group.[38,39] The large negative $\Delta S^{\ddagger}_{kcat}$ values for the substrates suggests that the transition-state complexes are substantially more ordered than the substrates' respective Michaelis complexes. This can be explained by the fact that more contacts are made in the transition-state complex (especially with the oxyanion hole), and the fact that a water molecule must become fixed to participate in the transition-state of the reaction.

The postulated models for 17E8's use of the side-chain•pocket interactions are shown in Figure 4.13. The side-chain contacts are used extensively with **2** in the Michaelis complex and much less so with **4**, as suggested by the ΔH_{KM} values and the ΔCp_{KM} for **2**. The side-chain contacts are used in converting the (IgG•**4**) complex to its transition-state complex, as suggested by the $\Delta H^{\ddagger}_{kcat}$ and $\Delta Cp^{\ddagger}_{kcat}$ values. Substrate **1** cannot make many contacts in either complex

161

and thus has been used as a control substrate to determine if the curvature in the temperature dependent plots indeed results from the extended side-chain•pocket contacts. The similar $\Delta H^{\ddagger}_{TS}$ and $\Delta S^{\ddagger}_{TS}$ values for **2** and **4** suggest that their transition-state complexes are highly similar. Thus, it seems that the side-chains for **2** and **4** are being used differently in the 17E8 catalyzed reactions.

One reason that enzymes are able to achieve differential binding of specific groups on substrates is because their active sites are often more complementary to the transition-state than to the Michaelis complex.[2,4,27,30,40] The existence of a linear correlation between $\ln(k_{cat}/K_M)$ and $\ln K_I$ and the lack of a correlation between $\ln K_M$ and $\ln K_I$ for alternative substrates and transition-state analogs with several enzymes is proof of this complementarity.[27,28,41-43] We have shown in our system that the $\ln(k_{cat}/K_M)$ values of an extensive panel of substrates correlate well with the binding of the corresponding phosphonates, indicating that the side-chain•pocket interactions are similarly presented by both the catalytic transition-state and the phosphonates.[9] The correlation between $\ln K_M$ and $\ln K_I$ in Figure 4.8 indicates that the side-chain•pocket interactions are similar in the Michaelis complex and in the transition-state for the

homologous alkyl series. This correlation suggests that part of 17E8's active site is complementary to both the ground state and the transition-state. This precludes the possibility that the side-chain•pocket can be used differentially between the two species. The substrates **4** and **5** deviate from the K_M-K_I correlation, which is consistent with the side-chains binding differently in the ground state and the transition-state.

IgG•2

↓

uniform binding of side-chain

(IgG•S)‡

differential binding of side-chain

↑

IgG•4
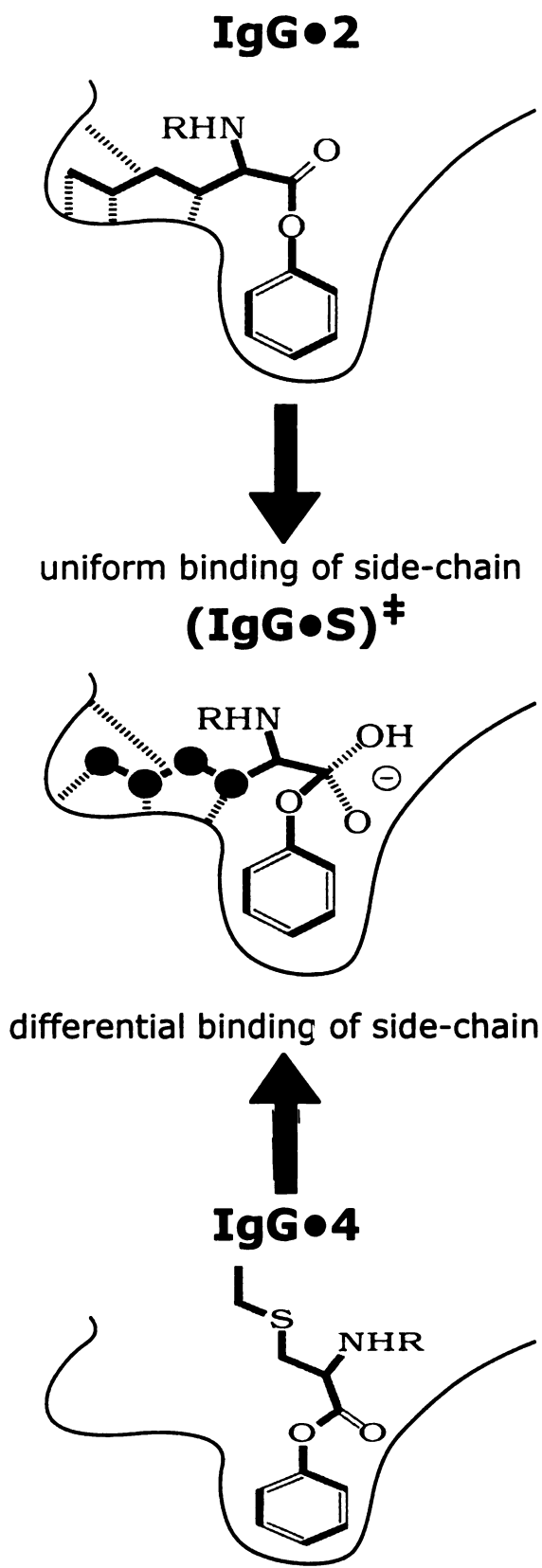
Figure 4.13 Postulated model of the of use side-chain•pocket interactions that result in uniform binding (substrate **2**) and differential binding (substrate **4**). In uniform binding, all the side-chain pocket interactions are made in the (IgG•S) complex and no additional interactions are formed in the (IgG•S)‡. In differential binding, the side-chain•pocket interactions are formed exclusively in the (IgG•S)‡.

Conclusions

In addition to engineering catalytic efficiency in the form of high k_{cat}/K_M values, an important concern in catalyst design is high turnover (large k_{cat} values). The properties of enzymes indicate that high turnover can be obtained by binding non-reactive portions of the substrate differentially between the ground state and the transition-state complexes. This points out a potentially significant limitation of generating catalytic antibodies with hapten molecules designed to mimic a transition-state. There may often be a subtle structural difference between the transition-state and the Michaelis complex for a chemical reaction that is not effectively exploited with a synthetic transition-state mimic. As a result, the antibodies generated against the transition-state analog also bind corresponding non-reactive portions of the substrate with high affinity. Thus, haptens program binding interactions needed to stabilize the transition-state, but don't enforce the differential use of binding energy of non-reactive portions of the substrate. This inevitably results in the unproductive stabilization of antibody bound ground state species. Thus, the development of new general strategies that can program or select for differential binding is undoubtedly an essential step for achieving truly efficient catalytic antibodies.

Experimental Section

General Methods and Reagents. Reactions requiring anhydrous conditions were carried out in flame-dried glassware under an atmosphere of argon. Anhydrous solvents were purchased from Aldrich. Chromatography solvents were purchased from Fisher Corp. and were used as received. Reagents were purchased either from Sigma or Aldrich and used as received unless noted otherwise. ^{1}H NMR and ^{13}C NMR were recorded on a General Electric 300-MHz instrument. The NMR samples were prepared in 5-mm tubes, and the chemical shifts are reported in parts per million (δ) relative to the standards TMS for samples in $CDCl_3$ and TSP (3-(trimethylsilyl)-1-propanesulfonic acid sodium salt) for samples in D_2O. Flash chromatography was performed with Merck silica gel 60 (230-400 mesh). Ion exchange chromatography was performed with diethylaminoethyl (DEAE) Sephadex A-25 (anion exchange) and Dowex 50WX2-100 (cation exchange). The resins were washed and prepared according to manufacturers' recommendations.

Synthesis of n-Formylated Amino Acid Ester Substrates, 1-8.

The racemic phenyl ester substrates were synthesized as described by Wade and Scanlan **[9]**. The synthesis of **5** is described by Guo *et al.***[26]** The L-enantiomer of the amino acid esters (**1**, **2**, and **4**)

were used in the temperature dependent studies. The synthesis of the enantiopure substrates is described in Wade and Scanlan **[9]**.

n-formyl-(S-methyl)-cysteine phenyl ester [3] Yield 0.65 g (80%)
^{1}HNMR (300 MHz, CDCl$_3$) δ 8.29 (s, 1H), 7.40 (t, J = 7.8 Hz, 2H), 7.27 (t, J = 7.2 Hz, 1H), 7.13 (d, J = 8.2 Hz, 2H), 6.64 (br d, J = 7.5 1H), 5.16 (dd, J = 7.8, 4.5 Hz, 1H), 3.16 (d, J = 5.1 Hz, 2H), 2.21 (s, 3H); ^{13}C NMR δ 160.8, 129.6, 126.4, 121.2, 50.6, 36.3, 16.4; MS (EI): 239.0(M+), 239.1, 194.1, 160.0, 146.0, 118.0, 101.0, 94.0, 90.0, 77.0, 61.0; HRMS calcd for C$_{12}$H$_{15}$N$_1$O$_3$S$_1$ 239.0616 found 239.0616.

n-formyl-(S-ethyl)-cysteine phenyl ester [4] Yield 0.75 g (90%)
^{1}HNMR (300 MHz, CDCl$_3$) δ 8.22 (s, 1H), 7.36 (t, J = 7.5 Hz, 2H), 2.23 (t, J = 7.2 Hz, 1H), 7.10 (d, J = 7.8 Hz, 2H), 6.56 (br s, 1H), 5.10 (dd, J = 9.0, 4.8 Hz, 1H), 3.12 (d, J = 4.5 Hz, 2H), 2.58 (dd, J = 7.5, 6.9 Hz, 2H), 1.52 (t, J = 7.2 Hz, 2H); ^{13}C NMR d 169.1, 160.8, 150.3, 129.6, 126.4, 121.2; MS (EI): 253.1(M+), 208.1, 160.0, 132.0, 115.0, 104.1, 94.0, 87.0, 75.0, 65.0; HRMS calcd for C$_{12}$H$_{15}$N$_1$O$_3$S$_1$ 253.0773 found 253.0774.

n-formyl-(O-methyl)-serine phenyl ester [6] Yield 0.73 g (88%)

^{1}HNMR (300 MHz, CDCl$_3$) δ 8.30 (s, 1H), 7.40 (t, J = 7.5 Hz, 2H), 7.26 (t, J = 7.8, 7.5 Hz, 1H), 7.10 (d, J = 7.5 Hz, 2H), 6.54 (br d, J = 5.4 1H), 5.08 (dt, J = 8.4, 2.7 Hz, 1H), 4.05 (dd, J = 9.3, 3.0 Hz, 1H), 3.77 (dd, J = 9.3, 3.0 Hz, 1H), 3.44 (s, 3H); ^{13}C NMR δ 160.7, 129.5, 126.3, 121.3, 72.2, 59.7, 51.5; MS (EI): 224.0(MH+), 224.1, 130.1, 102.1, 94.0, 85.0, 74.1, 65.0; HRMS calcd for C$_{11}$H$_{14}$N$_1$O$_4$ 224.0923 found 224.0915.

n-formyl-(O-ethyl)-serine phenyl ester [7] Yield 0.54 g (60%)

^{1}HNMR (300 MHz, CDCl$_3$) δ 8.30 (s, 1H), 7.40 (t, J = 7.8, 7.5 Hz, 2H), 7.26 (t, J = 6.9 Hz, 1H), 7.10 (d, J = 7.8 Hz, 2H), 6.56 (br d, J = 5.4 Hz, 1H), 5.10 (dd, J = 8.4, 3.0 Hz, 1H), 4.08 (dd, J = 9.3 ,2.4 Hz, 1H), 3.79 (dd, J = 9.3, 2.4 Hz, 1H), 1.52 (q, J = 6.9 Hz, 2H) 1.22 (t, J = 6.9 Hz, 3H); ^{13}C NMR d 160.6, 129.5, 126.2, 121.3, 70.1, 67.1, 51.5, 15.0; MS (EI): 238.1(MH+), 238.1, 144.0, 133.0, 116.0, 94.0, 82.9, 70.0, 60.0; HRMS calcd for C$_{12}$H$_{15}$N$_1$O$_4$ 237.1001 found 237.0995.

n-formyl-(O-methyl)-homoserine phenyl ester [8] Yield 0.57 g (63%) ^{1}HNMR (300 MHz, CDCl$_3$) δ 8.26 (s, 1H), 7.39 (t, J = 7.8 Hz, 2H), 7.25 (t, J = 7.2 Hz, 1H), 7.10 (d, J = 7.8 Hz, 2H), 6.85 (br d, J =

5.4 Hz, 1H), 5.10 (dt, J = 7.2, 5.4 Hz, 1H), 3.58 (t, J = 5.7 2H), 3.35

(s, 3H), (q, J = 5.4 Hz, 2H) 1.22 (t, J = 6.9 Hz, 3H); ^{13}C NMR δ 170.3,

160.8, 150.5, 129.4, 126.0, 121.2, 68.9, 58.9, 49.7, 15.0; MS (EI):

238.1(MH+), 179.1, 158.0, 116.1, 94.0, 82.9, 70.0, 65.0, 56.0; HRMS

calcd for $C_{12}H_{16}N_1O_4$ 238.1079 found 238.1087.

Synthesis of n-Formylated Phenyl Phosphonates (see Figure 4.2,

and text for phosphonates used). The phosphonates were

prepared by the route similar to that described by Guo *et al.*[26]

The use of aldehydes with different side-chains yielded the series.

Phenyl [1-(1-N-Formylamino)alkyl]phosphonates

2-(S-ethyl)-ethyl (corresponding substrate is **4** in Figure 4.2) Yield:

0.20 g (44%) ^{1}H NMR (300 MHz, D$_2$O) δ 8.22 (s, 1H), 7.45 (t, J = 8 Hz,

2H), 7.23 (t, J = 8.0 Hz, 1H), 7.19 (d, J = 9 Hz, 2H), 4.44 (ddd, J =

15.2, 12, 3.2 Hz, 1H), 3.22 (ddd, J = 14.4, 4.8, 3.2 Hz, 1H), 2.80

(ddd, J = 14.4, 12, 6 Hz, 1H), 2.61 (dq, J = 7.2, 2.4 Hz, 2H), 1.20 (t, J

= 7.2 Hz, 3H) LSIMS-MS(-) 288.4 m/z (MH$^-$-HCl)

3-(S-methyl)-propyl (corresponding substrate is **5**) (44%) ^{1}H NMR

(300 MHz, D$_2$O) δ 8.16 (s, 1H), 7.41 (t, J = 6.8 Hz, 2H), 7.22 (t, J =

7.6 Hz, 1H), 7.17 (d, J = 8.4 Hz, 2H), 4.45 (ddd, J = 14.8, 11.2, 3.2

Hz, 1H), 2.69 (ddd, J = 13.6, 8.4, 4.8 Hz, 1H), 2.80 (dt, J = 13.2, 8.4 Hz, 1H), 2.17 (m, 1H), 2.11 (s, 3H), 1.96 (s, 1H) LSIMS-MS(-) 288.4 m/z (MH$^-$-HCl).

Steady-state Kinetics of the Phenyl Esters. Michaelis-Menton parameters for the substrates were determined by continuous measurement at 270 nm (phenol release ε = 1400 M$^{-1} \cdot$cm^{-1}) using a Uvikon 930 (Kontron Instrument) UV-vis spectrophotometer. All assays were performed with cuvette holders thermostated at 24.5 ± 0.5°C with a Lauda RM6 temperature control unit. Cells of 1 cm pathlength (0.5 mL) were used in each experiment. The buffer used in all kinetic experiments was 50 mM sodium borate-150 mM NaCl, pH 8.7. The antibody concentrations used in the experiments ranged from 0.2 µM to 1.4 µM. All substrates were soluble at these substrate concentrations. The substrate concentrations used were: **1:** 800 µM to 30 mM ; **2:** 30 µM to 1 mM; **3:** 650 µM to 22 mM; **4:** 200 µM to 25 mM; **5:** 200 µM to 25 mM; **6-8:** 400 µM to 45 mM. The reactions were initiated by adding 20 mL of the substrate stock in DMSO to a solution of 13-25 mL of 17E8 (in PBS) and 455-467 mL of pH 8.7 borate buffer. In the background reactions, the IgG was replaced with PBS. All catalyzed assays were performed in

170

triplicate. The background reactions were performed in duplicate. The catalyzed rate was obtained by subtracting the average of the background reaction rate from the rate of the catalyzed reaction. The data (v vs [S]) from the experiments were fit with the KaleidaGraph (Synergy Software) curve fitting program using the Michaelis-Menton equation.

pH-rate Dependence of 17E8 Catalysis. The steady-state kinetic parameters of 17E8 catalysis of **4** at different pH values were obtained in the same manner as described above for the experiments performed at pH 8.7. The following buffer systems were used in this analysis: 50 mM $NaHPO_4$, 150 mM NaCl, pH 7.2; 50 mM Tris, 150 mM NaCl, pH 7.8; 50 mM borate, 150 mM NaCl, pH 8.4, and pH 8.7; 50 mM CHES, 150 mM NaCl, pH 9.0, pH 9.5, pH 9.8, and 10.0. The buffer system used for **2** is listed in ref **[26]**. The parameters for the pH values > 10 were not obtained due to a high background reaction. The k_{cat} values were plotted as a function of pH and fit to the equation described in the legend of Figure 4.5 using the KALIEDGRAPH plotting program.

Temperature Dependence of Catalysis. All reactions were performed in 50 mM borate, 150 mM NaCl (pH 8.0). The steady-

171

state kinetic parameters of 17E8 catalysis of **1**, **2**, and **4** at the different temperatures were obtained in the same manner as described above for the experiments performed at 24.5°C. The temperature range covered for each of the substrates was from 5°C to 40°C. The lnk_{cat}, K_M, and k_{cat}/K_M values for the different temperatures were plotted as a function of $1/T$ (K) and fit to the equation described in the legends of Figure 4.9, 4.11, and 4.12 using the KALEIDAGRAPH plotting program.

References

(1) Jencks, W. P. Economics of enzyme catalysis. *Cold Spring Harbor Symp. Quant. Biol.* **1987**, *LII*, 65-73.

(2) Jencks, W. P. *Catalysis in Chemistry and Enzymology*; Dover Publications: Mineola, **1969**.

(3) Fersht, A. R. Catalysis, binding, and enzyme-substrate complementarity. *Proc. R. Soc. Lond.B.* **1974**, *187*, 397-407.

(4) Fersht, A. *Structure and Mechanism in Protein Science: A Guide to Enzyme Catalysis and Protein Folding*; W.H. Freeman and Company: New York, 1999.

(5) Pauling, L. Molecular architecture and biological reactions. *Chem. Eng. News.* **1946**, *24*, 1375-1377.

(6) Avis, J. M.; Fersht, A. R. Use of binding energy in catalysis: Optimization of rate in a multistep reaction. *Biochemistry* **1993**, *32*, 5321-5326.

(7) Whitty, A.; Fierke, C. A.; Jencks, W. P. Role of binding energy with coenzyme A in catalysis by 3-oxoacid coenzyme A transferase. *Biochemistry* **1995**, *34*, 11678-11689.

(8) Wells, T. N. C.; Fersht, A. R. Use of binding energy in catalysis analyzed by mutagenesis of the tyrosyl-tRNA synthetase. *Biochemistry* **1986**, *25*, 1881-1886.

(9) Wade, H.; Scanlan, T. S. Remote binding energy in antibody catalysis: Studies of a catalytically unoptimized specificity pocket. *J. Am. Chem. Soc.* **1999**, *121*, 1434-1443.

(10) Wade, H.; Scanlan, T. S. The structural and functional basis of antibody catalysis. *Ann. Rev. Biophys. Biomol. Struct.* **1997**, *26*, 461-493.

(11) Ulrich, H. D.; Mundorff, E.; Santarsiero, B. D.; Driggers, E. M.; Stevens, R. C.; Schultz, P. G. The interplay between binding

energy and catalysis in the evolution of a catalytic antibody. *Nature* **1997**, *389*, 271-275.

(12) Stewart, J. D.; Benkovic, S. J. Transition-state stabilization as a measure of the efficiency of antibody catalysis. *Nature* **1995**, *375*, 388-391.

(13) Benkovic, S. J. Catalytic antibodies. *Ann. Rev. Biochem.* **1992**, *61*, 29-54.

(14) Wade, H.; Scanlan, T. S. P1-S1 interactions control the enantioselectivity and hydrolytic activity of the norleucine phenylesterase catalytic antibody 17E8. *J. Am. Chem. Soc.* **1996**, *118*, 6510-6511.

(15) Bizzozero, S. A.; Baumann, W. K.; Dutler, H. Kinetic investigation of the α-chymotrypsin-catalyzed hydrolysis of peptide substrate. The relationship between the peptide structure c-terminal to the cleaved bond and reactivity. *Eur. J. Biochem.* **1982**, *122*, 251-258.

(16) Bauer, C.-A.; Thompson, R. C.; Blout, E. R. The active centers of *Streptomyces griseus* protease 3 and α-chymotrypsin: enzyme-substrate interactions remote from the scissile bond. *Biochemistry* **1976**, *15*, 1291-1296.

(17) Thompson, R. C.; Blout, E. R. Dependence of the kinetic parameters for elastase-catalyzed amide hydrolysis on the length of peptide substrates. *Biochemistry* **1973**, *12*, 57-65.

(18) Thompson, R. C. Binding of peptides to elastase: Implication for the mechanism of substrate hydrolysis. *Biochemistry* **1974**, *13*, 5495-5501.

(19) Stroud, R. M. A family of protein-cutting proteins. *Amer. Sci.* **1974**, *231*, 74-88.

(20) Fersht, A. R.; Dingwall, C. An editing mechanism for the methionyl-tRNA synthetase in the selection of amino acid in protein synthesis. *Biochemistry* **1979**, *18*, 1250-1255.

(21) Dorovska, V. N.; Varfolomeyev, S. D.; Kazanskaya, N. F.; Klyosov, A. A.; Martinek, K. The influence of the geometric

174

properties of the active centre on the specificity of α-chymotrypsin catalysis. *FEBS Lett.* **1972**, *23*, 122-124.

(22) Berezin, I. V.; Kazanskaya, N. F.; Klyosov, A. A.; Martinek, K. On the relationship between structure and reactivity of α-chymotrypsin substrates. *FEBS Lett.* **1971**, *15*, 125-128.

(23) Hansch, C.; Leo, A.; Hoekman, D. *Exploring QSAR: Hydrophobic, Electronic, and Steric Constants*; American Chemical Society: Washington, D.C., 1995.

(24) Zhou, G. W.; Guo, J.; Huang, W.; Fletterick, R. J.; Scanlan, T. S. Crystal structure of a catalytic antibody with a serine protease active site. *Science* **1994**, *265*, 1059-1064.

(25) Guo, J.; Huang, W.; Zhou, W.; Fletterick, R. J.; Scanlan, T. S. Mechanistically different catalytic antibodies obtained from immunization with a single transition-state analog. *Proc. Natl. Acad. Sci., USA* **1995**, *92*, 1694-1698.

(26) Guo, J.; Huang, W.; Scanlan, T. S. Kinetic and mechanistic characterization of an efficient hydrolytic antibody: Evidence for the formation of an acyl intermediate. *J. Am. Chem. Soc.* **1994**, *116*, 6062-6069.

(27) Mader, M. M.; Bartlett, P. A. Binding energy and catalysis: The implications for transition state analogs and catalytic antibodies. *Chem. Rev.* **1997**, *97*, 1281-1301.

(28) Bartlett, P. A.; Marlowe, C. K. Phosphonamidates as Transition-State Analogue Inhibitors of Thermolysin. *Biochemistry* **1983**, *22*, 4618-4624.

(29) Wolfenden, R. Transition state analog inhibitors and enzyme catalysis. *Annu. Rev. Biophys. Bioeng.* **1976**, *5*, 271-306.

(30) Gandour, R. D.; Schowen, R. L. *Transition states of biochemical processes*; Plenum Press: New York, 1978.

(31) Fukuda, M.; Kunugi, S. Pressure dependence of thermolysin catalysis. *Eur. J. Biochem.* **1984**, *142*, 565-570.

(32) Fukuda, M.; Kunugi, S. Kinetic studies of wheat carboxypepridase-catalyzed reaction: Difference in pressure and temperature dependence of peptidase and esterase activities. *J. Biochem.* **1987**, *101*, 233-240.

(33) Hinz, H.-J.; Weber, K.; Flossdorf, J.; Kula, M.-R. Thermodynamic studies on the specificity of L-isoleucine•tRNA ligase of *Escherichia coli* MRE 600. *Eur. J. Biochem.* **1976**, *71*, 437-442.

(34) Ross, P. D.; Subramanian, S. Thermodynamics of protein association reactions: Forces contributing to stability. *Biochemistry* **1981**, *20*, 3096-3102.

(35) Sturtevant, J. M. Heat capacity and entropy changes in processes involving proteins. *Proc. Natl. Acad. Sci.* **1977**, *74*, 2236-2240.

(36) Baldwin, R. L. Temperature dependence of the hydrophobic interaction in protein folding. *Proc. Natl. Acad. Sci.* **1986**, *83*, 8069-8072.

(37) Edsall, J. T.; Gutfreud, H. *Biothermodynamics. The study of biochemical processes at equilibrium*; John Wiley and Sons: New York, 1983.

(38) Creighton, T. E. *Proteins: Structure and Molecular Properties*; Second ed.; W.H. Freeman and Company: New York, 1993.

(39) Edsall, J. T. Apparent molal heat capacities of amino acids and other organic compounds. *J. Am. Chem. Soc.* **1935**, *57*, 1506-1507.

(40) Wolfenden, R. Enzyme catalysis: Conflicting requirements of substrate access and transition state affinity. *Molecular and Cellular Biochemistry* **1974**, *3*, 207-211.

(41) Bartlett, P.; Otake, A. Fluoroalkenes as peptide isosteres: Ground state analogs inhibitors of thermolysin. *J. Org. Chem.* **1995**, *60*, 3107-3111.

(42) Bartlett, P. A.; Giangiordano, M. A. Transition state analogy of phosphonic acid inhibitors of pepsin. *J. Org. Chem* **1996**, *61*, 3433-3438.

(43) Phillips, M. A.; Kaplan, A. P.; Rutter, W. J.; Bartlett, P. A. Transition state characterization: A new approach combining inhibitor analogs and variation in enzyme structure. *Biochemistry* **1992**, *31*, 959-963.

Chapter 5. A Thermodynamic Analysis of Transition-state Analog Binding and Transition-state Stabilization

Abstract

In this chapter, a calorimetric investigation of the binding of several phosphonate ligands to the catalytic antibody 17E8 is reported. We find that the forces that contribute to phosphonate binding correlate well with those that are responsible for the stabilization of the catalytic transition-state as determined from kinetic studies with alternative substrate analogs. In addition, we find that closer examination of the thermodynamic parameters associated with binding reveal some thermodynamic differences between phosphonate binding and the desired catalytic features of a hydrolytic active site. The most significant difference involves the energetic contribution from electrostatic interactions to phosphonate binding and the importance of coulombic interactions to the stabilization of an anionic transition-state. These thermodynamic differences illustrate what may be a limitation of using transition-state analogs and binding screens to obtain efficient hydrolytic antibodies.

Introduction

Transition-state stabilization by binding transition-states tightly has been an important principle for generating catalytic antibodies.[1-3] The three dimensional structures of several hydrolytic antibody•hapten complexes reveal the noncovalent interactions that are responsible for the tight binding of the phosphonate antigens (Figure 5.1).[4-7] These same interactions are presumably used to stabilize the transition-states of the reactions that the antibodies catalyze. Although the activation of the immune system using phosphonate antigens has been reliable for generating antibodies with catalytic properties, the hydrolytic activities of these catalysts are low compared to enzymes that catalyze analogous reactions.[1,8] In addition, there seems to be a maximal rate acceleration of $\sim 10^4$ that is difficult to surpass using phosphonates.[1]

Understanding how catalytic antibodies use binding energy and determining the molecular forces that drive transition-state analog binding may help identify the barriers to achieving antibodies of higher efficiencies. Determining the thermodynamic relationship between the binding of the transition-state analog and the stabilization of the transition-state may also help one to design rational and random mutagenesis experiments in protein engineering of catalytic antibodies.[9-12]

17E8, which catalyzes the efficient enantioselective hydrolysis of the phenyl esters of n-formylated amino acids, has been shown to be a 'well-behaved' system to study the correlation between transition-state analog binding and the stabilization of the hydrolytic transition-state (Figure 5.2). The kinetic activity of several substrate analogs and the binding of their corresponding phosphonate analogs correlate directly, indicating that the phosphonates are good mimics of the catalytic transition-state and good probes of transition-state•17E8 interactions.[13]

In this study, titration calorimetry is used to study the thermodynamic forces that drive the association between phosphonate transition-state analogs and the catalytic antibody 17E8. Several phosphonates are used to determine the contributions of the hydrophobic effect, electrostatic interactions, and van der Waals interactions to the free-energy of transition-state analog binding. These forces, as determined from the thermodynamic values, correlate well to those as determined from kinetic experiments with substrate analogs. A closer look at the thermodynamic parameters associated with phosphonate binding reveal possible thermodynamic differences between phosphonate binding to 17E8 and the desired binding interactions between 17E8 and the catalytic transition-state.
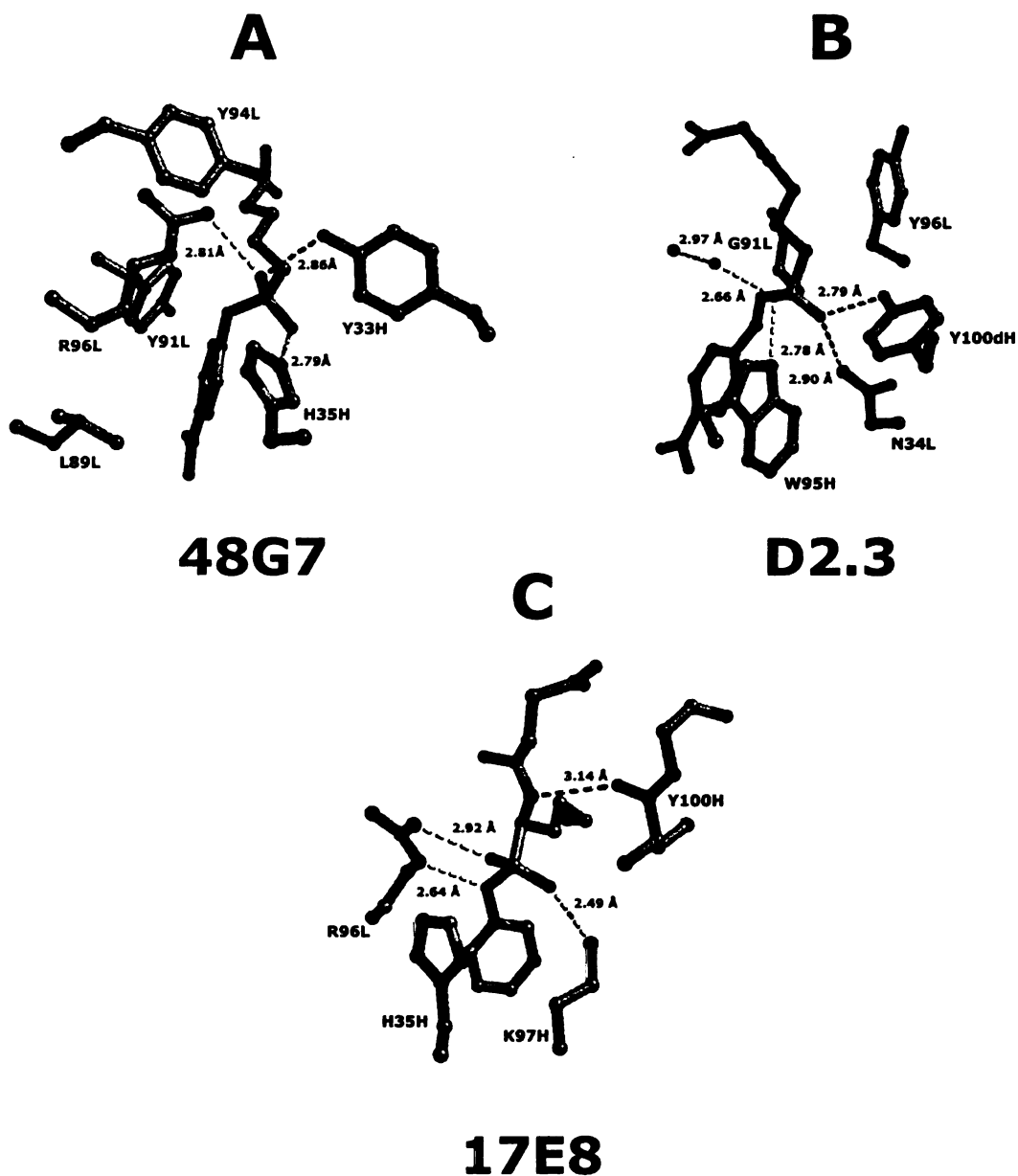
Figure 5.1 Important active site interactions of three hydrolytic antibodies with the corresponding phosphonate transition state analog. These interactions are presumed to be responsible for stabilizing the rate limiting anionic transition state of the corresponding hydrolytic reaction. **A.** 48G7 **B.** D2.3 **C.** 17E8
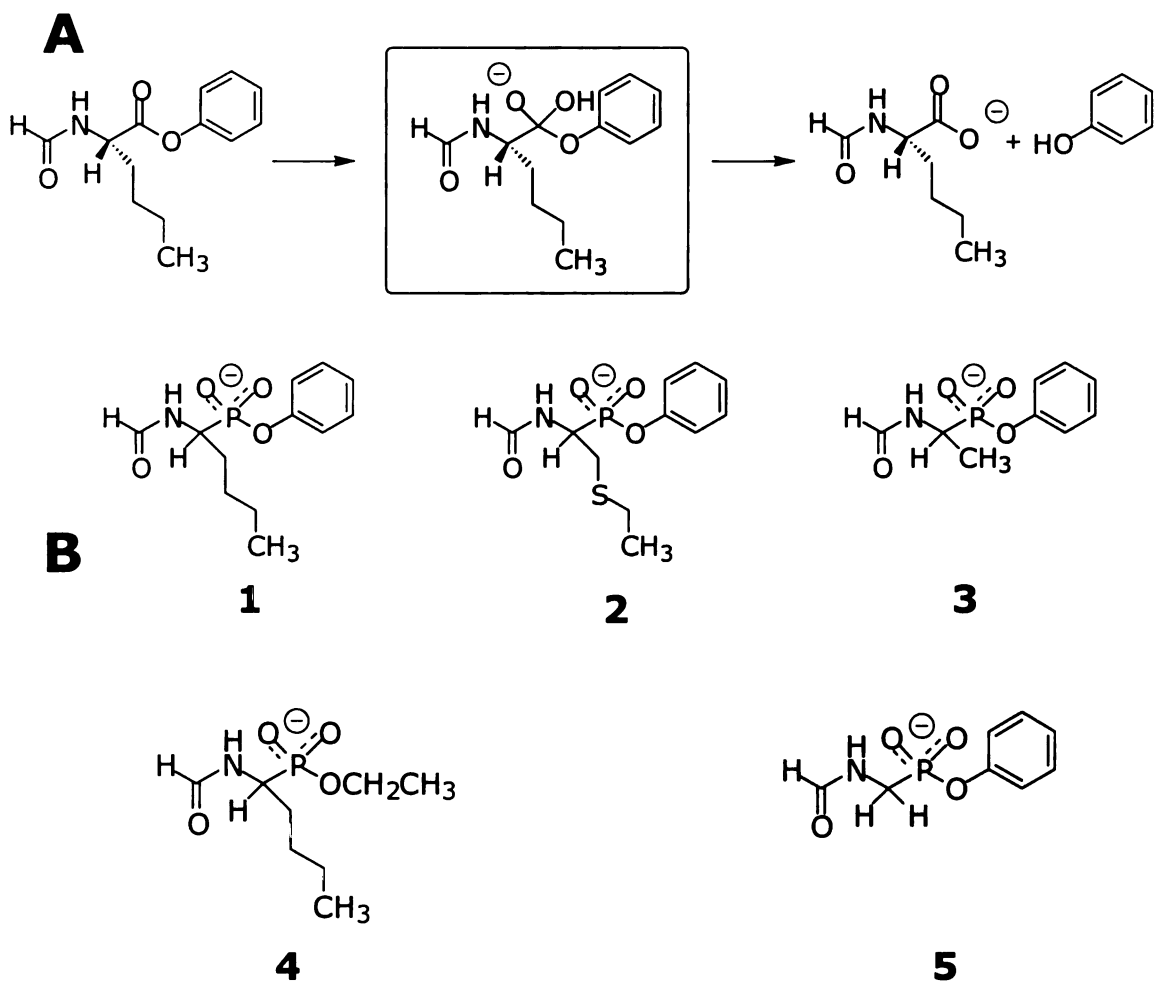
Figure 5.2 A. Reaction catalyzed by 17E8. (Boxed) Putative tetrahedral intermediate formed during reaction. **B.** Phosphonates used in calorimetric experiments (calorimetric experiments were not performed on **4** and **5**).

	[1]	[2]	[3]
$K_a \times 10^{-5} (M^{-1})$	6 ± 1	3 ± 1	0.34 ± 0.08
ΔH_{bind} (kcal/mol)	-4.0 ± 0.2	-2.9 ± 0.2	-1.7 ± 0.2
ΔG_{bind} (kcal/mol)	-7.9 ± 0.1	-7.5 ± 0.2	-6.2 ± 0.1
ΔS_{bind} (cal/(mol•K))	13 ± 1	16 ± 2	15 ± 1

Table 5.1 Thermodynamic parameters associated with the binding of **1**, **2**, and **3**. The calorimetric experiments were performed at 24.5 ± 1.0 °C in 50 mM phosphate, 150 mM NaCl, pH 7.2. Racemic mixtures of the phosphates were used. The thermodynamic values reflect the binding of one enantiomer. The errors associated with the parameters (K_a, ΔG°_{bind}, and ΔH°_{bind}) were obtained from the calculated fit to the one sites model (Wiseman Isotherm) using the program OMEGA (MicroCal, Inc). The free energy change, and the entropy change, were calculated from the equation, $\Delta G^{\circ}_{bind} = -RT\ln K_a = \Delta H^{\circ}_{bind}-T\Delta S^{\circ}_{bind}$. The errors associated with the ΔS°_{bind} (standard state = 1.0 M) parameter were determined through the propagation of errors associated with ΔG°_{bind} and ΔH°_{bind}.

Results

Thermodynamic Parameters Associated with Transition-state Analog Binding. The thermodynamic parameters associated with the binding of **1**, **2**, and **3** at 25°C and pH 7.2 are shown in Table 5.1 (standard state = 1.0 M). The association constants (and free-energy changes, $\Delta G°_{bind}$) for the binding of **1** and **2** are similar, whereas **3** binds about 20-fold less tightly. The enthalpy of the binding, $\Delta H°_{bind}$, of the phosphonates follows the same trend as that of $\Delta G°_{bind}$. The entropy of binding, $\Delta S°_{bind}$, is positive and similar in magnitude for all of the phosphonates and contributes more favorably to the free-energy of binding than does the enthalpy of binding for **2** ($T\Delta S°_{bind}$ = + 4.8 kcal/mol), and **3** ($T\Delta S°_{bind}$ = + 4.5 kcal/mol). Both $\Delta S°_{bind}$ and $\Delta H°_{bind}$ contribute equally to $\Delta G°_{bind}$ for **1** ($T\Delta S°_{bind}$ = + 3.8 kcal/mol).

Temperature Dependence of Transition-state Analog Binding. The temperature dependence of the thermodynamic parameters of binding for **1**, **2**, and **3** was examined from 10°C to 30°C at pH 7.2 in PBS (Table 5.2). The $\Delta H°_{bind}$ decreased in a linear fashion over the temperature range (Figure 5.3). The temperature dependence of $\Delta H°_{bind}$ can be described by equation (1) (see legend Figure 5.3).[14,15] The following $\Delta Cp°_{bind}$ values were obtained for the phosphonates: - 118 cal/(mol•K) for **1**, - 65 cal/(mol•K) for **2**,

and - 53 cal/(mol•K) for **3**. The ΔG°_{bind} was fairly constant over the temperature range, while the entropy (and enthalpy) were significantly dependent on the temperature (Figure 5.4).
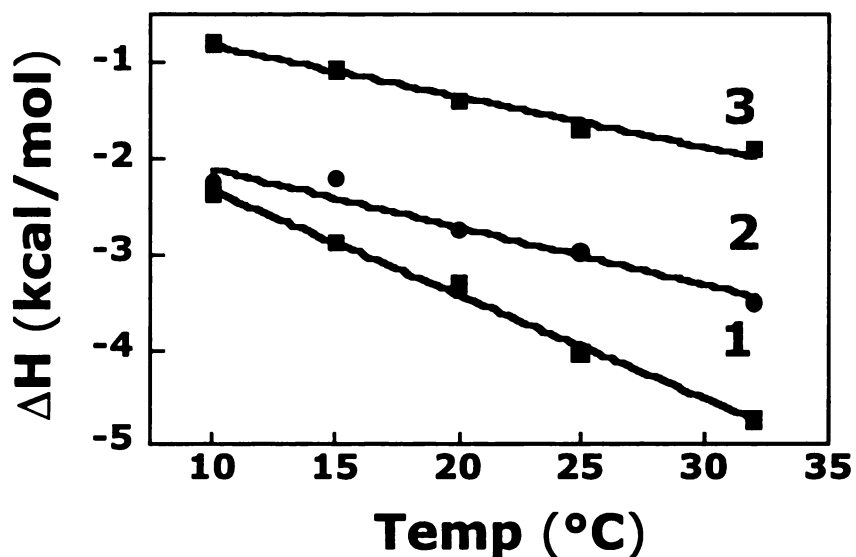
Figure 5.3 Temperature dependence of ΔH°_{bind} for **1**, **2**, and **3**. See legend for Table 5.2 for accompanying notes. The linear fit to the equation represents the relationship described by equation (1):

$$\Delta H^{\circ}_{bind} = \Delta H_0 + \Delta Cp^{\circ}_{bind}(T - T_0) \quad (1),$$

where ΔH_0 is the binding enthalpy at an arbitrary reference temperature T_0, and ΔCp°_{bind} is the heat capacity change of binding. The following ΔCp°_{bind} values and correlation coefficients were obtained from the fits: **1**, - 118 ± 8 cal/(mol•K), R = 0.993; **2**, - 65 ± 9 cal/(mol•K), R = 0.972; **3**, - 53 ± 5 cal/(mol•K), R = 0.989.

ΔG°_{bind} (kcal•mol^{-1})

Temp (°C)	[1]	[2]	[3]
10	-8.5 ± 0.1	-7.9 ± 0.1	-6.6 ± 0.2
15	-8.4 ± 0.1	-7.8 ± 0.1	-6.9 ± 0.1
20	-7.9 ± 0.1	-7.8 ± 0.1	-6.7 ± 0.1
25	-7.9 ± 0.1	-7.5 ± 0.2	-6.2 ± 0.1
30	-8.2 ± 0.1	-7.6 ± 0.1	-6.4 ± 0.1

ΔH°_{bind} (kcal•mol^{-1})

Temp (°C)	[1]	[2]	[3]
10	-2.4 ± 0.1	-2.3 ± 0.1	-0.77 ± 0.06
15	-2.9 ± 0.1	-2.2 ± 0.1	-1.1 ± 0.1
20	-3.3 ± 0.1	-2.7 ± 0.1	-1.4 ± 0.1
25	-4.0 ± 0.2	-2.9 ± 0.2	-1.7 ± 0.2
30	-4.7 ± 0.1	-3.5 ± 0.1	-1.9 ± 0.1

ΔS°_{bind} (cal•mol^{-1}•K^{-1})

Temp (°C)	[1]	[2]	[3]
10	20 ± 1	19 ± 1	20 ± 1
15	19 ± 1	19 ± 1	19 ± 1
20	15 ± 1	17 ± 1	18 ± 1
25	13 ± 1	16 ± 1	15 ± 1
30	12 ± 1	14 ± 1	15 ± 1

Table 5.2 Temperature dependence of the thermodynamic parameters for the binding of **1, 2,** and **3**. The experiments were performed at the indicated temperatures (± 1.0 °C) in 50 mM sodium phosphate, 150 mM NaCl, pH 7.2. The errors associated with the parameters (K_a, ΔG°_{bind}, and ΔH°_{bind}) were obtained from the calculated fit to the one–site model (Wiseman isotherm) using the program OMEGA (MicroCal, Inc). See the legend to Table 5.1 for other details.
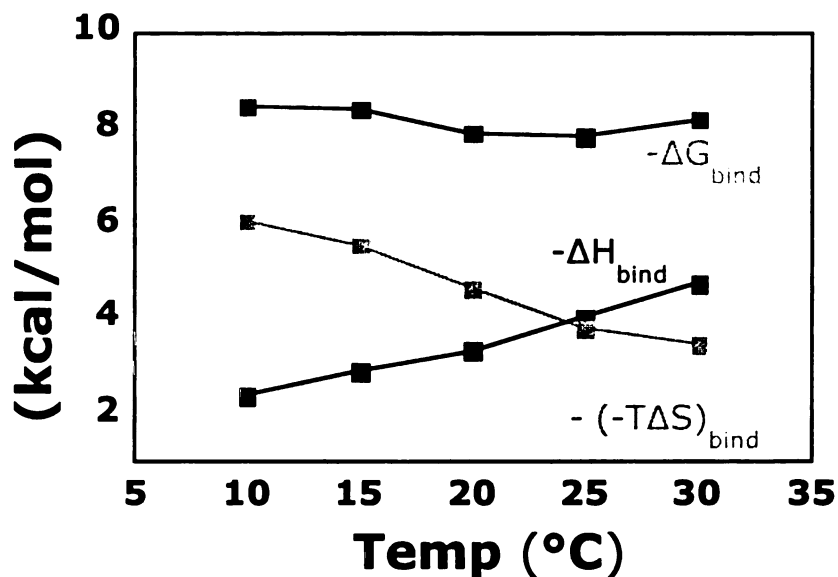
Figure 5.4 Graphical representation of the thermodynamic parameters associated with the dissociation of the **1•17E8** complex. Partitioning experiments involving the transfer of nonpolar molecules from a nonpolar medium to an aqueous media are used to determine the thermodynamic parameters associated with the hydrophobic effect. In the phosphonate binding experiments, the nonpolar moieties are transfered from the aqueous media to the more hydrophobic media. Therefore, the dissociation constant is more relevant in determining the magnitude of the hydrophobic effect associated with phosphonate binding than is the association constant. The values ΔS°_{bind} and ΔH°_{bind} are associated with the K_a, and the - ΔS°_{bind} and - ΔH°_{bind} values are associated with the K_d.
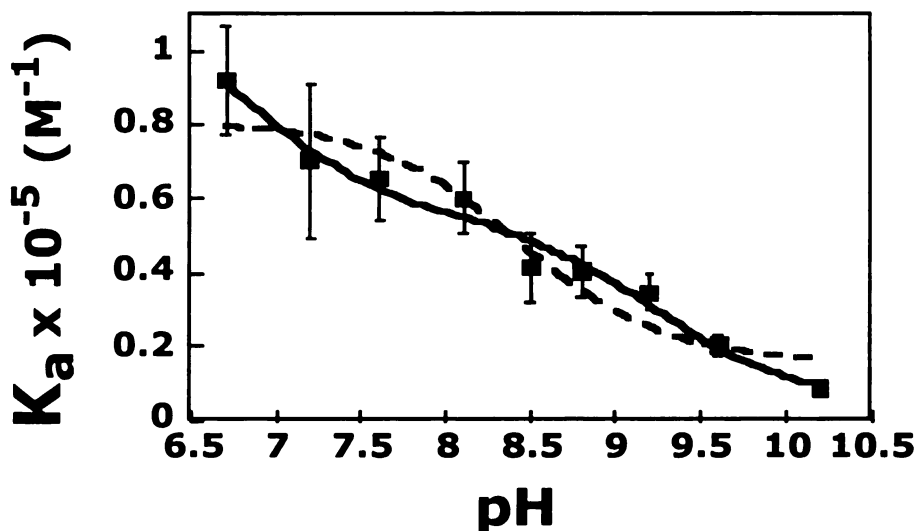
Figure 5.5 pH Dependence of Transition-state Analog Binding. Calculated fits to the experimental data derived from models in which transition-state analog binding is coupled to one (dashed fit) and to two (solid fit) antibody ionizations. The model involving one antibody ionization (Figure 5.5a) is described by equation (2):

$$K_{a(obs)} = K_{A1}\left(1 + \frac{K_3}{[H^+]}\right) \Big/ \left(1 + \frac{K_1}{[H^+]}\right) \quad (2),$$

where K_1 represents the proton dissociation constant for the unbound antibody, and K_3 represents that for the antibody•phosphonate complex. $K_{a(obs)}$ is the observed association constant at the different pH values, and K_{A1} is the association constant for phosphonate binding to the fully protonated antibody. The model involving two antibody ionizations (Figure 5.5b) is described by equation (3):

$$K_{a(obs)} = K_{A1}\left(1 + \frac{K_3}{[H^+]} + \frac{K_3 K_4}{[H^+]^2}\right) \Big/ \left(1 + \frac{K_1}{[H^+]} + \frac{K_1 K_2}{[H^+]^2}\right) \quad (3),$$

where K_1 and K_2 represent the first and second proton dissociation constants for the unbound antibody, respectively, and K_3 and K_4 represents the first and second ionization constants for the antibody•phosphonate complex, respectively. The values determined from the use of equation (2) are as follows: $pK_1 = 8.4 \pm 0.2$, $pK_3 = 9.1 \pm 0.4$, and $K_{A1} = 8.1 \pm 0.6 \times 10^5$ (M^{-1}). The correlation coefficient (R) for the fit to equation (2) is 0.957. The values determined from the use of equation (3) are as follows: $pK_1 = 7.1 \pm 0.6$, $pK_2 = 9.2 \pm 0.3$, $pK_3 = 6.7 \pm 0.7$, $pK_4 = 10.3 \pm 1$ and $K_{A1} = 1.2 \pm 0.5 \times 10^6$ (M^{-1}). The correlation coefficient (R) for the fit to equation (3) is 0.989.

A

$$IgGH_2 + L \xrightleftharpoons{K_1} IgGH- + L + H+$$

$$KA_1 \Updownarrow \qquad\qquad KA_2 \Updownarrow$$

$$IgGH_2{\bullet}L \xrightleftharpoons{K_3} IgGH-{\bullet}L + H+$$

B

$$IgGH_2 + L \xrightleftharpoons{K_1} IgGH^- + L + H^+ \xrightleftharpoons{K_2} IgG^{2-} + L + 2H^+$$

$$K_{A1} \Updownarrow \qquad\qquad K_{A2} \Updownarrow \qquad\qquad K_{A3} \Updownarrow$$

$$IgGH_2{\bullet}L \xrightleftharpoons{K_3} IgGH^-{\bullet}L + H^+ \xrightleftharpoons{K_4} IgG^{2-}{\bullet}L + 2H^+$$
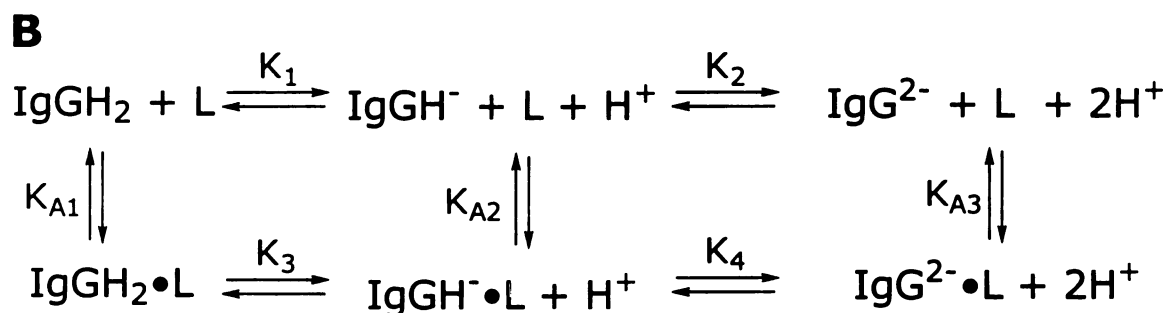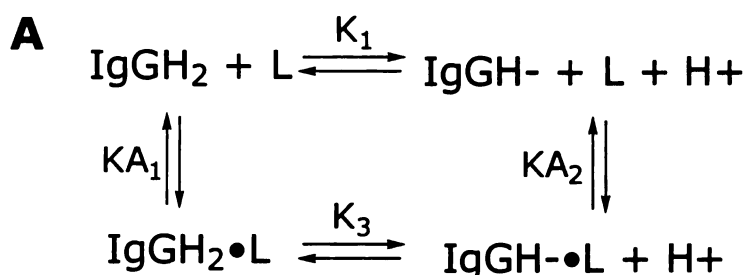
Figure 5.6. Ionization Behavior and Binding of **1** to 17E8. **A.** Model in which transition–state analog binding is coupled to one antibody ionization. **B.** Model in which transition–state analog binding is coupled to two antibody ionizations. Model **B** is favored over **A** for reasons discussed in the text. The association constants to the mono-protonated antibody and the fully protonated antibody were determined from the equations $K_{A2} = \dfrac{K_{A1}K_3}{K_1}$ and

$K_{A3} = \dfrac{K_{A2}K_4}{K_2}$, respectively. The determined values are $(4 \pm 1) \times 10^5$ M^{-1} and

$(3 \pm 2) \times 10^4$ M^{-1}, respectively. The association constants for **1** to the bis-protonated, K_{A1}, equals $(1.2 \pm 0.5) \times 10^6$ M^{-1}.

Figure 5.7
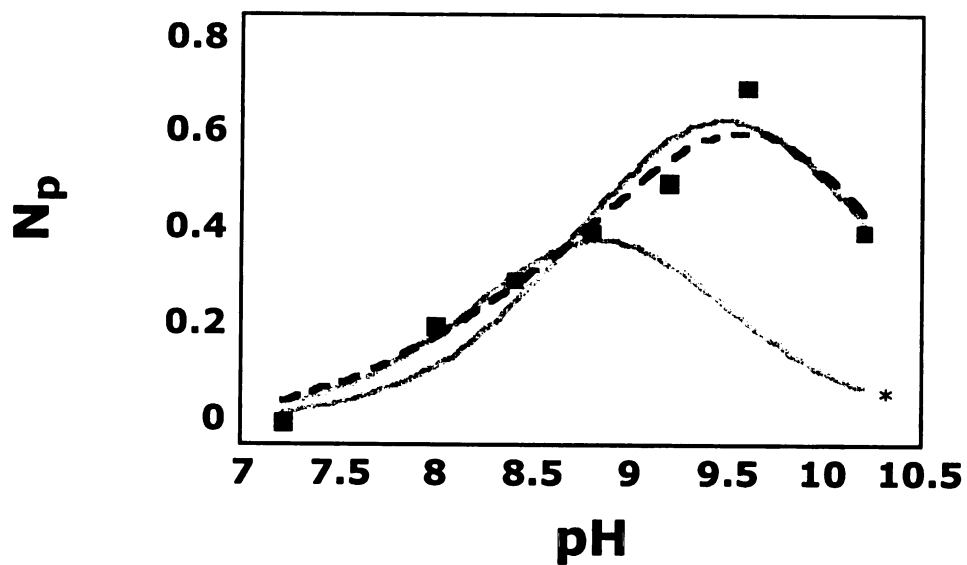
Figure 5.8
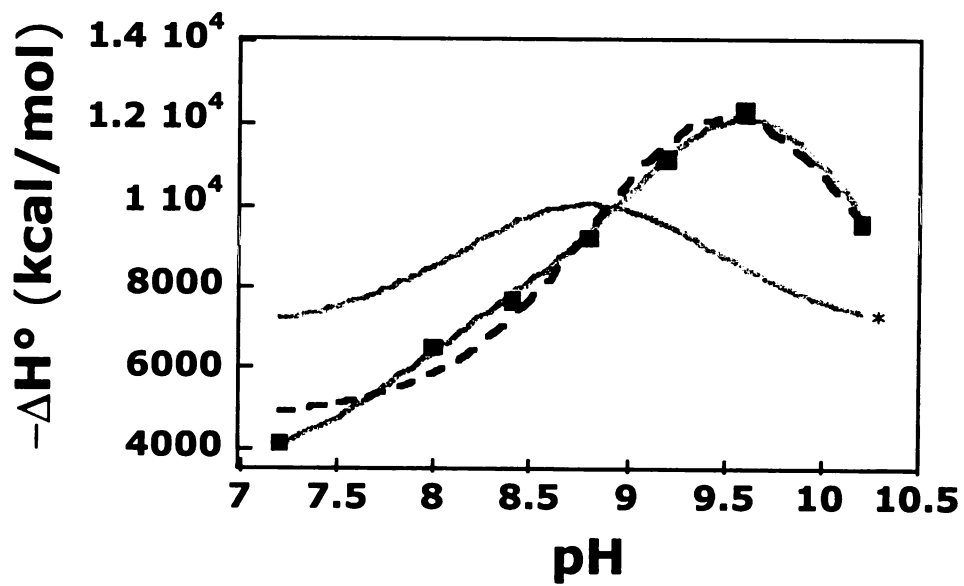
Figure 5.7 Proton linkage to Transition-state Analog Binding. Shown are the calculated fits to the equations which describes difference between the fractional saturation of protons in the free antibody and the antibody complexes. This difference yields the change in the number of protons bound by the antibody upon binding of the phosphonate ligand. The N_p values were determined as described in the text (see equation (4)). Equation (5), which is represented by the dashed fit, corresponds to a model in which one antibody ionization contributes to the change in the number of protons bound by complexation. Equation (6), which is represented by the solid fit, corresponds to a model involving the contribution of two antibody ionizations. The equation involving one ionization is as follows:

$$N_p = \frac{K^B[H^+]}{1+K^B[H^+]} - \frac{K^F[H^+]}{1+K^F[H^+]} \quad (5),$$

where K^B is the proton binding constant for the complexed antibody, K^F is the proton binding constant for the free antibody, respectively. The equation involving two antibody ionizations is as follows:

$$N_p = \left(\frac{K_1^B[H^+]}{1+K_1^B[H^+]} - \frac{K_1^F[H^+]}{1+K_1^F[H^+]} \right) - \left(\frac{K_2^B[H^+]}{1+K_2^B[H^+]} - \frac{K_2^F[H^+]}{1+K_2^F[H^+]} \right) \quad (6),$$

where K^B_1 and K^B_2 are the proton binding constants for the complexed antibody, K^F_1 and K^F_2 are the proton binding constants for the free antibody, respectively. The pK_a values determined from equation (5) are as follows: pK^B = 10.1 ± 0.1 and pK^F = 8.8 ± 0.1. The correlation coefficient for the fit is R = 0.956. The pK_a values determined from equation (6) are as follows: pK^B_1 = 10.2 ± 0.2, pK^B_2 = 8.3 ± 1.0, pK^F_1 = 9.1 ± 0.4, and pK^F_2 = 8.1 ± 0.8. The correlation coefficient for the fit is R = 0.973.

Figure 5.8 Binding Enthalpy Dependence on pH. Shown are the calculated fits to the experimental data derived from models in which the enthalpy of transition-state analog binding includes contributions from one (dashed line, equation (7)) and two antibody ionizations (solid line, equation (8)). The equation for the one ionization model is as follows:

$$\Delta H^o = \Delta H_o + \left(\frac{K^B[H^+]}{1+K^B[H^+]} \right) \Delta H_1 - \left(\frac{K^F[H^+]}{1+K^F[H^+]} \right) \Delta H_2 \quad (7),$$

where K^B is the proton binding constant for the complexed antibody, K^F is the proton binding constant for the free antibody, ΔH_o is the enthalpy that is independent of pH, and ΔH^o is the observed binding enthalpy after accounting for proton transfer effects (see equation (4)). ΔH_1 and ΔH_2 are the enthalpies of protonation of the antibody•phosphonate complex and the free antibody, respectively. The equation that includes the contributions from two antibody ionizations is as follows:

$$\Delta H^o = \Delta H_o + \left(\frac{K_1^B[H^+]}{1+K_1^B[H^+]} - \frac{K_1^F[H^+]}{1+K_1^F[H^+]} \right) \Delta H_1 + \left(\frac{K_2^B[H^+]}{1+K_2^B[H^+]} - \frac{K_2^F[H^+]}{1+K_2^F[H^+]} \right) \Delta H_2 \quad (8),$$

where K^B_1 and K^B_2 are the first and second proton binding constants for the complexed antibody, respectively, and K^F_1 and K^F_2 are the proton binding constants for the free antibody, respectively. ΔH_1 and ΔH_2 are the protonation enthalpies of the two different sites. The equation is derived from a model that assumes that the heat of protonation doesn't change upon complexation. The following equation:

$$\Delta H^o = \Delta H_o + \left(\frac{K_1^B[H^+]}{1+K_1^B[H^+]} \right) \Delta H_1 + \left(\frac{K_2^B[H^+]}{1+K_2^B[H^+]} \right) \Delta H_2 - \left(\frac{K_1^F[H^+]}{1+K_1^F[H^+]} \right) \Delta H_3 - \left(\frac{K_2^F[H^+]}{1+K_2^F[H^+]} \right) \Delta H_4 \quad (9),$$

takes into consideration changes in the heats of protonation upon complexation. The enthalpies obtained from the use of equation (7) are as follows: $\Delta H_o = -5.2 \pm 1.3$ kcal/mol, $\Delta H_1 = -13.6 \pm 2.3$ kcal/mol, and $\Delta H_2 = -14.0 \pm 1.5$ kcal/mol (R = 0.985). Using the equation in which the heat of protonation is not taken into consideration yields a very poor fit with an R value of 0.395 for the one ionization model. The K^B and K^F values were taken from values obtained with the use of the N_p vs pH relationship (equation (5)–one ionization). The enthalpies obtained from the use of equation (8) are as follows: $\Delta H_o = -3.2 \pm 0.2$ kcal/mol, $\Delta H_1 = -15.1 \pm 0.4$ kcal/mol, and $\Delta H_2 = -13.5 \pm 1.5$ kcal/mol (R = 0.998). The K^B and K^F values were taken from values obtained with the use of the N_p vs pH relationship (equation (6)–two ionizations). Consideration of changing heats of protonation upon complexation yields the following values: ΔH_o, - 1.7 ± 0.3 kcal/mol; ΔH_1, - 18.2 ± 0.5 kcal/mol; ΔH_2, - 19.3 ± 0.9 kcal/mol; ΔH_3, - 20.0 ± 1.8 kcal/mol; ΔH_4, - 17.4 ± 1.3 kcal/mol. The correlation coefficient of the fit is 0.999. The curved marked by the asterisk is corresponds to the one ionization model (equation (7)) fitted with pK_a values obtained from the use of equation (3).

pH Dependence of Transition-state Analog Binding. The

pH dependence of the binding of **1** was studied over the range of 6.7

to 10.2. The variation of the association constant over the pH range is

shown in Figure 5.4. The value is largest occurs at pH 6.7 (K_a = 9.2 x

10^5 M^{-1}) and decreases with increasing pH (K_a = 9 x 10^4 M^{-1} at pH

10.2). The experimental data were fit both to two models: one

consisting of one ionizable residue (dashed fit-equation (2), Figure

5.4; also see Figure 5.5a); and one that consists of two ionizable

residues (solid fit-equation (3), Figure 5.4; also see Figure 5.5b). The

pK_a values obtained from the model involving one ionizable residue are

8.4 (pK_1) and 9.1 (pK_3). These pK_a values correspond to the free

antibody and the antibody•phosphonate complex, respectively. The

pK_a values obtained from the fit describing the contribution of two

ionizable residues are 7.1 (pK_1), 9.2 (pK_2), 6.8 (pK_3), and 10.3 (pK_4).

The pK_1 and pK_2 values correspond to ionizations of the free antibody,

whereas pK_3 and pK_4 correspond to those of the antibody•hapten

complex. The data appear to fit better the model described by

equation (3), but the errors associated with the determined pK_a values

are larger, and therefore, less determined than those obtained with

equation (2). One reason that the pK_a values determined with the fit

to equation (3) are not well determined as data is probably due to the

fact that data could not be obtained in the acidic and basic plateau

regions of the curve. The values that are determined from the model described by equation (3) are consistent with those observed in the pH dependencies of N_p and ΔH° (see below). Fitting N_p and ΔH° pH–dependences with the pK_a values obtained from the fit to equation (2) results in very poor fits (see Figure 5.5 and 5.6).

The ΔH°_{bind} is independent of the buffer system used at pH 7.2 (PBS, ΔH°_{bind} = - 4.0 kcal/mol; MOPS, - 4.5 kcal/mol; and Tris - 4.1 kcal/mol), ruling out a change in the protonation state of 17E8 upon binding of **1** at this pH. In contrast, the large variation in the ΔH°_{bind} of **1** in the glycine (ΔH°_{bind} = - 5.7 kcal/mol), and borate (- 9.4 kcal/mol) buffer systems at pH 9.2 indicates a change in the protonation state of 17E8 upon binding at this pH. By using equation (4):

$$\Delta H^\circ_{bind} = \Delta H^\circ + N_p\Delta H^\circ_{ion} \ (4),$$

where N_p is the number of protons absorbed or released upon binding, ΔH°_{bind} is the observed enthalpy, ΔH° is the intrinsic enthalpy, and ΔH°_{ion} is the ionization enthalpy of the buffer system, we estimate that ~ 0.7 protons are absorbed upon phosphonate binding at pH 9.2.**[14,15]**

The variation of N_p with pH is shown in Figure 5.7. The difference between the fractional saturation of protons in the free antibody and the fractional saturation of protons for the antibody

194

complex yields the change in the number of protons bound by the antibody upon binding.[16,17] This relationship can be used to determine the pK_a of the residues in the free 17E8 antibody and the 1•17E8 complex (see equations (5) and (6) in Figure 5.7 legend). The variation of N_p over the pH is consistent with the proton absorption associated with one residue over the pH range. The pK_a values of the residues determined (using equation (5)) for the free and bound antibody are 9.0 and 10.2, respectively (Figure 5.6). The curve fit to two antibody ionizations (using equation (6)) is also included. This curve fit also suggests that only one pK_a value changes upon phosphonate binding). This result is consistent with the pH dependence of the association constant that suggests that only one of the antibody ionizations is significantly shifted upon phosphonate binding.

The variation of the enthalpy ($\Delta H°$) with pH, after accounting for buffer effects, is shown in Figure 5.8. The $\Delta H°$ value is largest at approximately pH 9.6 ($\Delta H° = -12.3$ kcal/mol) and decreases with increasing and decreasing pH ($\Delta H° = -3.2$ kcal/mol at pH 6.7 and -7.7 kcal/mol at pH 10.2). The $\Delta H°$ values include the enthalpy of the protonation reaction of the residue(s) on the bound and free antibody and the enthalpy of binding of the phosphonate. The enthalpy-pH dependence data were fit to two models: one that includes

contributions from one antibody ionization (equation (7)) and one that includes contributions from two ionizations (equations (8) and (9)) (Figure 5.8). A good fit is obtained for all curves using the pK_a values determined from the N_p vs pH data, whereas the pK_a values afforded by the K_a–pH (equations (2) and (3)) dependence gave poor fits (see curves marked with asterisks in Figures 5.7 and 5.8). The fit to the model that includes two antibody ionizations (equations (8) and (9)) did not afforded a significantly better fit to the experimental data than the model that includes only one antibody ionization (equation (7)), suggesting that the inclusion of the additional parameters is not warranted. The observation of one ionization in the ΔH_{bind}–pH relationship is not surprising although two are seen in the K_a-pH dependence. Because $\Delta H_{bind} \approx \Delta H_o + \sum_i \Delta n_i \Delta H_i$, where ΔH_i is the protonation enthalpy of the ith ionizable group and ΔH_o represents the intrinsic binding enthalpy, the shape of the enthalpy–pH dependence curve can be dominated by the proton uptake (see N_p–pH dependence, Figure 5.7), especially when the enthalpy of the proton uptake is large as it is in this case. The pH independent enthalpy, ΔH_o, obtained from the fit to equation (7), is - 5.2 ± 1.3 kcal/mol. The calculated enthalpies of protonation of the residues in question are − 13.6 ± 2.3 kcal/mol (ΔH_1) and − 14.0 ± 1.5 kcal/mol (ΔH_2).

The estimated ΔH° is plotted against proton uptake by 17E8 in

Figure 5.9. This plot can be used to determine the average ΔH_p

(slope) for proton absorption upon the formation of the 1•17E8

complex and the average ΔH_{bind} (intercept) for 1•17E8 complex

formation in the absence of proton absorption. The determined

enthalpy for proton absorption upon binding is - 12.3 ± 0.7 kcal/mol.

The proton absorption independent enthalpy for binding determined

from the plot is - 4.2 ± 0.3 kcal/mol. These values are consistent with

those obtained from the ΔH°-pH relationship.

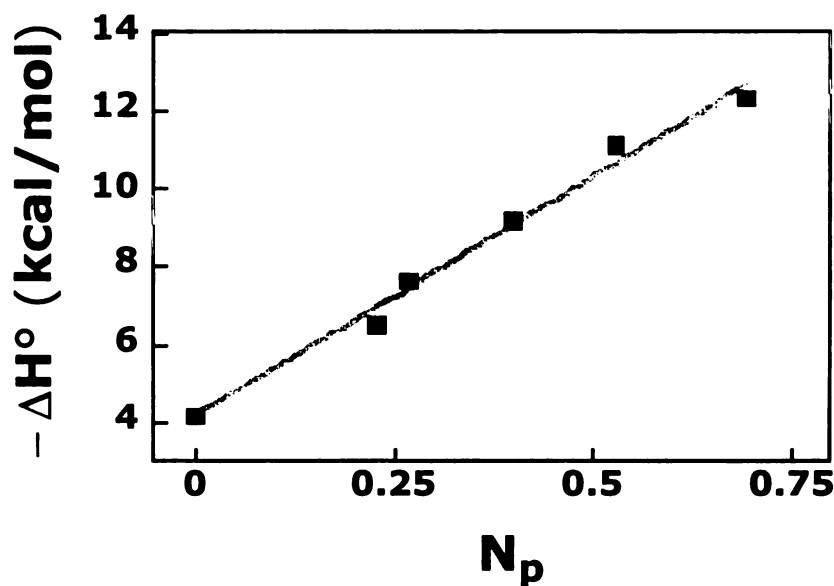**Figure 5.9** Enthalpy change for proton absorption and the proton absorption independent enthalpy change for 1•17E8 formation. The curve was calculated using a linear fit. The average enthalpy change for proton absorption determined from the fit is - 12.3 ± 0.7 kcal/mol. The determined proton absorption-independent binding enthalpy is - 4.2 ± 0.3 kcal/mol. The correlation coefficient for the fit is R = 0.993.

Discussion

The thermodynamics of binding for all of the phosphonates is governed by a small favorable enthalpic (ΔH°_{bind} = - 4.0 to - 1.7 kcal/mol) and a significant favorable entropic (ΔS°_{bind} = + 13 to + 16 cal/(mol•K)) contribution. The $T\Delta S^{\circ}_{bind}$ contributes more favorably to the ΔG°_{bind} than does the ΔH°_{bind} for **2** and **3**; ΔH°_{bind} and $T\Delta S^{\circ}_{bind}$ contribute equally for **1**. The enthalpic component of ΔG_{bind} is somewhat smaller than expected based on calorimetric studies of most small molecule-protein binding reactions, where ΔH_{bind} often exceeds - 10 kcal/mol.[18,19] In addition, the favorable ΔS°_{bind} contribution is surprising as the thermodynamics of many bimolecular association reactions is adversely affected by the entropic cost of bringing two molecules together (typically $\sim$ - 20 cal/(mol•K), 1 M standard state).[20-24]

The magnitude of ΔH°_{bind} and ΔS°_{bind} suggests that water may play a significant role in phosphonate binding.[19,25,26] This role can be explained in terms of the hydrophobic effect and electrostatic interactions. The transfer of both hydrophobic and charged groups from an aqueous environment to a more hydrophobic environment are characterized by near zero enthalpic changes, and large favorable entropic changes.[19,25-29] The favorable entropic changes in both cases result from the release of tightly bound water molecules that

198

solvate the hydrophobic and charged moieties on the uncomplexed

ligand and in the ligand binding site of the uncomplexed antibody.

Despite the anionic character of the phosphonates, the role of

the hydrophobic effect is evident from the temperature dependence of

phosphonate binding. The ΔCp°_{bind} value obtained from the

temperature dependence of ΔH°_{bind} is largest for the formation of the

1•17E8 complex followed by the **2**•17E8 and the **3**•17E8 complexes.

The ΔCp°_{bind} values corresponding to the complexes are consistent

with a dominant role of the hydrophobic effect on ligand binding as the

hydrophobicities of the side-chains follow the same trend: **1**

(pentane), log P = 3.39; **2** (diethyl sulfide), log P = 1.95; **3** (ethane),

log P = 1.81 (see legend for Figure 4.4).**[30]** Furthermore, the data

in Figure 5.4 show that the entropy of dissociation (- ΔS_{bind}) of **1** is

least favorable at low temperatures and becomes more favorable with

increasing temperature, while the opposite trend is observed for the

enthalpy of dissociation (- ΔH°_{bind}) of **1**, further indicating an important

contribution from the hydrophobic effect.**[26,27,31,32]** Moreover,

the magnitude of the difference in the ΔCp°_{bind} values between **1** and **3**

is consistent with the hydrophobic effect. Model compound data

suggest that the addition of a methylene group is expected to add ~

15 - 20 cal/(mol•K) to the magnitude of the ΔCp of transferring the

molecule from the hydrocarbon solvent to water.**[33,34]** The

difference of ~ 60 cal/(mol•K) between **1** and **3** is larger than the expected amount. This can be accounted for by the fact that two hydrophobic surfaces, namely the side-chain of the phosphonate and the antibody pocket, are being removed from water upon binding. In addition to the hydrophobic effect, the unfavorable increases in the ΔG°_{bind} and ΔH°_{bind} values resulting from the methylene group removal from the side-chain of **1** to yield **3** indicate a small energetic contribution from van der Waals interactions.

The contribution of the hydrophobic effect and van der Waals interactions to phosphonate binding correlates with the previously observed contribution of the hydrophobic effect to overall transition-state stabilization determined by kinetic studies with alternative substrates that contain side-chains of varying hydrophobicities.[13] The hydrophobic parameter, π, correlates well with the logarithmic values of k_{cat}/K_M for a series of substrates and with the K_I (ΔG°_{bind}) values for a series of phosphonates.

The thermodynamic data for the binding of the transition-state analogs also provides evidence for a contribution from electrostatic interactions. The removal of the side-chain methylene groups of **1** to yield **3** does not significantly alter the favorable $T\Delta S^{\circ}_{bind}$ contribution to phosphonate binding suggesting that the electrostatic interactions involving the phosphonate moiety and 17E8 may make a significant

contribution to the $T\Delta S^{\circ}_{bind}$ parameter. Additional evidence for the

participation of electrostatic interactions comes from a shift in the pK_a

value of a residue upon binding. The pK_a shift of (9 → 10) of a binding

site residue is apparent in the K_a-pH, N_p-pH, and ΔH°-pH dependencies

(Figures 5.5, 5.7, and 5.8). The estimated relationship between the

contribution of the electrostatic interactions to the ΔG°_{bind} and a pK_a

shift is:

$$\Delta G_{elec} = 2.303 RT (pK_a^F - pK_a^B) \ (10),$$

where pK_a^F and pK_a^B are the pK_a values associated with the residue in

the free and bound species, respectively.[19,25,29] The pK_a^F and

pK_a^B values in this system are 9 and 10, respectively. The estimated

ΔG°_{elec} value obtained from this equation for the 17E8 system is

approximately - 1.5 kcal/mol. This value is much smaller than the

ΔG°_{bind} (- 7.9 kcal/mol) and the ΔG°_u (- 10.2 kcal/mol) values

suggesting that the electrostatic interactions contribute little to

phosphonate binding. We believe that the ΔG°_{elec} value obtained from

equation (10) underestimates the actual ΔG°_{elec} value because it does

not account for the interactions between the phosphonate and the

residue Arg96L (see Figure 5.1), the pK_a value of which is presumably

too high to be observed in the pH range studied. The value obtained

from equation (10) also is much smaller than that obtained from

equation (11):

201

$$-T\Delta S_{elec} = 1.37\Delta G°_{elec} \quad (11),$$

where ΔS_{elec} is the unitary entropy associated with the of binding of **3** where most of the side-chain•pocket interactions have been removed.[25,28,35] The $\Delta G°_{elec}$ value obtained from equation (11) is - 4.8 kcal/mol. This value likely overestimates the actual $\Delta G°_{elec}$ value as it contains energetic contributions from interactions involving the phenol group and the remaining side•chain pocket interactions.

The importance of electrostatics in the 17E8 hydrolytic function is also apparent from the pH dependence of 17E8 catalysis.[36] The k_{cat}-pH rate profile is bell-shaped and characterized by the pK_a values of 9 and 10 with the maximum rate occurring at pH 9.5. The kinetic pK_a value of 10 has been assigned to the residue Lys97 on the 17E8 heavy chain.[37] Similarly, we believe that the residue that undergoes the pK_a shift of 9 to 10 upon phosphonate binding is Lys97. The experimentally determined value of the $\Delta H_{protonation}$ from the N_p-ΔH relationship (- 12.3 ± 0.7 kcal/mol) and the ΔH-pH relationship (- 13.6 ± 2.3 and - 14.0 ± 1.5 kcal/mol) are similar to the calorimetrically determined protonation heat of lysine in water ($\sim$ - 11 – 13 kcal/mol).[27] This further supports the assignment of this pK_a shift to Lys97H. The three dimensional structure of 17E8•**1** complex reveals that this residue forms a salt bridge with the phosphonate moiety on the transition-state analog, suggesting that it assists in the

electrostatic stabilization of the anionic transition-state.[37] Deprotonation of this residue results in a loss of this stabilization and a significant loss in catalysis. Correspondingly, the deprotonation of Lys97H results in reduction of binding affinity of **1**. Interestingly, the loss of binding of **1** ($\Delta\Delta G_{bind} \approx 1.5$ kcal/mol) associated with deprotonation of this residue is smaller than the corresponding loss of catalysis ($\Delta\Delta G^{\ddagger} > 3.2$ kcal/mol). There seems to be another pK_a that is apparently important in phosphonate binding. Its contribution to binding is only apparent in the K_a–pH relationship with a value between 7–8 (Figure 5.5). At this time, we cannot assign the residue associated with this value. It does not shift significantly upon phosphonate binding.

The correlation of phosphonate binding forces to catalysis indicates that active site properties that are elicited by phosphonates translate into catalysis. At first glance it would seem as if there is no apparent reason why catalyst screens based on transition-state analog binding rarely yield more efficient catalysts. The discussion below suggests that a closer look at some of the thermodynamic details associated with transition-state analog binding may yield insight into why this may be the case.

Enzymes stabilize transition-states primarily by lowering the enthalpy of activation relative to that of the corresponding uncatalyzed

203

reaction that occurs in solution.[38] This would also be expected of antibodies that catalyze the pseudo-first order ester hydrolysis reaction. The binding interactions between the phosphonate moiety and the side-chains in antibody•hapten complexes provide evidence that these catalysts contain pre-organized polar environments that lower the enthalpic and entropic requirements of activation relative to those for the uncatalyzed solution reactions (Figure 1).[4,5,7,37,39,40] These pre-organized active sites are functionally similar to the oxyanion hole in serine proteases and contain hydrogen bond donors from charged and uncharged amino acids and mediating water molecules.[41-45] These active site dipoles are shielded from bulk solvent upon formation of the catalyst•transition-state complex which prevents the dissipation of their electric field. This results in a large enthalpic stabilization of the charge-separated transition-state due to stronger coulombic interactions than those that would occur unshielded in bulk aqueous solution.[44-47] A favorable entropic component (relative to solution) results from the fact that the active site is pre-organized, and that water solvent molecules need not be immobilized to interact with the transition-state.

It might be desirable for the thermodynamics of phosphonate binding to an esterolytic antibody to be governed by a large favorable enthalpic component. This enthalpic component should be dominated

by interactions between the mono-anionic part of the phosphonate and the antibody since it is these interactions that give rise to the differential binding of the transition-state and the substrate, which results in increased turnover numbers (k_{cat}).[1,8,48,49] A large favorable enthalpic component would be indicative of a large coulombic interaction between the anionic phosphonate and an active site oxyanion hole that has a strong electrostatic field.[22,27,29]

Several lines of evidence suggest that these charged interactions make a small contribution to the observed ΔG°_{bind} and ΔH°_{bind} values. The binding of the phosphonate with the one carbon side-chain (**3**) is characterized by a small ΔH°_{bind} value of - 1.7 kcal/mol. This binding enthalpy includes contributions from interactions involving the remaining side-chain carbon, the phenol group, and the anionic part of the phosphonate. It is not unreasonable to expect the contribution from the van der Waals interactions involving the phenol group and the antibody to be similar to those from the side-chain•pocket interactions. After accounting for the contributions of these non-electrostatic interactions to ΔH°_{bind}, it becomes apparent that interactions involving the anionic moiety likely make a negligible or even unfavorable enthalpic contribution to binding. In addition, the removal of the side-chain from **1** (to yield **4**), and of many of the binding interactions involving the phenol moiety (examined with **5**)

result in unfavorable increases in ΔG°_{bind} of $\sim$ 5 kcal/mol (data not shown). This suggests that the interactions involving the anionic moiety do not dominate the energetics of phosphonate binding.

The thermodynamic values associated with phosphonate binding in this study do not reflect the desired properties for catalysis in the antibody active site. On the other hand, the values are consistent with what is known about the thermodynamic characteristics of hydrophobic and electrostatic interactions. These characteristics include smaller than typical favorable enthalpic, and larger than typical favorable entropic contributions to binding (see above).[25,27,29,32,50] Thus, there seem to be thermodynamic differences between the binding of phosphonates to hydrolytic antibodies and the desired properties of an efficient hydrolytic active site.

A component of the thermodynamic differences includes the desolvation processes of phosphonate binding to the uncomplexed antibody and the formation of the electronically similar transition-state•antibody complex from the free ester and antibody (Figure 5.11). Although the requirement of desolvating the charge(s) in the active site of the antibody is similar in each process, the energetic price to desolvate the uncharged ester substrate is lower than the price of desolvating the anionic phosphonate. Because the substrate

does not become charged in solution, there is never an extra energetic cost of desolvating a charge. This solvation difference between substrates and TS analogs may have important implications for obtaining catalysts from binding screens (see below). These solvation differences between transition-state analog binding and the formation of the transition-state from substrates may contribute to the poor correlation between the rate enhancements of many protein catalyzed reactions and the relative binding affinities of transition-state analogs and substrates.
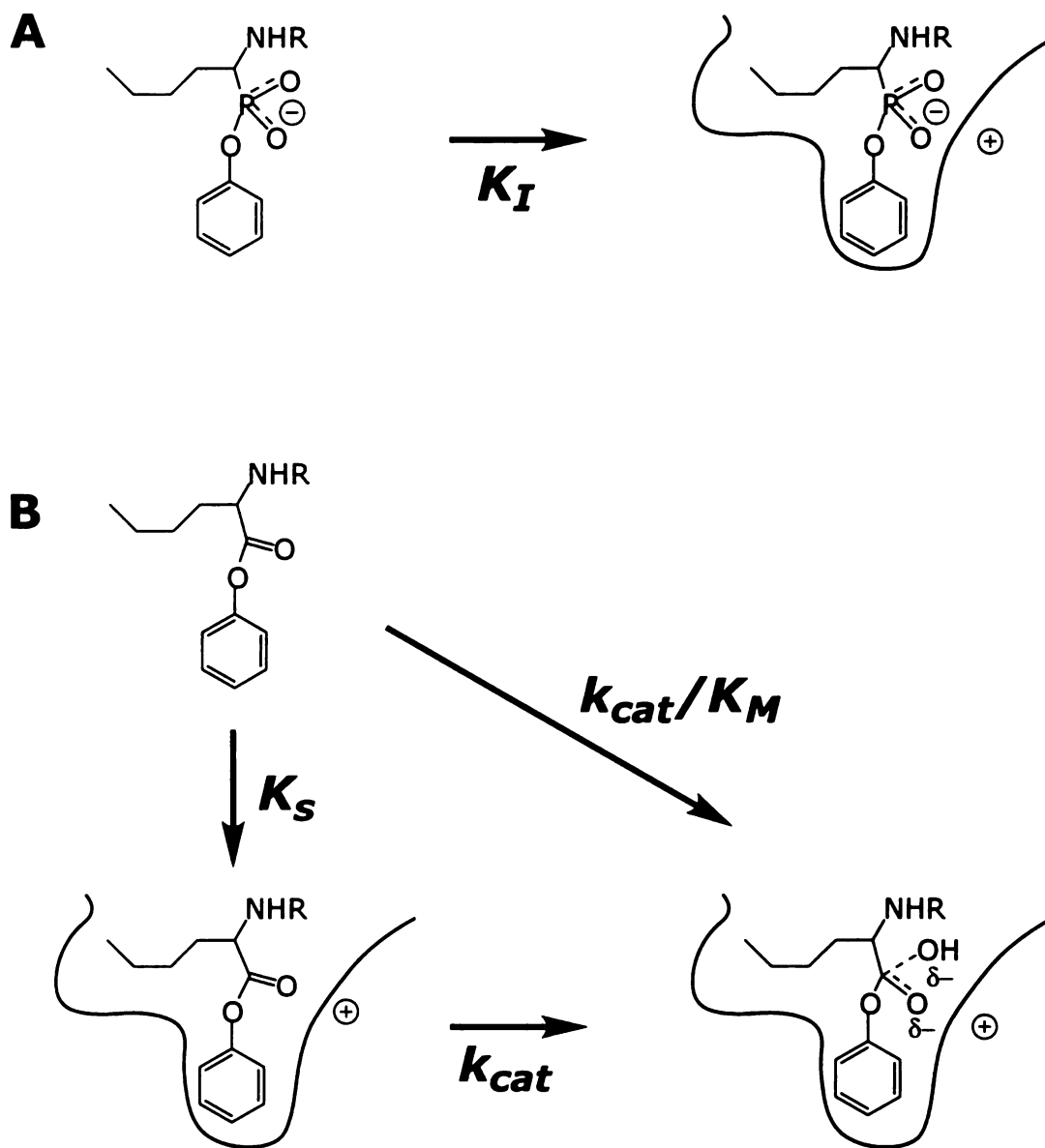
Figure 5.11 Differences between transition state analog binding (**A**) and transition–state formation (**B**).

The stabilization of transition-states often involves electrostatic and polar interactions.[51-54] Because the desolvation of charged groups on ligands and proteins often is not equally compensated by the coulombic attraction between interacting groups in the ligand•protein complex, electrostatic complementarity does not always contribute favorably to the free-energy of association.[25,29,55] Therefore, candidate protein catalysts obtained from screens based purely on transition-state analog binding will not necessarily contain active sites with stronger electric fields. Having such fields is not likely to increase the binding affinity of the TS analog because of the higher desolvation penalty associated with the more highly charged groups that contribute to the field. In contrast to binding, stronger coulombic interactions between a transition-state and an antibody are likely to facilitate catalysis.[47,56-58] It has also been suggested that the creation of such a highly charged site is likely to compromise protein stability and that this strain is compensated by tertiary interactions in the protein.[59-61] The fact that there are more solutions for binding and fewer for catalysis is probably a manifestation of this conundrum. For example, in phage display experiments involving 17E8, polar to non-polar mutations that maintained or increased phosphonate binding were observed.[11,12] However, these substitutions drastically reduced catalysis. In addition, the phosphonates used to generate

esterolytic antibodies are of similar size and bind to their respective

antibodies with similar affinities. The number of positively charged

residues in the antibody active site that directly interact with the

phosphonates ranges from 0 to 2 (Figure 5.1). The structures of

several esterolytic antibody•hapten complexes indicate that the

immune system has many energetically degenerate solutions for

interacting with phosphonate moieties, including hydrogen bonds from

tyrosine hydroxyl groups, histidine imido nitrogen protons, peptide

amide nitrogen protons, lysine side-chain amino protons, arginine

side-chain guanidinium protons, and mediating water

molecules.[4,5,7,37,39,40,62]

Conclusions

This thermodynamic study of the binding of several phosphonates to the catalytic antibody 17E8 reveals that the forces responsible for binding the transition-state analogs correlate well with 17E8's catalytic mechanism which most likely involves hydroxide attack on the ester substrate, and probably does not involve an acyl-antibody intermediate (described in ref. 34). The hydroxide attack mechanism is supported by several mutagenesis studies and by the fact that tetrahedral phosphonates have been shown to be good transition-state analogs.[12,13] The phosphonate binding data also correlate with the forces that are responsible for the stabilization of the catalytic transition-state as determined from kinetic studies with alternative substrate analogs. However, the thermodynamic parameters reveal some essential differences between phosphonate binding and the desired catalytic features of a hydrolytic antibody's interactions with a charged transition-state. These thermodynamic differences may illustrate quantitatively a limitation of using binding screens to obtain efficient hydrolytic antibodies. The results from this study also extend beyond catalytic antibodies, and include RNA, DNA, and other protein (or peptide) based catalysts.

Experimental Section

Materials. All molecular biology grade buffers used were purchased from commercial suppliers (Aldrich, Sigma, and Fisher) and were used without further purification. The phosphonate ligands (Figure 5.2) used in the studies were synthesized as described by Wade and Scanlan.[13]

Antibody Preparation: 17E8 was isolated from ascites fluid and purified by protein A affinity chromatography as described by Guo *et al* with several modifications.[36] After loading ascites fluid/binding buffer (1.5 M Glycine, 3 M NaCl, pH 9.5) mixture on to protein A matrix, the column with washed with several column volumes of PBS (50 mM phosphate, 150 mM NaCl, pH 7.2) until an OD_{280} of ~ 0.2. The column was then washed with 0.1 M sodium acetate pH 5.0 until an OD_{280} of <0.02. The antibody was then eluted with 0.1 M glycine pH 2.6. The fractions were immediately neutralized with 1.0 M Tris•HCl pH 9.0. The fractions containing protein were pooled and dialyzed against PBS.

Isothermal Titration Calorimetry. The free-energy and enthalpy of inhibitor binding was measured with an Omega titration microcalorimeter (MicroCal, Inc.) coupled with a nanovolt preamplifier whose design and operation have been described.[15,64] The protein concentrations used to obtain the binding isotherms ranged from

212

0.015 mM to 0.040 mM. The phosphonate ligand concentrations used were as follows: **1**, 0.5 mM; **2**, 0.5 mM; **3**, 1.0 mM. The phosphonate concentrations reflect the concentration of only the S-enantiomer. All buffers used in the calorimetry experiments were degassed and passed through a 0.2 μm filter prior to use. The ligand solutions were prepared with the degassed and filtered buffers solutions. The protein was exchanged into the desired degassed buffer solution by gel filtration using PD-10 columns (Pharmacia) that were pre-equilibrated with the desired buffer. Typically, a concentrated stock solution (~ 100 mM) of the protein in PBS (pH 7.2) was added to the column and then eluted with the desired buffer. The eluted sample was then diluted with the desired buffer to the appropriate concentration (see above) and passed through a 0.2 μm filter. The pH of the resulting solution always matched that of the desired buffer conditions. In addition, experiments performed with protein samples exhaustively dialyzed against the appropriate buffer gave identical results with those in which the same was prepared as described above. Also, the heats of dilution obtained from experiments in which ligand was injected against buffer matched those that were obtained from injections that were continued past saturation in the ligand binding experiments that were performed under the same buffering conditions.

The shape of the isotherms is governed by the parameter c, where $c = K[M_T]_o$, K is the association constant of the ligand, and $[M_T]_o$ is the total macromolecule concentration. It has been determined that the c value should range from 1 to 1000 for the optimum determination of the binding constant. In the experiments performed in this paper c was approximately 20 for **1** and **2** and 2 for **3** under all conditions. The stoichiometry (n) value obtained from the least-squares regression using a one-site model (Origin program -described below) ranged from 1.9 to 2.1, which is expected since the intact antibody was used in the experiments.

pH-dependence of Thermodynamic Parameters of Binding.

The thermodynamic parameters were analyzed as a function of pH using the same method described in the calorimetry section above. These experiments were performed at 24.5 ± 1°C. The following buffer systems were used in this analysis (pH values are within ± 0.1 pH unit of the indicated values): 50 mM Bis-Tris 150 mM NaCl, pH 6.7; 50 mM MOPS 150 mM NaCl pH 7.2; 50 mM $NaHPO_4$ 150 mM NaCl pH 7.2; 50 mM Tris 150 mM NaCl pH 7.2, 7.6, 8.1, 8.5, 8.8; 50 mM CHES 150 mM NaCl pH 9.2, 9.6; 50 mM glycine 150 mM NaCl pH 9.2; 50 mM CAPS 150 mM NaCl pH 10.2; 50 mM Borate 150 mM NaCl pH 8.1, 8.5, 8.8, 9.2, 9.6, 10.2.

Data analysis. The titration isotherm data was analyzed using the program ORIGIN v2.9 (MicroCal, Inc). The data were fit to a single site binding model using the Wiseman Isotherm.**[14,15,64]** The variations of the parameters obtained from the titration data (temperature dependence, pH dependence, etc.) were fit to the equations in the text using the KaleidaGraph (Synergy Software) plotting program. The parameters obtained from the fit (including errors) are in the Figure legends along with the correlation coefficient for the fit to the equation.

References

(1)   Benkovic, S. J. Catalytic antibodies. *Ann. Rev. Biochem.* **1992,** *61*, 29-54.

(2)   Hilvert, D. Catalytic antibodies. *Curr. Opin. Struct. Biol.* **1994,** *4*, 612-617.

(3)   Lerner, R. A.; Benkovic, S. J.; Schultz, P. G. At the crossroads of chemistry and immunology: catalytic antibodies. *Science* **1991,** *252*, 659-667.

(4)   Wedemayer, G. J.; Patten, P. A.; Wang, L. H.; Schultz, P. G.; Stevens, R. C. Structural insight into the evolution of an antibody combining site. *Science* **1997,** *276*, 1665-1670.

(5)   Wedemayer, G.; Wang, L. H.; Patten, P. A.; Schultz, P. G.; Stevens, R. C. Crystal structures of the free and liganded forms of an esterolytic catalytic antibody. *J. Mol. Biol.* **1997,** *268*, 390-400.

(6)   Wade, H.; Scanlan, T. S. P1-S1 interactions control the enantioselectivity and hydrolytic activity of the norleucine phenylesterase catalytic antibody 17E8. *J. Am. Chem. Soc.* **1996,** *118*, 6510-6511.

(7)   MacBeath, G.; Hilvert, D. Hydrolytic antibodies: variation on a theme. *Chem. & Biol.* **1996,** *3*, 433-445.

(8)   Mader, M. M.; Bartlett, P. A. Binding energy and catalysis: the implications for transition state analogs and catalytic antibodies. *Chem. Rev.* **1997,** *97*, 1281-1301.

(9)   Janda, K. M.; Lo, C.-H. L.; Li, T.; Barbas III, C. F.; Wirsching, P.; Lerner, R. A. Direct selection for a catalytic mechanism from combinatorial antibody libraries. *Proc. Natl. Acad. Sci. USA* **1994,** *91*, 2532-2536.

(10) Gram, H.; Marconi, L. A.; Barbas III, C. F.; Collet, T. A.; Lerner, R. A.; Kang, A. S. In vitro selection and affinity maturation of antibodies from a naive combinatorial immunoglobulin library. *Proc. Natl. Acad. Sci. USA* **1992,** *89*, 3576-3580.
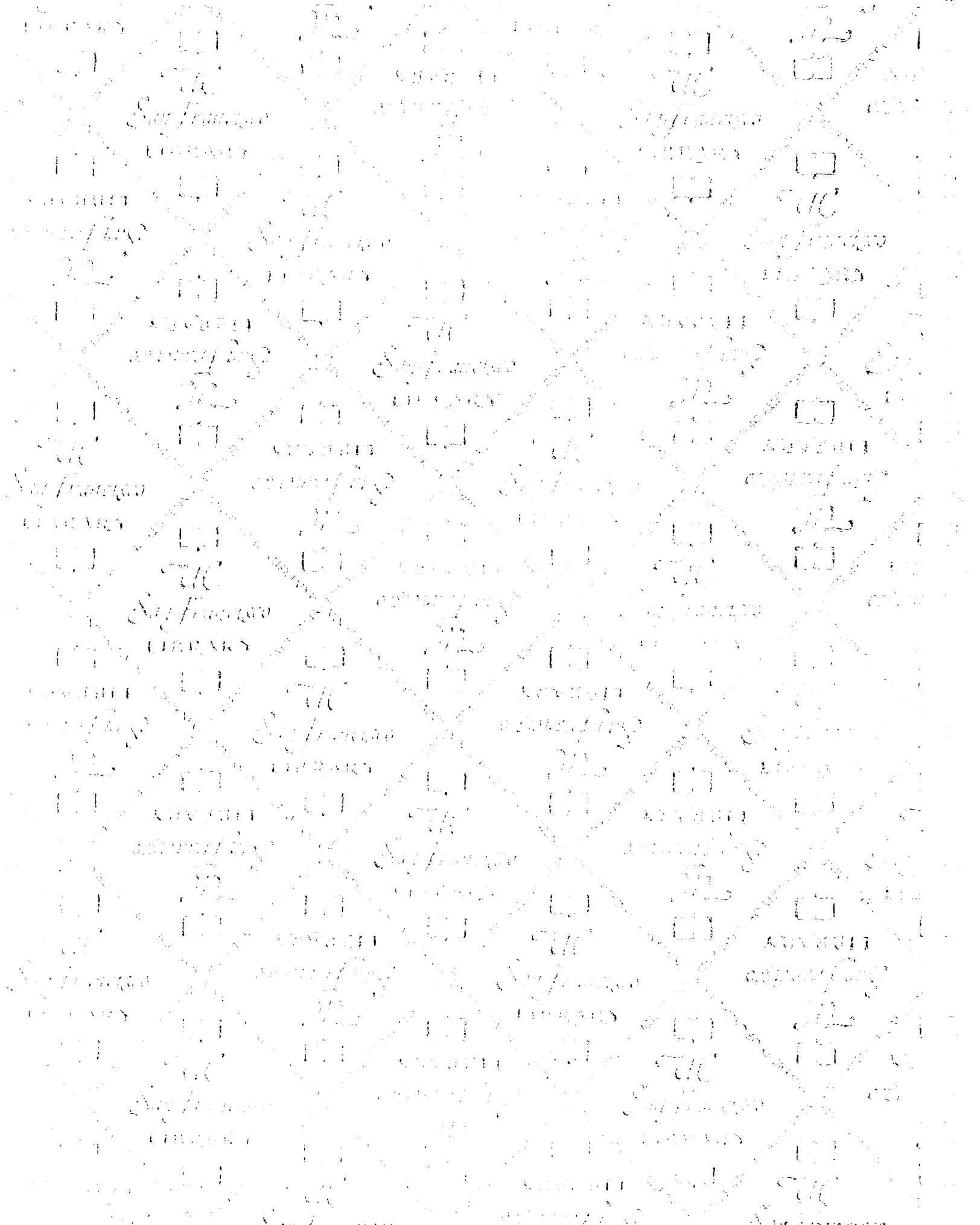
216

(11) Arkin, M. R.; Wells, J. A. Probing the importance of second sphere residues in an esterolytic antibody by phage display. *J. Mol. Biol.* **1998**, *284*, 1083-1094.

(12) Baca, M.; Scanlan, T. S. S.; Stephenson, R. C.; Wells, J. A. Phage display of a catalytic antibody to optimize affinity for transition state analog binding. *Proc. Natl. Acad. Sci.* **1997**, *94*, 10063-10068.

(13) Wade, H.; Scanlan, T. S. Remote binding energy in antibody catalysis: Studies of a catalytically unoptimized specificity pocket. *J. Am. Chem. Soc.* **1999**, *121*, 1434-1443.

(14) Indyk, L.; Fisher, H. F. *Theoretical aspects of isothermal titration calorimetry*; Johnson, M. L. and Ackers, G. A., Ed.; Academic Press: New York, 1998; Vol. 295, pp 350-364.

(15) Freire, E.; Mayorga, O. L.; Straume, M. Isothermal titration calorimetry. *Analytical Chemistry* **1990**, *62*, 950A-959A.

(16) Baker, B.; Murphy, K. P. Evaluation of linked protonation states in protein binding reactions using isothermal titration calorimetry. *Biophysical Journal* **1996**, *71*, 2049-2055.

(17) Xie, D.; Gulnik, S.; Collins, L.; Gustachina, E.; Suvorov, L.; Erickson, J. W. Dissection of pH dependence of inhibitor binding energetics for an aspartic protease: Direct measurement of the protonation states of the catalytic aspartic acid residues. *Biochemistry* **1997**, *36*, 16166-16172.

(18) Biltonen, R. L.; Langerman, N. *Microcalorimetry for biological chemistry: Experimental design, data analysis, and interpretation*; Hirs, C. H. W. and Timasheff, S. N., Ed.; Academic Press: New York, 1979; Vol. 61, pp 287-319.

(19) Eftink, M.; Biltonen, R. *Thermodynamics of interacting biological systems*; Beezer, A. E., Ed.; Academic Press: New York, 1980.

(20) Murphy, K. P.; Xie, D.; Thompson, K. S.; Amzel, L. M.; Freire, E. Entropy in biological binding processes: Estimation of translational entropy loss. *Prot. Struct. Funct. Gen.* **1994**, *18*, 63-67.

(21) Finkelstein, A. V.; Janin, J. The price of lost freedom: entropy of bimolecular complex formation. *Prot. Eng.* **1989,** *3*, 1-3.

(22) Jencks, W. P. *Catalysis in Chemistry and Enzymology*; Dover Publications: Mineola, 1969.

(23) Page, M. I. Binding energy and enzymic catalysis. *Biochem. Biophys. Res. Commun.* **1976,** *72*, 456-461.

(24) Page, M. I. Entropy, binding energy, and enzymic catalysis. *Angew. Chem. Int. Ed. Engl.* **1977,** *16*, 449-459.

(25) Kauzmann, W. Some factors in the interpretation of protein denaturation. *Adv. Prot. Chem.* **1959,** *14*, 1-63.

(26) Dill, K. Dominant forces in protein folding. *Biochemistry* **1990,** *29*, 71337155.

(27) Edsall, J. T.; Wyman, J. *Biophysical Chemistry*; Academic Press: New York, 1958; Vol. 1.

(28) Flogel, M.; Albert, A.; Biltonen, R. The magnitude of electrostatic interaction in inhibitor binding and during catalysis by ribonuclease A. *Biochemistry* **1975,** *14*, 2616-2621.

(29) Honig, B.; Nicholls, A. Classical electrostatics in biology and chemistry. *Science* **1995,** *268*, 1144-1149.

(30) Hansch, C.; Leo, A.; Hoekman, D. *Exploring QSAR: Hydrophobic, Electronic, and Steric Constants*; American Chemical Society: Washington, D.C., 1995.

(31) Privalov, P. L.; Gill, S. J. Stability of protein structure and hydrophobic interactions. *Adv. Prot. Chem.* **1988,** *39*, 191-234.

(32) Edsall, J. T.; Gutfreud, H. *Biothermodynamics. The study of biochemical processes at equilibrium*; John Wiley and Sons: New York, 1983.

(33) Baldwin, R. L. Temperature dependence of the hydrophobic interaction in protein folding. *Proc. Natl. Acad. Sci.* **1986,** *83*, 8069-8072.

(34) Murphy, K. P.; Privalov, P. L.; Gill, S. J. Common features of protein unfolding and dissolution of hydrophobic compounds. *Science* **1990,** *247,* 559-561.

(35) Flogel, M.; Biltonen, R. L. The pH dependence of the thermodynamics of the interaction of 3'-cytidine monophosphate with ribonuclease A. *Biochemistry* **1975,** *14,* 2610-2615.

(36) Guo, J.; Huang, W.; Scanlan, T. S. Kinetic and mechanistic characterization of an efficient hydrolytic antibody: evidence for the formation of an acyl intermediate. *J. Am. Chem. Soc.* **1994,** *116,* 6062-6069.

(37) Zhou, G. W.; Guo, J.; Huang, W.; Fletterick, R. J.; Scanlan, T. S. Crystal structure of a catalytic antibody with a serine protease active site. *Science* **1994,** *265,* 1059-1064.

(38) Wolfenden, R.; Snider, M.; Ridgeway, C.; Miller, B. The temperature dependence of enzyme rate enhancements. *J. Am. Chem. Soc.* **1999,** *121,* 7419-7420.

(39) Charbonnier, J.-B.; Carpenter, E.; Gigant, B.; Golinelli-Pimpaneau, B.; Eshhar, Z.; Green, B. S.; Knossow, M. Crystal structure of the complex of a catalytic antibody Fab fragment with a transition state analog: Structural similarities in esterase-like catalytic antibodies. *Proc. Natl. Acad. Sci., USA* **1995,** *92,* 11721-11725.

(40) Charbonnier, J.-B.; Golinelli-Pimpanaeu, B.; Gigant, B.; Tawfik, D. S.; Chap, R.; Schindler, D. G.; Kim, S.-H.; Gren, B. S.; Eshhar, Z.; Knossow, M. Structural convergence in the active sites of a family of catalytic antibodies. *Science* **1997,** *275,* 1140-1142.

(41) Rao, S. N.; Singh, U. C.; Bash, P. A.; Kollman, P. A. Free energy perturbation calculations on binding energy and catalysis after mutating Asn 155 in subtilisin. *Nature* **1987,** *328,* 551-554.

(42) Kraut, J. Serine proteases: structure and mechanism of catalysis. *Ann. Rev. Biochem.* **1977,** *46,* 331-358.

(43) Stroud, R. M. A family of protein-cutting proteins. *Amer. Sci.* **1974,** *231,* 74-88.

(44) Warshel, A.; Naray-Szabo, G.; Sussman, F.; Hwang, J.-K. How do serine proteases really work? *Biochemistry* **1989,** *28,* 3629-3637.

(45) Warshel, A.; Aqvist, J.; Crieghton, S. Enzymes work by solvation substitution rather than by desolvation. *Proc. Natl. Acad. Sci..,* *USA* **1989,** *86,* 5820-5824.

(46) Warshel, A. Calculations of enzymatic reactions: Calculations of pK$_a$, proton tranfer reactions, and general acid catalysis in enzymes. *Biochemistry* **1981,** *3167-3177,* 3167-3177.

(47) Warshel, A. Energetic of enzyme catalysis. *Proc. Natl. Sci., USA* **1978,** *75,* 5250-5254.

(48) Jacobs, J. W.; Schultz, P. G.; Sugasawara, R.; Powell, M. Catalytic antibodies. *J. Am. Chem. Soc.* **1987,** *109,* 2174-76.

(49) Schultz, P. G.; Lerner, R. A.; Benkovic, S. J. Catalytic antibodies. *Chem. Eng. News* **1990,** *68,* 26-40.

(50) Ross, P. D.; Subramanian, S. Thermodynamics of protein association reactions: Forces contributing to stability. *Biochemistry* **1981,** *20,* 3096-3102.

(51) Creighton, T. E. *Proteins: Structure and Molecular Properties*; Second ed.; W.H. Freeman and Company: New York, 1993.

(52) Fersht, A. *Structure and Mechanism in Protein Science: A Guide to Enzyme Catalysis and Protein Folding*; W.H. Freeman and Company: New York, 1999.

(53) Lolis, E.; Petsko, G. A. Transition-state analogues in protein crystallography: probes of the structural source of enzyme catalysis. *Ann. Rev. Biochem.* **1990,** *59,* 597-630.

(54) Kyte, J. *Mechanism in Protein Chemistry*; Garland Publishing: New York, 1995.

(55) Gilson, M. K.; Honig, B. The Inclusion of Electrostatic Hydration Energies in Molecular Mechanics Calculations. *Journal of Computer-Aided Molecular Design* **1991,** *5,* 5-20.

(56) Warshel, A. Electrostatic origin of the catalytic power of enzymes and the role of preorganized active sites. *J. Biol. Chem.* **1998,** *273*, 27035-27038.

(57) Warshel, A.; Florian, J. Computer simulations of enzyme catalysis: Finding out what has been optimized by evolution. *Proc. Natl. Acad. Sci., USA* **1998,** *95*, 5950-5955.

(58) Cannon, W. R.; Benkovic, S. J. Solvation, reoganization energy, and biological catalysis. *J. Biol. Chem.* **1998,** 26257-26260.

(59) Herzberg, O.; Moult, J. Analysis of the steric strain in the polypeptide backbone of protein molecules. *Prot. Struct. Func. Gen.* **1991,** *11*, 223-229.

(60) Warshel, A.; Sussman, F.; Hwang, J. Evaluation of the catalytic free energies in genetically modified proteins. *J. Mol. Biol.* **1988,** 139-159.

(61) Scoichet, B. K.; Baase, W. A.; Kuroki, R.; Matthews, B. W. A relationship between protein stability and protein function. *Proc. Natl. Acad. Sci.* **1995,** *92*, 452-456.

(62) Kristensen, O.; Vassylyev, D. G.; Tanaka, F.; Morikawa, K.; Fujii, I. A structural basis of transition state stabilization in antibody-catalyzed hydrolysis: Crystal structures of an abzyme at 1.8 Å resolution. *J. Mol. Biol.* **1998,** *281*, 501-511.